CHALMERS
UNIVERSITY OF TECHNOLOGY

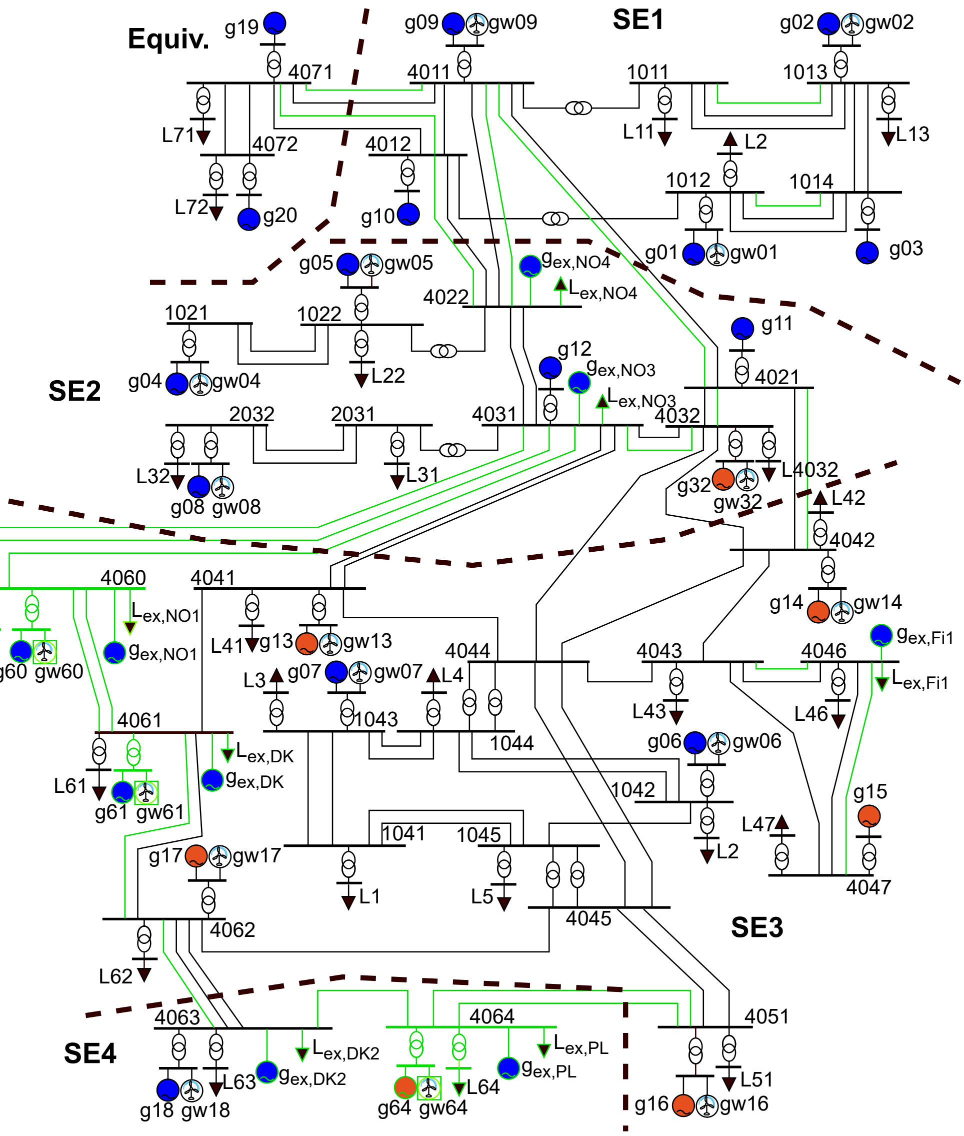

Phasor Data based Power Oscillation Damping in the Power System

Master's thesis in Electrical Power Engineering

Simon Johansson & Maciej Tomala

Department of Electric Engineering
CHALMERS UNIVERSITY OF TECHNOLOGY
Gothenburg, Sweden 2022

Master's thesis 2022:06

Phasor Data based Power Oscillation Damping in the Power System

Simon Johansson & Maciej Tomala

CHALMERS
UNIVERSITY OF TECHNOLOGY

Department of Electrical Engineering
Division of Electric Power Engineering
Chalmers University of Technology
Gothenburg, Sweden 2022

Phasor Data based Power Oscillation
Damping in the Power System
Simon Johansson & Maciej Tomala

Examiner: Peiyuan Chen, Department of Electrical Engineering
Supervisor: Daniel Karlsson, DNV
Co-supervisor: Mohammad Reza Safari Tirtashi, DNV

Master's Thesis 2022:06
Department of Electrical Engineering
Division of Electric Power Engineering
Chalmers University of Technology
SE-412 96 Gothenburg
Telephone +46 31 772 1000

Cover: Diagram of the edited Nordic32.

Typeset in LaTeX
Printed by Chalmers Reproservice
Gothenburg, Sweden 2022

Phasor Data based Power Oscillation Damping in the Power System
Simon Johansson & Maciej Tomala
Department of Electric Engineering
Chalmers University of Technology

Abstract

With the rapid shift towards renewable energy sources there is a concern regarding power system stability. Power oscillation is a phenomena frequently occurring in power systems as a consequence of disturbances and resulting actions to stabilise the system. With the growing interest and availability of Phasor Measurement Units (PMU) in the system this opens up for new possibilities of both monitoring and control. This thesis has investigated both of these aspects.

Dynamic Mode Decomposition (DMD) is a dimensional reduction algorithm which can take in time series data and then extract relevant system information. It proved useful in extracting mode information as frequency and damping ratio from both a single input as well as multiple. The modal analysis performed by DMD corresponded to the analysis performed by the modern Power System Analysis tool PowerFactory, which was used during this thesis.

Another way of creating a damping signal, as compared to the traditional Power System Stabiliser (PSS) structure most commonly used, is the phasor Power Oscillation Damping (phasor POD) algorithm. It focuses on extracting an oscillatory component from a signal which can thereafter be manipulated to create a control signal. A comparison was made between using local power as a feedback signal and a wide-area signal. The wide-area signal was equal to a scaled estimation of power transfer using bus angles retrieved from PMUs. The results show both methods damp power oscillations satisfactory. However, the use of a wide-area control signal can be risky because generators can change their oscillation pattern. Adapting the tuning for the phasor POD to better correlate to the dominating mode improved the damping. However, based on the analysis, the use of Wide-Area Control System (WACS) does not provide any additional benefits as compared to the use of a local feedback signal. On the other hand, it is easier to separate the inter-area mode from the WACS signal than from the local signal.

Simulations were done connected to changes in the production to better represent a future scenario with more Renewable Energy based Sources (RES). The inter-area mode frequency increases with the decrease in system inertia as expected. Re-tuning for the change in frequency results in improved damping performance when compared to the old settings.

Keywords: DMD, inter-area oscillations, Nordic32, Phasor POD, PMU, PowerFactory, power oscillation damping, wide-area.

Acknowledgements

We would like to thank Daniel Karlsson who came up with the topic for this thesis, which turned out to be much larger and more complex than we could then imagine. We would also like to thank Peiyuan Chen, both as an examiner and a professor for his continuous positive guidance. We would like to thank Sharon Müller for allowing us to use his modified version of the Nordic32 model in PowerFactory. We want to give thanks to Lucas Thomée for helping us with technicalities connected to management as well as Arvid Björemark for his positive spirit around the office. Lastly we want to give a big thanks to Mohammad Reza who after joining the project gave a new dimension to it. Your support, broad knowledge and personal interest really deepened our own knowledge as well as inspired us to learn more. Thank you.

Simon Johansson and Maciej Tomala, Gothenburg, June 2022

List of Acronyms

Below is the list of acronyms that have been used throughout this thesis listed in alphabetical order:

AVR	Automatic Voltage Regulator
DMD	Dynamic Mode Decomposition
FACTS	Flexible AC Transmission Systems
GPS	Global Positioning System
HVDC	High Voltage Direct Current
MMF	Magnetomotive Force
OCC	Open Circuit Characteristics
PMU	Phasor Measurement Unit
POD	Power Oscillation Damping
PSS	Power System Stabilizer
RES	Renewable-based Energy Sources
SC	Synchronous Condenser
SG	Synchronous Generator
SMIB	Single-Machine Infinite Bus
SVC	Static Var Compensator
SVD	Singular Value Decomposition
TCSC	Thyristor-Controlled Series Compensator
TSO	Transmissions System Operator
WACS	Wide-Area Control System
WAMPAC	Wide-Area Monitoring Protection and Control
WAMS	Wide-Area Measurement System
WAPOD	Wide-Area Power Oscillation Damper

Nomenclature

Below is the nomenclature of indices, sets, parameters, and variables that have been used throughout this thesis. The symbols are listed in alphabetical order in each category. The sets, parameters, and variables are also defined in the text, where they first appear.

Indices

i, k, n, m	Indices for position in matrices
t	Index for time step

Sets

$\mathbf{A}$	System state matrix
$\tilde{\mathbf{A}}$	Projected state matrix
b	Set of initial values
$\mathbf{B}$	System input matrix
$\mathbf{C}$	System output matrix
$\mathbf{D}$	System feedforward matrix
$\mathbf{g}$	Set of nonlinear functions relating states
λ	Set of eigenvalues
Ω	Diagonal set of frequencies
p	Set of participation factors
$\mathbf{\Phi}$, $\mathbf{R}$	Set of right eigenvectors
$\mathbf{\Psi}$	Set of left eigenvectors
$\mathbf{\Sigma}$, $\mathbf{U}$, $\mathbf{V}$	Matrices from the SVD operator
$\mathbf{u}$	Set of system inputs
$\mathbf{x}$	Set of system states
$\dot{\mathbf{x}}$	Set of system state derivatives
$\mathbf{x}_0$	Set of system states at equilibrium
$\mathbf{X_1}$	Set of inputs for DMD
$\mathbf{X_2}$	Set of time shifted inputs for DMD
$\mathbf{X}_{\text{aug},1}$	Set of augmented inputs for DMD
$\mathbf{X}_{\text{aug},2}$	Set of augmented and time shifted inputs for DMD

$\mathbf{y}$	Set of system outputs

Parameters

β	Matrix ratio
k	Cut-off frequency
K_{POD}	Gain for the POD
K_{sd}	Saturation coefficient
r	Truncation rank
s	Size of data-stacking
T_{W}	Time constant
θ_{POD}	Phasor POD compensation angle

Variables

δ	Rotor angle
E', E_{B}, E_{t}, V_{r}, V_{s}	Bus voltages
D	Load-damping constant
$\Delta\omega_{\mathrm{r}}$	Rotational speed deviation
H	Inertia constant
K_{D}	Damping torque coefficient
K_{S}	Synchronising torque coefficient
ω	Rotational speed
ω_{n}	Natural frequency
ω_{osc}	Inter-area frequency
P	Scaled power signal used for wide-area damping
P_{e}	Electrical power
P_{m}	Mechanical power
P_{pgt}	Local electrical power
P_{sum}	Power transfer between the price areas SE2 and SE3
$P_0(t)$	Signal containing the average component
$\tilde{P}_{\mathrm{osc}}(t)$	Signal containing the oscillatory component
$\underline{P}_{\mathrm{ph}}$	Phasor component
Ψ_{at}, Ψ_{at0}, Ψ_{I}	Flux linkages
σ	Damping constant
T_{e}	Electrical torque
T_{m}	Mechanical torque
V_{POD}	Control signal from the phasor POD
Z	Impedance
ζ	Damping ratio

Contents

List of Acronyms **ix**

Nomenclature **xi**

1 Introduction **1**
1.1 Background 1
1.2 Aim 2
1.3 Task 2
1.4 Scope 2

2 Modelling and Analysis of Power Oscillations **3**
2.1 Generator Theory and Control 3
2.1.1 Single-Machine Infinite Bus System 3
2.1.2 Classical Generator Model 4
2.1.3 Including Effect of Field Winding Dynamic and Flux Saturation . . 7
2.1.4 Automatic Voltage Regulator and Power System Stabiliser 9
2.2 Modal Analysis of Linearised System Model 11
2.3 Data-based Modal Analysis 13
2.3.1 Phasor Measurement Unit 13
2.3.2 Dynamic Mode Decomposition 14
2.3.2.1 Retrieving the Dynamic Matrix A 15
2.3.2.2 Truncation 16
2.3.2.3 The Dynamic Properties 17
2.3.2.4 Participation Factor and Modal Analysis 18
2.4 Real-Life Examples of Inter-Area Oscillations 19
2.4.1 Nordic System 19
2.4.2 European System 19
2.4.3 Other Systems 19
2.4.4 Incidents Based on Inter-Area Oscillations 19
2.5 The Nordic Power System Model 20
2.5.1 The Nordic34 Model 20
2.5.2 The 2018 Scenario 24
2.5.3 Assumptions of the Fully-Renewable Scenario 27

3 Implementation of Power Oscillation Damping **29**
3.1 DMD-based Modal Analysis with Phasor Measurements 29
3.2 Extracting Oscillating Component of a Signal 33
3.2.1 Washout Filter 33
3.2.2 Low-Pass Filter Based Approach 34

3.3 Evaluation of Phase Angle Compensation 38
3.3.1 Analytical Evaluation Based on Linearised System 39
3.3.2 Numerical Approach 40
3.4 Gain Tuning of Phasor POD 41
3.4.1 Local Signal Based 42
3.4.2 Wide-Area Signal Based 43

4 Results **45**
4.1 Description of Case Studies 45
4.2 Use of Local vs. Wide-Area Signal for Damping 46
4.2.1 Impact from Simultaneous Control of Generators 49
4.2.2 Effect of Measurement Location for PMUs 53
4.3 Fully-Renewable Scenario 54

5 Further Discussions **57**
5.1 Participation Factor & Truncation 57
5.2 Local Signal vs. Wide-Area Signal 58
5.2.1 Input Signals 58
5.2.2 Gain Setting 58
5.2.3 Phasor POD 58
5.2.4 Operation Scenario 59
5.2.5 Security 59
5.2.6 Potential Uses 59
5.3 Grid Reinforcements in the Future 59
5.4 Sustainable and Ethical Aspects 60
5.5 Future Work 60

6 Conclusions **61**

References **65**

A Appendix A. Generator Modelling **I**

B Appendix B. DSL Models **III**

C Appendix C. Local vs. Wide-Area Damping **IX**
C.1 Generator g17 IX
C.2 Generator g64 XII
C.3 Wind Turbine Damping for Future Scenario XIV

1
Introduction

This chapter begins by giving a background of the thesis and why it is a topic of interest. Thereafter the aim and the plan on how to achieve it is presented. With a topic of such size, some limitations had to be made which are presented in the scope.

1.1 Background

Since its first introduction in the 1980s, the synchronised Phasor Measurement Unit (PMU) with its further development have proven to be useful in Wide-Area Measurement Systems (WAMS) [1]. There is a growing interest in the world for these systems and most modern power systems around the world are now installing WAMS consisting of PMUs [2]. These units measure the quantities of voltage and current which together with a Global Positioning System (GPS) are time synchronised and can therefore provide a real-time image of the current state of the power system. Any deviation in the system can be detected instantaneously and necessary actions can be performed.

There are different oscillations occurring in the power system. There are large temporary oscillations caused by faults or other disturbances but another kind of oscillations are inter-area oscillations. These latter oscillations are caused by generators within large interconnected power systems oscillating against each other. These oscillations usually have a frequency between 0.2-0.8 Hz and cause concern regarding instability [3]. Within the Nordic system there are two critical inter-area modes of 0.29 and 0.55 Hz caused by generators in the north swinging against those in the south [4]. If the damping ratio of these modes is low, specific measures have to be taken to dampen them. Examples of some of these measures are Power System Stabilisers (PSSs) acting on Automatic Voltage Regulators (AVRs) on generators, Flexible AC Transmission Systems (FACTS) or Supplementary control of HDVC links [5].

The shift towards more Renewable-based Energy Sources (RES) in the power system will lead to definite changes to the existing infrastructure. Their non-continuous nature will most likely lead to more problems regarding stability issues. Wind power seems to not directly affect oscillation modes, but with its alternating behaviour (as with other renewables) the need for compensation will change the overall topology of the grid [6]. A conclusion that can be drawn from this is that the future power systems will have to be able to handle these changes in real time along side the fluctuations. With the increase of PMUs together with new solutions, a shift should be possible from WAMS towards Wide-Area Monitoring, Protection and Control (WAMPAC). This thesis work aims to be part of assisting the movement towards a power system suited for these new stability issues.

1.2 Aim

The aim of the thesis was to compare how local versus wide-area signals can be used for damping inter-area power oscillations with generators. A measurement based method for characterising the system state was also investigated to be able to use PMU data to extract information for damping purposes.

1.3 Task

The project can be divided into the following parts:

1. Literature study:
   (a) Background information regarding the necessity of power oscillation damping.
   (b) Algorithm for detecting power oscillations.
   (c) Implementation of large scale power system model in PowerFactory.
2. PowerFactory:
   (a) Build/load power system model according to Nordic32.
   (b) Create power oscillations in the software.
   (c) Implement algorithm for power oscillation detection.
   (d) Implement equipment and control for the chosen method of damping.
   (e) Run simulation tests.
3. Document theory and results in a thesis report along side the period of the project.

1.4 Scope

There are theoretically many ways to damp power oscillations. By just looking at the power transfer equation and seeing the available parameters gives an overview of the possibilities for power oscillation damping. Some of the methods involve voltage control on generators (AVR), Static Var Compensator (SVC), Thyristor-Controlled Series Compensator (TCSC), governor control on generators but also load modulation.

Investigating and testing all of these methods would not be possible within the time span of this project and a selection is therefore needed. Due to the wide spread availability of synchronous generators these were targeted for damping.

To narrow down the scope as much as possible, existing models of a power system will be used for the simulations. The Nordic32 network is deemed sufficient when studying the topic area, without any major changes, due to its dynamic properties. The algorithms for oscillation classification will be taken from previous works.

2

Modelling and Analysis of Power Oscillations

This chapter goes through necessary points needed and used to analyse power oscillations in the power system. There is a large part regarding generators, how power oscillations emerge and are observed which then transitions into necessary modelling of generators for tuning purposes. A walk through of theory connected to modal analysis is then done for comparison between the traditional and measurement based techniques. Lastly are some historical events caused by inter-area power oscillations.

2.1 Generator Theory and Control

This section goes through theory connected to synchronous generators and their control. An introduction into modal analysis is also made connected to the other theory presented.

2.1.1 Single-Machine Infinite Bus System

When studying the behaviour of a single machine connected to a large power system this can be done through what is called a Single-Machine Infinite Bus (SMIB) system [7]. By representing the connected machine as in Figure 2.1 the behaviour of the machine can be analysed while still keeping the correct system behaviour. The size of the system relative to the generator makes it so the Thevenin's voltage remains virtually constant, giving rise to the term infinite bus. The external system R_e and X_e represents the grid. In a real setting these values can be approximated by calculating the Thevenin equivalent impedance from doing a short circuit at the bus between the transformer and the infinite bus. Even though the system conditions remains the same when the analysed machine is perturbed, the conditions representing the external system is not necessarily the same but changes with load and grid topology.

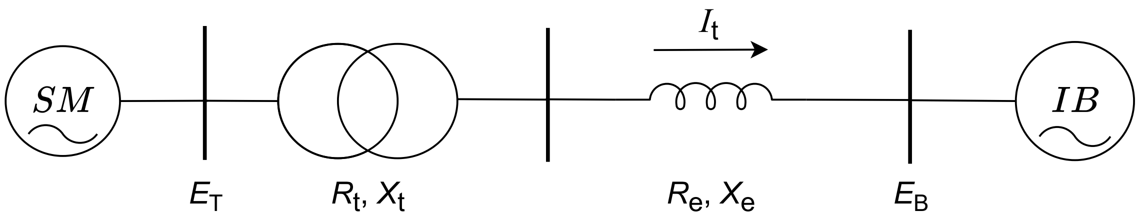

Figure 2.1: Single-machine infinite bus model.

2.1.2 Classical Generator Model

The system shown in Figure 2.1 can be linearised to analyse the system behaviour when a disturbance takes place. By neglecting the resistance and representing the generator with the classical model [7] the system can be represented as in Figure 2.3. Figure 2.2 shows the classical generator model.

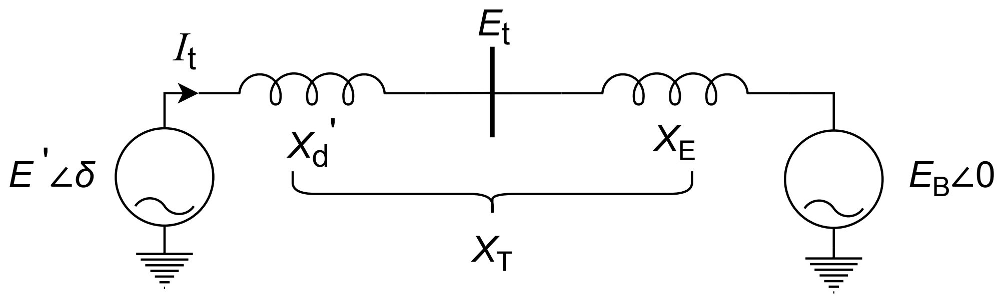

Figure 2.2: Illustration of the classical generator model.

With the stator resistance neglected the air-gap power is equal to the air-gap torque when in per unit. Therefore

$$T_{\mathrm{e}} = P_{\mathrm{e}} = \frac{E' E_{\mathrm{B}}}{X_{\mathrm{T}}} \sin\delta \tag{2.1}$$

where T_{e} is the electrical air-gap torque being equal to the power, X_{T} being the the total reactance including X'_{d} and X'_{E} and the voltages consisting of the generator voltage E' and the infinite bus voltage E_{B}. Linearising at an initial operating condition where $\delta = \delta_0$ gives

$$\Delta T_{\mathrm{e}} = \frac{\partial T_{\mathrm{e}}}{\partial \delta}\Delta\delta = \frac{E' E_{\mathrm{B}}}{X_{\mathrm{T}}} \cos\delta_0(\Delta\delta). \tag{2.2}$$

Linearising the equation of motion in per unit with $\frac{d}{dt}\delta = \omega_0 \Delta\omega_{\mathrm{r}}$ gives

$$\frac{\mathrm{d}}{\mathrm{dt}}\Delta\omega_{\mathrm{r}} = \frac{1}{2H}\left(T_{\mathrm{m}} - T_{\mathrm{e}} - K_{\mathrm{D}}\Delta\omega_{\mathrm{r}}\right), \tag{2.3}$$

where ω_{r} is per unit speed, δ rotor angle in electrical radians, w_0 base rotor electrical speed in radians per second. Substituting (2.2) results in

$$\frac{\mathrm{d}}{\mathrm{dt}}\Delta\omega_{\mathrm{r}} = \frac{1}{2H}\left(\Delta T_{\mathrm{m}} - K_{\mathrm{S}}\Delta\delta - K_{\mathrm{D}}\Delta\omega_{\mathrm{r}}\right) \tag{2.4}$$

where K_{S} is the synchronising torque coefficient given by

$$K_{\mathrm{S}} = \left(\frac{E' E_{\mathrm{B}}}{X_{\mathrm{T}}}\right)\cos\delta_0. \tag{2.5}$$

Linearising further as in [7], writing in vector matrix and solving for the characteristic equation results in the natural frequency being

$$\omega_{\mathrm{n}} = \sqrt{K_{\mathrm{S}} \frac{\omega_0}{2H}}. \tag{2.6}$$

Figure 2.3 shows a block diagram representation of the SMIB system with a classical generator model, graphically illustrating (2.4). The factors K_{S} and K_{D} represents the different torque components connected the machines stability. The synchronising torque K_{S} is connected to a machines ability to stay synchronised to the system and is linked to the change of $\Delta\delta$. A lack thereof would result in an aperiodic drift in the rotor angle. The damping torque K_{D} is in phase with the speed deviation $\Delta\omega_{\mathrm{r}}$ and a lack of sufficient damping torque results in rotor oscillations.

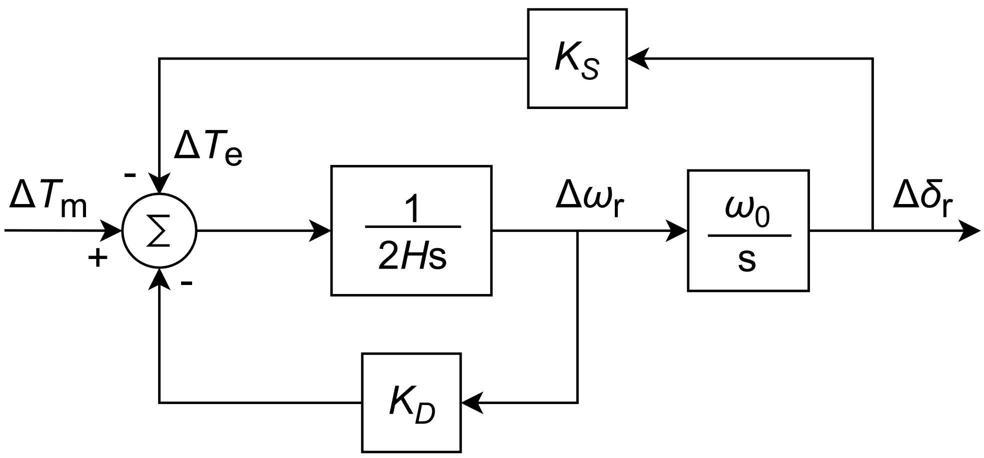

Figure 2.3: Block diagram of the representation of SMIB as a classical generator model.

The power system is constantly affected by transient disturbances. These can be small like load changes in the system or larger disturbances like for example disconnection of lines due to faults. When power system stability is analysed, the active power transfer between generators is used and can be written as

$$P_{\mathrm{e}} = \frac{V_{\mathrm{s}} V_{\mathrm{r}}}{Z} \sin(\delta) \tag{2.7}$$

where P_{e} is the electric power, V_{s} and V_{r} are the sending and receiving voltages, δ the angle difference between the voltages and Z is the equivalent impedance. Assume a simplified model of the electric grid seen in Figure 2.4 containing a generator, two transmission lines with impedances Z_{A} and Z_{B} and an infinite bus. The notation F_{A} represents a 3-phase fault on the transmission line.

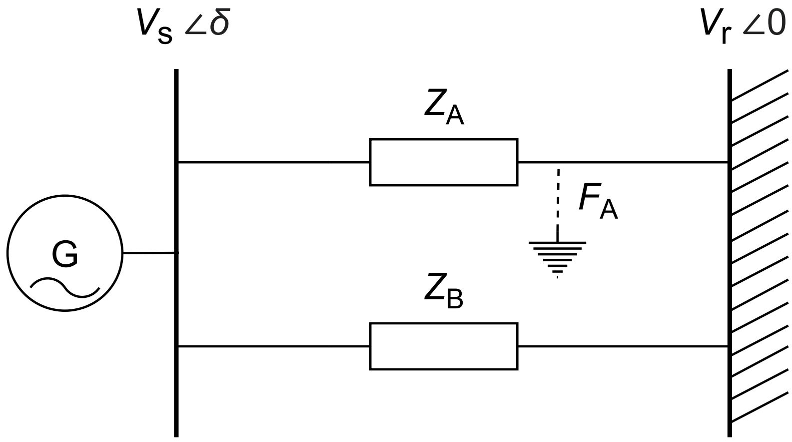

Figure 2.4: Generator connected to an infinite bus through two lines. F_A indicates a 3-phase fault on the transmission line.

Before a fault occurs the system is operating at an angle of δ_0 on curve A as seen in Figure 2.5. A fault occurring changes the equivalent impedance Z and P_e drops down to B. At this point there is now a power imbalance resulting in the generator speeding up. As it does the transfer angle δ increases leading to more active power being drawn from the generator terminal. This will continue until the transfer angle results in an active power transfer P_e greater than the mechanical power input P_m leading to the generator starting to decelerate. When the fault is cleared and the transmission line is disconnected the operating curve changes to C and the generator will start to decelerate. The new operation point will now be δ_1 until the faulted transmission line is reconnected.

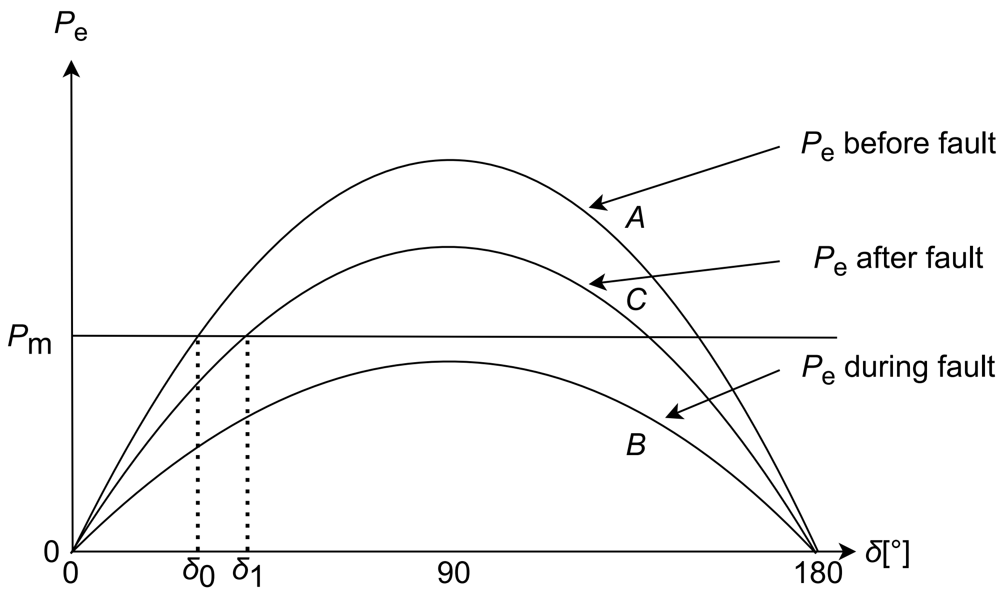

Figure 2.5: P-δ curves for different operations conditions.

The behaviour of the generator for the different stages is described by the traditional swing equation as

$$\frac{\mathrm{d}\omega}{\mathrm{dt}} = \frac{1}{2H}\left(P_{\mathrm{m}} - P_{\mathrm{e}} - D\Delta\omega\right) \tag{2.8}$$

where ω is the rotational speed of the generator, H is the inertia constant and D is the load-damping constant taking into account the frequency dependency of composite load. The longer the fault is active the less time the generator have to regain stability. If, according to the equal area criterion, the critical clearing angle is higher than the intersection of the electrical and mechanical power the machine will go out of synchronism.

When it comes to synchronous generator modelling there are multiple different models representing the machine. This originates from the more detailed parameter definitions not being possible to derive by measurements. The parameters which can be measured and are used in most power system softwares are shown in Table 2.1 and are called standard parameters.

Table 2.1: Synchronous generator parameters.

Parameters	
Synchronous reactance	X_{d}
	X_{q}
Transient reactance	X'_{d}
	X'_{q}
Subtransient reactance	X''_{d}
	X''_{q}
Transient OC time constant	T'_{d}
	T'_{q}
Subtransient OC time constant	T''_{d}
	T''_{q}
Stator leakage inductance	X_{l}
Stator resistance	R_{a}

2.1.3 Including Effect of Field Winding Dynamic and Flux Saturation

Modelling saturation is a complex problem due to several parameters being involved. A few assumptions are therefore made to simplify the task [7]:

- The leakage inductance is independent of saturation. This assumption does not significantly affect the results due to the leakage flux path being mostly through air and not through the iron.

- Leakage fluxes do not contribute to the saturation due to it only travelling through the main flux path for a small part of its path.

- The saturation relationship between the resultant air-gap flux and the magneto-motive force (MMF) under loaded conditions are the same as under no load. The saturation characteristics can therefore be represented by the Open Circuit Characteristic (OCC) saturation curve.

- There is no magnetic coupling between the d and q-axis resulting from the nonlinearities caused by the saturation, meaning currents in the windings of one axis does not produce flux linking with the other axis windings.

The above assumptions introduce the possibility of representing the saturation effects in the d-axis as in (A.2). An approximation of the saturation coefficient K_{sd} can be derived by doing a fit to a saturation curve and then using the parameters in (A.3). Initially the coefficient can be defined as

$$K_{\mathrm{sd}} = \frac{\Psi_{\mathrm{at}}}{\Psi_{\mathrm{at0}}}. \tag{2.9}$$

Defining a parameter

$$\Psi_{\mathrm{I}} = \Psi_{\mathrm{at0}} - \Psi_{\mathrm{at}} \tag{2.10}$$

the expression becomes

$$K_{\mathrm{sd}} = \frac{\Psi_{\mathrm{at}}}{\Psi_{\mathrm{at}} + \Psi_{\mathrm{I}}}, \tag{2.11}$$

where Ψ_{I} is the difference between the unsaturated and the saturated curve. Figure 2.6 illustrates the characteristic of the different parameters in relation to the OCC.

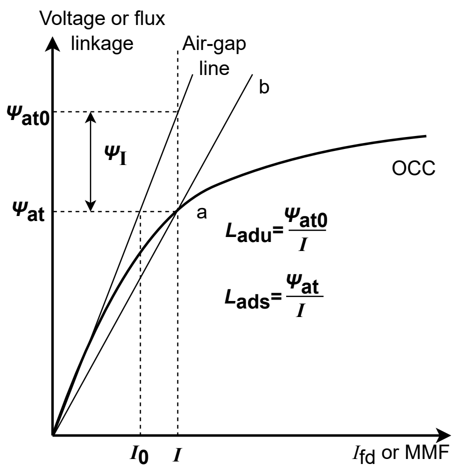

Figure 2.6: Saturation effects in relation to Open-circuit characteristics [7].

The saturation curve can be divided into three segments: unsaturated (I), saturated (II) and fully saturated (III). For segment I, the $\Psi_{\mathrm{I}} = 0$ due to the linearity, for segment II, Ψ_{I} can be expressed as a mathematical function and segment III is again linear and can be expressed as

$$\Psi_{\mathrm{I}} = \Psi_{\mathrm{G2}} + L_{\mathrm{ratio}} \left(\Psi_{\mathrm{at}} - \Psi_{\mathrm{T2}} \right) - \Psi_{\mathrm{at}}. \tag{2.12}$$

Figure 2.7 shows the definition of the segments with the corresponding parameters. By using two points on the curve a fit to a mathematical function can be achieved, Ψ_I can for example be expressed as an exponential function on the form

$$\Psi_\mathrm{I} = A_\mathrm{sat} e^{B_\mathrm{sat}(\Psi_\mathrm{at} - \Psi_\mathrm{T1})}. \tag{2.13}$$

Finally, the calculated results can be used together with (A.3) to get an estimation of the saturation.

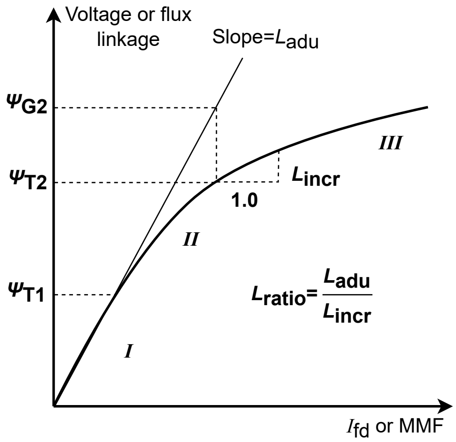

Figure 2.7: Segments in the saturation characteristics [7].

Depending on the type of machine the saturation relations between the axes vary. Due to the q-axis flux path being mostly in air, L_aq does not vary significantly with saturation and K_sq can therefore be assumed to be zero [7]. For the round rotor machines both axes are affected by saturation and can therefore be modelled.

2.1.4 Automatic Voltage Regulator and Power System Stabiliser

The Automatic Voltage Regulator (AVR) is the control system responsible for sending the control signals to the exciter which regulates the terminal voltage. To improve the power systems dynamic performance a PSS can be added to the control of the AVR.

The basis for PSS is that it should provide damping by introducing an electric torque in phase with the rotor speed deviation. Due to the relatively long response time of the generator field winding dynamic and certain exciter systems, appropriate phase compensation is necessary. Furthermore filtering and gain is needed to remove unwanted signal content and set a suitable control signal amplitude. A PSS control structure can be explained by the use of three blocks:

- Gain
- Signal washout
- Phase compensation

The gain corresponds to the introduced damping and should be set to achieve maximum damping while still considering the overall system stability. The signal washout is a high-pass filter set to allow oscillations in w_r to pass unchanged while at the same time acting on changes in speed. The phase compensation is used to correct for the frequency dependency and should allow all the frequencies of interest to be compensated while still remaining within certain stability limits. It is desirable to not have a perfect phase compensation to utilise the synchronising torque. An undercompensation of 20-40° is therefore preferable [8]. Figure 2.8 shows a traditional PSS control structure.

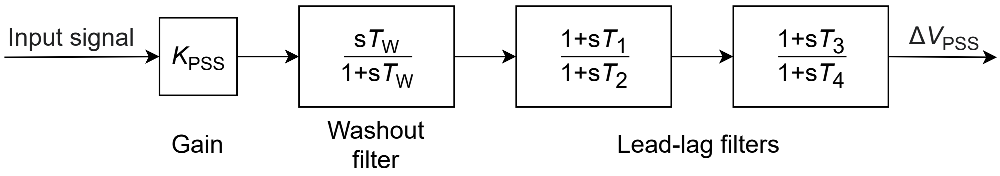

Figure 2.8: Traditional PSS block diagram.

There are a few alternatives when it comes to which signal to use for the control with their respective pros and cons. PSS commonly uses shaft speed, terminal frequency and/or power as input signals [7], but there is also a possibility of using accelerating power [8]–[10]. Many modern types of PSS use a combination of input signals to overcome the weaknesses of the single input signal. From the relation in (2.8) it can be seen the power is lagging the speed by 90°. When using the power as input signal it is therefore necessary to compensate for this additional difference.

When doing modelling of synchronous generator dynamics a model called the classical model is used with its corresponding parameters. These parameters are connected to the standard parameters through certain relations. In Figure 2.9 a complete model is shown containing all the parameters for a complete model.

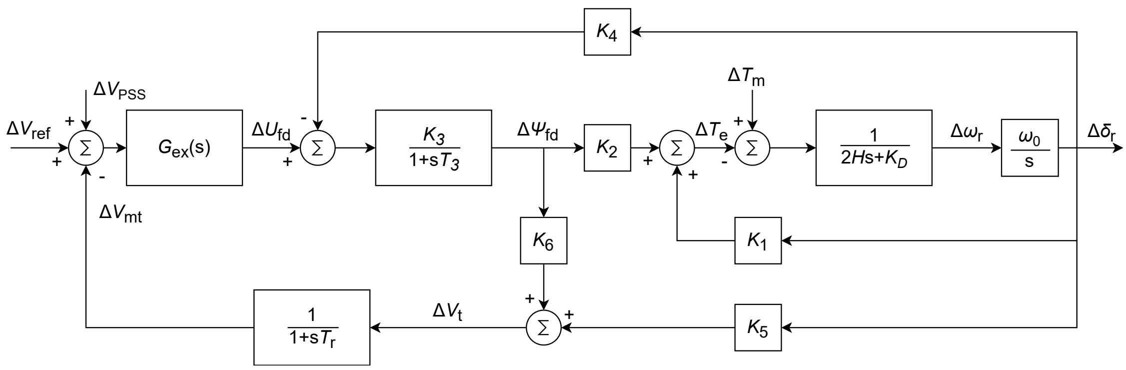

Figure 2.9: Block diagram of the classic generator model [7].

To achieve successful damping of power oscillations a positive damping torque should be supplied by the control system. To achieve this the control signal needs a gain as well as the correct phase shift. Looking at the generator response from the input signal to the electrical torque produced in the machine this information can be derived. If only the phase is of interest the same analysis can be done looking at the response to the terminal voltage produced due to the phase characteristics being the same. Figure 2.10 illustrates the open loop response on the torque ΔT_e from an input signal ΔV_{PSS}. The parameters required for phase analysis of the transient model shown in Figure 2.10 are displayed in Appendix A.

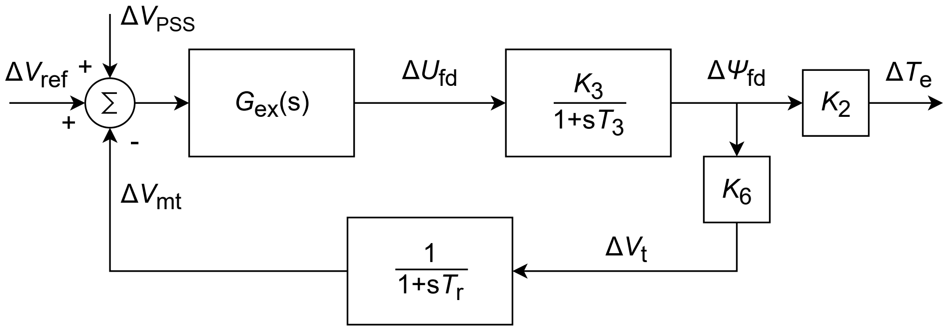

Figure 2.10: Block diagram of the transient model [7].

2.2 Modal Analysis of Linearised System Model

Analysis of power system stability is closely linked to linear algebra. Traditionally the method of setting up the dynamic equations representing the system and then evaluating its properties has been done, but with more advanced technical equipment a shift towards a data analysis approach is possible. The different methods are not separated when it comes to the understanding of the fundamental concepts and these will therefore be presented briefly.

The dynamics of the power system can be described by a set of first order nonlinear ordinary differential equations which on vector form is expressed as [7]:

$$\dot{\mathbf{x}} = \mathbf{f}(\mathbf{x}, \mathbf{u}, t) \tag{2.14}$$

where the vectors are

$$\mathbf{x} = \begin{bmatrix} x_1 \\ x_2 \\ \vdots \\ x_n \end{bmatrix} \quad \mathbf{u} = \begin{bmatrix} u_1 \\ u_2 \\ \vdots \\ u_n \end{bmatrix} \quad \mathbf{f} = \begin{bmatrix} f_1 \\ f_2 \\ \vdots \\ f_n \end{bmatrix} \tag{2.15}$$

with $\mathbf{x}$ known as the state, contains the state variables and $\mathbf{u}$ contains the inputs to the system. While $\dot{\mathbf{x}}$ denotes the derivatives of the state variables and t is time, which is not necessarily expressed explicitly. Additionally the output variables of the system are of interest and these are expressed as vectors:

$$\mathbf{y} = \mathbf{g}(\mathbf{x}, \mathbf{u}) \tag{2.16}$$

with

$$\mathbf{y} = \begin{bmatrix} y_1 \\ y_2 \\ \vdots \\ y_m \end{bmatrix} \quad \mathbf{g} = \begin{bmatrix} g_1 \\ g_2 \\ \vdots \\ g_m \end{bmatrix} \tag{2.17}$$

where $\mathbf{y}$ and $\mathbf{g}$ are the vectors containing the outputs as well as the nonlinear functions relating state, input and output variables. The state variables describe the dynamic behaviour of the system and together with the input variables any other system variable can be determined. In reality the state variables can be connected to physical quantities as angle, voltage or speed but can also only be mathematical variables connected to differential equations describing the system.

The choice of state variables is not unique but this does not mean that the state of the system is not unique. Different choices of state variables can provide the same information about the system. The system state may be represented in a n-dimensional Euclidean space, called state space. The different choices of state variables can be described as using a different coordinate system for achieving the system representation.

When doing analysis on dynamic systems it is interesting to look at singular points due to them being characteristic of the system behaviour. These are points satisfying

$$\mathbf{f}(\mathbf{x}_0) = 0 \tag{2.18}$$

where $\mathbf{x}_0$ is the state vector $\mathbf{x}$ at the equilibrium point (singular point). If the functions in $\mathbf{f}$ are linear then the system is linear and only one equilibrium point exists. This is not the case for nonlinear systems where multiple points can exist.

When doing a traditional small signal analysis a linearisation is done around the equilibrium point which is to be investigated. With the assumption the changes are small, Taylor series expansion is used to express the nonlinear functions. This results in the following expressions:

$$\Delta\dot{\mathbf{x}} = \mathbf{A}\Delta\mathbf{x} + \mathbf{B}\Delta\mathbf{u} \tag{2.19}$$

$$\Delta\mathbf{y} = \mathbf{C}\Delta\mathbf{x} + \mathbf{D}\Delta\mathbf{u} \tag{2.20}$$

where $\mathbf{x}$ is the state vector, $\mathbf{y}$ the output vector, $\mathbf{u}$ input vector, $\mathbf{A}$ state matrix, $\mathbf{B}$ input matrix, $\mathbf{C}$ output matrix and $\mathbf{D}$ is a kind of feedforward matrix defining input properties directly affecting the output.

When looking at stability for a system it is the eigenvalues of the state matrix $\mathbf{A}$ which provides this information.

$$\mathbf{A}\boldsymbol{\phi} = \lambda\boldsymbol{\phi} \tag{2.21}$$

describes the fundamental equation with $\boldsymbol{\phi}$ being the right eigenvector and $\boldsymbol{\lambda}$ the eigenvalues. By solving for the eigenvalues λ_i through

$$\det(\mathbf{A} - \lambda\mathbf{I}) = 0 \tag{2.22}$$

the corresponding eigenvectors can be derived

$$\phi_i = \begin{bmatrix} \phi_{1i} \\ \phi_{2i} \\ \vdots \\ \phi_{ni} \end{bmatrix}, \tag{2.23}$$

with each column vector being connected to the ith eigenvalue, $i = 1, 2, ..., n$. For a real matrix $\mathbf{A}$ the eigenvalues always appear in conjugate pairs as

$$\lambda_i = \sigma_i \pm \mathrm{j}\omega_i. \tag{2.24}$$

The time characteristics of the eigenvalues are given by $e^{\lambda_i t}$ meaning the real part represents the damping and the imaginary the oscillatory part. The frequency and damping ratio can be expressed as

$$f_i = \frac{\omega_i}{2\pi} \tag{2.25}$$

$$\zeta_i = \frac{-\sigma_i}{|\lambda_i|} = \frac{-\sigma_i}{\sqrt{\sigma_i^2 + \omega_i^2}}. \tag{2.26}$$

2.3 Data-based Modal Analysis

This section starts of by introducing the PMU and its functionality. The use of PMU data is then combined with an advanced algorithm with the purpose of performing measurement based modal analysis.

2.3.1 Phasor Measurement Unit

The fundamental relation of active power flow seen in (2.7) has caused voltage phasors in the power system to be of special interest. Even though this is the case, there was no good way of measuring these quantities historically. It was not until the growth of GPS in the 1980s that the development of the first modern PMU could really take place. Jumping forward to today, most modern power systems around the world are in the process of installing PMUs for WAMS [2], and there are already applications utilising PMUs for WAMPAC.

In Norway a Wide-Area Power Oscillation Damper (WAPOD), controlling a SVC together with PMU signals, has been implemented and tested with good results [11]. In China additional damping is being provided by several HVDC links, by using PMUs, to help the traditional PSS during stressed conditions [12]. With more PMUs and better data analysing tools the development of WAMPAC systems will be able to reach even further and ensure better overall stability in the power system.

First, consider a sinusoidal signal

$$x(t) = A\cos(\omega t + \phi) \tag{2.27}$$

with an amplitude A, frequency ω and phase ϕ. This equation can also be written in the form of

$$x(t) = \mathrm{Re}\left\{Ae^{\mathrm{j}(\omega t+\phi)}\right\} = \mathrm{Re}\left[\left\{e^{\mathrm{j}(\omega t)}\right\}X_{\mathrm{m}}e^{\mathrm{j}\phi}\right]. \tag{2.28}$$

With the understanding that the frequency is ω the term $e^{\mathrm{j}(\omega t)}$ representing the frequency can be suppressed. With this the signal can be expressed with a phasor representation according to

$$X \equiv \frac{A}{\sqrt{2}}e^{\mathrm{j}\phi} = \frac{A}{\sqrt{2}}(\cos\phi + \mathrm{j}\sin\phi). \tag{2.29}$$

The PMU can supply all of the mentioned quantities of a signal. These can then be used to generate a control signal for damping purposes. In [11] the phasors from two different locations are used while [12] discusses the use of frequency as input. Figure 2.11 illustrates how a phasor representation can be made from a sinusoidal signal.

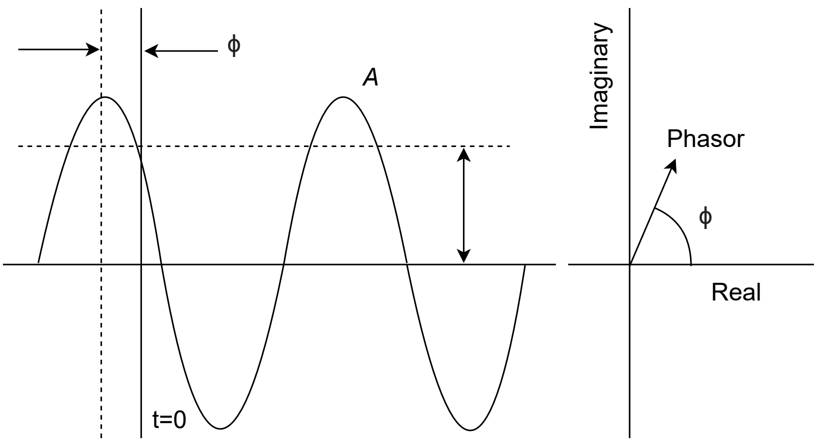

Figure 2.11: Representation of the PMU phasor from a sinusoidal signal.

2.3.2 Dynamic Mode Decomposition

Dynamic Mode Decomposition (DMD) is an algorithm which extracts information regarding the behaviour of a system. The method originally comes from the fluid dynamics field [13], [14], but has lately been implemented and used for Power System application [15]–[20]. Together with PMU data DMD can estimate the state space matrix **A** in (2.19) representing the system dynamics. When it comes to large power systems with many nonlinear dynamics it is practically impossible to fully comprehend its behaviour. DMD can use the PMU data to create a temporary linear model of the actual power system, this dynamic representation can then be updated continuously to capture the changes caused by for example production changes, load changes or drastic topology changes as disconnecting lines etc. This creates great possibilities of analysing the system small signal stability, which typically is a complex analysis, continuously.

2.3.2.1 Retrieving the Dynamic Matrix A

As previously pointed out in (2.19) the purpose of the dynamic matrix (state space matrix) is to link the current state to the future state. This can be described in discrete form as

$$\mathbf{X}_{k+1} = \mathbf{A}\mathbf{X}_k. \tag{2.30}$$

The matrixes $\mathbf{X}_k$ and $\mathbf{X}_{k+1}$ are constructed by time-shifting the matrices containing the PMU signals as

$$\mathbf{X_1} = \begin{bmatrix} | & | & & | \\ \mathbf{x}_1 & \mathbf{x}_2 & \cdots & \mathbf{x}_{m-1} \\ | & | & & | \end{bmatrix} \tag{2.31a}$$

$$\mathbf{X_2} = \begin{bmatrix} | & | & & | \\ \mathbf{x}_2 & \mathbf{x}_3 & \cdots & \mathbf{x}_{m} \\ | & | & & | \end{bmatrix} \tag{2.31b}$$

where $\mathbf{x}_1$ is a column vector containing all the first samples from all the signals and so on. Additionally one must perform something called data stacking to increase the information provided for the calculation and therefore increase the accuracy. This is especially important if used on a single signal. The data stacking is done by creating augmented matrices with time-shifted matrices as new rows. The augmented matrices looks like

$$\mathbf{X}_{\text{aug},1} = \begin{bmatrix} x_1 & x_2 & \cdots & x_{m-s} \\ x_2 & x_3 & \cdots & x_{m-s+1} \\ \vdots & \vdots & \ddots & \vdots \\ x_s & x_{s+1} & \cdots & x_{m-1} \end{bmatrix} \tag{2.32a}$$

$$\mathbf{X}_{\text{aug},2} = \begin{bmatrix} x_2 & x_3 & \cdots & x_{m-s+1} \\ x_3 & x_4 & \cdots & x_{m-s+2} \\ \vdots & \vdots & \ddots & \vdots \\ x_{s+1} & x_{s+2} & \cdots & x_{m} \end{bmatrix} \tag{2.32b}$$

where s represents the amount of time-shifts performed which should be sufficiently large. According to [15] it should be between 30-40 % of the measurement snapshot number m.

This can result in rather large amount of data which is why [15] successfully implements a randomisation technique originally proposed in [21] to reduce the amount of rows of the augmented matrices. This somewhat reduces the accuracy but significantly reduces computation time [15].

For a small system the matrix $\mathbf{A}$ can be directly calculated by just using the Moore-Penrose pseudoinverse † as

$$\mathbf{A} = \mathbf{X}_2\mathbf{X}_\mathbf{1}^{\dagger}. \tag{2.33}$$

Due to the size of the matrices in the power system applications this is not suitable. DMD therefore uses Singular Value Decomposition (SVD) which extracts the necessary information into much smaller matrices. It is then possible to use rank reduction reducing the data size leading to less computation cost while also removing noise. The SVD results in

$$\mathbf{X_1} \approx \mathbf{U\Sigma V}^*, \tag{2.34}$$

where $\mathbf{U} \in \mathbb{C}^{n\times r}$, $\mathbf{\Sigma} \in \mathbb{C}^{r\times r}$, and $\mathbf{V} \in \mathbb{C}^{m\times r}$. The notation * symbolises conjugate transpose and r is rank, if no rank reduction is used the matrices would be $\mathbf{U} \in \mathbb{C}^{n\times n}$, $\mathbf{\Sigma} \in \mathbb{C}^{n\times n}$, and $\mathbf{V} \in \mathbb{C}^{m\times n}$. For the augmented matrices the sizes would be much larger. Combining (2.33) and (2.34) leads to

$$\mathbf{A} = \mathbf{X}_2\mathbf{V\Sigma}^{-1}\mathbf{U}^*. \tag{2.35}$$

To achieve a reduced rank dynamic matrix the full size $\mathbf{A}$ is projected onto the ortogonal basis produced by the SVD as

$$\tilde{\mathbf{A}} = \mathbf{U}^*\mathbf{A}\mathbf{U} = \mathbf{U}^*\mathbf{X_2}\mathbf{V\Sigma}^{-1}. \tag{2.36}$$

The lower rank dynamic model is now defined as

$$\tilde{\mathbf{x}}_{k+1} = \tilde{\mathbf{A}}\tilde{\mathbf{x}}_k. \tag{2.37}$$

2.3.2.2 Truncation

Truncating with a rank r reduces the size of the matrices from the SVD and increases the computation speed. There are multiple ways of choosing the size of r [22]. One method is to analyse the energy of the diagonal values in $\mathbf{\Sigma}$ and extract r corresponding to a percentage of choice. The higher percentage the more accurate the recreation of the signal will be, but a too large value might include noise from the signal, decreasing the accuracy of the recreation. A value between 90-99 % is mentioned by [22].

Another method, called the hard threshold method, functions by looking at the "elbow" or "knee" from the logarithmic plot of $\mathbf{\Sigma}$ and extract the r at the point where the curve sharply turns. Numerically it can be calculated as

$$\tau = (4/\sqrt{3})\sqrt{n}\gamma \tag{2.38}$$

if the input matrix $\mathbf{X}$ is a square matrix $\mathbf{R}^{n\times n}$. While if the matrix is non-square $\mathbf{R}^{n\times m}$ with m $\ll$ n, then the rank is calculated as

$$r = \lambda(\beta)\sqrt{n}\gamma \tag{2.39}$$

$$\lambda(\beta) = \left(2(\beta+1) + \frac{8\beta}{(\beta+1) + (\beta^2 + 14\beta + 1)^{1/2}}\right)^{1/2}, \tag{2.40}$$

with β=m/n and γ being the know noise in the input signal. If m $\ll$ n then β=n/m. If the noise on the other hand is unknown the equation changes to

$$r = \omega(\beta)\sigma_{\mathrm{med}} \tag{2.41}$$

using the median of the singular values $\mathbf{\Sigma}$ and $\omega(\beta) = \lambda(\beta)/\mu_\beta$, where μ_β has to be solved numerically as

$$\int_{(1-\beta)^2}^{\mu_\beta} \frac{\left[\left((1+\sqrt{\beta})^2 - t\right)\left(t - (1-\sqrt{\beta})^2\right)\right]^{1/2}}{2\pi t} dt = \frac{1}{2}. \tag{2.42}$$

2.3.2.3 The Dynamic Properties

The dynamic behaviour is now extracted by computing the eigenvalue and eigenvectors on $\tilde{\mathbf{A}}$ which follows the standard form

$$\tilde{\mathbf{A}}\mathbf{R} = \lambda\mathbf{R}, \tag{2.43}$$

where $\mathbf{R}$ is a matrix with the right eigenvectors and λ a matrix with the eigenvalues on the diagonal. The original signals can now be recreated and future states can also be estimated by first converting to a continuous-time model

$$\omega_k = \ln(\lambda_k)/\Delta t, \tag{2.44}$$

where ω_k are the eigenvalues in continuous time and Δt are the sampling time. The DMD exact modes [23] are calculated by

$$\mathbf{\Phi} = \mathbf{X}_2\mathbf{V}\mathbf{\Sigma}^{-1}\mathbf{R}. \tag{2.45}$$

These are the exact eigenvectors of the matrix $\mathbf{A}$. This formula should be used to find dynamic modes associated with zero eigenvalues but otherwise

$$\mathbf{\Phi} = \mathbf{UR} \tag{2.46}$$

should be used to get the modes referred to as projected DMD modes. The initial values for the signals are provided through

$$\mathbf{b} = \mathbf{\Phi}^{\dagger}\mathbf{x_1} \tag{2.47}$$

where $\mathbf{\Phi}$ is a matrix with the eigenvectors of $\mathbf{A}$. Equation (2.47) can be derived by setting the initial time to zero in (2.48). The signals are then reconstructed by

$$\mathbf{x}(t) = \sum_{k=1}^{n} \phi_k \exp(\omega_k t) b_k = \mathbf{\Phi} \exp(\mathbf{\Omega} t)\mathbf{b} \tag{2.48}$$

with $\mathbf{\Omega}$ being a diagonal matrix with the continuous ω_k.

2.3.2.4 Participation Factor and Modal Analysis

The participation factor is a measure of how different state variables contribute to the modes in a system. In power systems this information is of vital importance to be able to target specific generators to be able to get the most efficient damping. From [7] the participation factor is defined as

$$\mathbf{p}_i = \begin{bmatrix} p_{1i} \\ p_{2i} \\ \vdots \\ p_{ni} \end{bmatrix} = \begin{bmatrix} \phi_{1i}\psi_{i1} \\ \phi_{2i}\psi_{i2} \\ \vdots \\ \phi_{ni}\psi_{in} \end{bmatrix} \tag{2.49}$$

with ϕ_{ki} and ψ_{ki} being the kth entry in the right and left eigenvectors,

$$\mathbf{\Phi}_i = \begin{bmatrix} \phi_{1i} \\ \phi_{2i} \\ \vdots \\ \phi_{ni} \end{bmatrix} \quad \mathbf{\Psi}_i = \begin{bmatrix} \psi_{1i} \\ \psi_{2i} \\ \vdots \\ \psi_{ni} \end{bmatrix}. \tag{2.50}$$

The modal analysis is done by looking at the DMD modes used for the recreation of the signal. If data stacking is used, a selection has to be made of the first rows still connected to the initial states. This is due to the data stacking changing the matrices dimensions.

The above method for calculating participation factor is of the simplest kind. There are other variants using more advanced methods. For more information about these the reader is referred to [24].

2.4 Real-Life Examples of Inter-Area Oscillations

Inter-area mode oscillations are oscillations caused by critical frequencies (also called modes) in the system created by groups of generators oscillating against another group of generators connected by weak ties. These modes are typically in the range 0.2-0.8 Hz and are mostly noticeable during small load and generator changes. Because of this they can be considered to be part of small signal stability problem [3], [7]. During other events such as faults and line disconnections these natural oscillation frequencies get enhanced and the oscillation can then sustain if not properly damped out.

Inter-area oscillations are complex phenomena and are affected by many things. They can be naturally initiated by disturbances occurring in the system but can also be started by different control actions. In [25] a thorough explanation is done connected to inter-area oscillations. By introducing mechanical torque steps for generators inter-area oscillations can be provoked, similarly different control actions resulting from disturbances can therefore affect how generators respond.

2.4.1 Nordic System

The Nordic system includes Norway, Sweden, Finland and the eastern part of Denmark. Analysis from the multiple PMUs in the system resulted in two critical inter-area modes being spotted. The first one of 0.29 Hz, created by the Finnish generators working in contrast to the rest of the system while the second mode of 0.55 Hz is created by generators in the north swinging against those in the south [4].

2.4.2 European System

A much larger system is the European system. It includes nearly all the European countries spanning from Portugal in the southwest to Turkey in the southeast and parts from northern Africa up to Denmark in the north [26]. Four different inter-area modes were found with frequencies of 0.2, 0.3 and two 0.5 Hz modes. The first mode was between the generators in southwest against the ones in northeast. The second mode involved the same generators in the southwest together with some in the northeast working against the ones in between. The last two concern generators in northeast and southeast, the later being more noticeable during power transfer from north to south [5].

2.4.3 Other Systems

Other systems worth mentioning are the six North American systems which with their large size similarly to the European system contain their own inter-area modes in different regions ranging from 0.16-0.73 Hz [27]. The largest system is the Western Interconnection system spanning over both Canada in the north and USA all the way to the border of Mexico. There have been many investigations of these systems and in particular the western system trying to understand the risk of inter-area oscillations since the blackout in 1996 [27].

2.4.4 Incidents Based on Inter-Area Oscillations

There have been several incidents throughout the last 30 years in all the above mentioned systems. Not all incidents are based on inter-area oscillations and the ones that are, are more common in the American systems than the rest [3], [27], [28]. Following are three examples of incidents based on the inter-area oscillations:

- August 10, 1996 Western Interconnection system disturbance: in a time span of 1:40 h, five different flashes to trees occurred resulting in areas of lower voltage levels being overloaded due to power distribution. The last flash started a fire and at this point the oscillations began and synchronised with the inter-area mode of 0.224 Hz. This began the procedure of generators trying to compensate for the oscillations and resulting in them being tripped alongside various connections between the four regions that the system was divided into. This event ended up in blackout of the system after 6:24 min after the last flash [29], [30].

- May 29, 2007 Danish Islanding: this incident occurred due to an unexpected current transformer explosion disconnecting two out of two 380 kV lines between Denmark main island and Germany. The two remaining lines of 220 kV tripped after 28 sec due to them being a weak connection and due to inter-area oscillations of 0.238 Hz and overload. In addition a HVDC line tripped after 58 s leaving Denmark on edge to blackout if not for the HVDC lines connected from Sweden and Norway. The system went back to normal operation after 5 min [3].

- August 4, 2000 Western Interconnection Inter-Area Natural Oscillations: smallest but not less important of these three occurred while one 500 kV and two 230 kV lines were tripped. This type of disconnection has been planned and studied, and while luckily it did not spread further it still caused a poorly damped oscillation identified as an inter-area mode of approximately 0.25 Hz. This event lasted for 60 s [27], [30].

2.5 The Nordic Power System Model

PowerFactory is a modern power system analysis software which can be used for a multiple of applications such as analysing generation, transmission, distribution and industrial systems [31]. It allows for advanced modelling with different control studies and has its own environment for implementing dynamic models called DSL.

2.5.1 The Nordic34 Model

Nordic32 is a fictitious representation of the Swedish and Nordic power system. It was made back in 1995 by Cigre Task Force 38.02.08 to illustrate the voltage collapse in Sweden in the year 1983 [32]. The system was intended for use when looking at transient stability and long term dynamics [33], the dynamic properties of the system and the model was similar at the time. The structure of the model is as follows:

- "North" with hydro generation and some load

- "Central" with much load and rather much thermal power generation

- "Southwest" with a few thermal units and some load

- "External" connected to the "North" consisting of a mixture of generation and load

It is a very simplified and standardised model. The number of nodes and generators are 32 & 20 respectively, together with some additional load and generator buses. The generators only use one excitation model with a few sets of data. The main system is designed for 400 kV but there are also regional systems of 220 and 130 kV. In short it is supposed to emulate the large hydro power transfer from the north down to a load area with thermal power.

This is no longer a good representation of the Swedish system. There are a few major factors behind this statement according to [32] and these are listed below:

- Important transmission lines are not modelled
- The model neglects connections to neighbouring countries (only Norway is included by the "External" part of Nordic32)
- The installed capacity no longer coincides
- The location of generation and load has changed

These discrepancies was the basis for [32] to try to update the original Nordic32 model to better represent the current Swedish transmission system. From here on out this model is called Nordic34 due to the two added nodes. This updated model with its base components was updated and used for the transient analysis in PowerFactory in this project.

Nordic34 takes into account the Swedish energy price bidding areas (SE1-SE4) which were introduced in 2011, due to the statistics being available independently for each area. The statistics used are from 2018 because it was the most resent data when the work was done. The factors taken into account when trying to update the model were:

- Installed capacity
- Power flow
- Production
- Export & import

Information connected to these points was the source for how the changes to the model would be implemented. The goal was to adapt the respective components in Nordic32 to match with the real power system with as few adjustments as possible. The changes done, taking into account the necessary simplifications as well as the complexity of the grid were:

- Adding new lines

  The transmission corridor Östersund-Gothenburg is missing in the original Nordic32. This was added in the form of a new node (4060) with four new transmission lines connected to it, two each going to node 4061 & 4031. In addition to this another node was added in the southern part (4064) to better represent the actual system.

- Amount and location of generators

  This was the most significant difference between the test system and the actual Swedish grid. The model was improved by increasing the production capacity to match with existing data and at the same time taking into account the location of the production units. Different generation types are lumped together resulting in only one Synchronous Generator (SG) on each bus. Changes were done to the existing generators rated power and a few additional generators were added and connected through step-up transformers. There are of course errors in the distribution of the production due to the actual spread of many smaller power plants but in large the mapping corresponds with the actual electrical power supply.

- Amount and location of loads

  A conclusion which was made was that the percentage of the total load for each area remained nearly constant during the year. The nodes in the model connected to the different areas was therefore assigned a percentage of the total area load. With the energy consumption varying this method allowed for a simple way of looking at different load scenarios based on the real data.

- Interconnection with neighbouring countries

  The transnational connections are modelled simply by having a generator and a load at the suitable locations to which the coupling points are located. The generators represent the import and loads the export of power. A SG representing a HVDC link to continental Europe is a poor representation and should be replaced if a more accurate behaviour is desirable. In addition to the already existing interconnection (External) seven more were added, connecting Norway, Denmark and Poland/Lithuania. The "External" link can represent the northern connection between Norway/Finland.

- Reinforcements

  When running simulations with the new load levels showed that multiple lines and transformers were overloaded. To compensate for this the affected components were reinforced. For the transmission lines a parallel system with the same characteristics were implemented while the ratings for the transformers were increased to the maximum apparent power seen during the year 2018.

- Reactive power supply

  To keep the nodes in the model within allowed voltage limits different reactive power supplies were added. Already included in the model were the SGs providing reactive power within their limits. These adjust themselves after the target voltage specified. In the cases when these units reached their limit, additional elements were installed in the form of Synchronous Condensers (SCs) & shunt elements. The choice between flexible SCs and static shunt elements was determined depending on if the voltage level varied or was constant. Due to SCs being a rare and expensive solution the goal was to add as few as possible of these. In this project, due to only one operation scenario being used with respect to production and load locations, the SCs were removed as they were not needed for voltage compensation.

The model was tested by comparing the real statistics from 2018 with the results from Quasi-Dynamic simulations based on the same data. The results showed good conformity except for the first three months of the year. The conclusions drawn for this was that the operation statistics were defective [32], especially in the SE1 area, being noticed by large errors in the power balance. The slack generator being located here therefore deviated substantially from the target value. Apart from that, with the implementations of voltage control, the voltage was kept between 0.9 and 1.05 p.u.

Overall Nordic34 seems to be a better representation than Nordic32. With the load and generator profiles being updated as well as the transmission line topology, it gives solid grounds for studies connected to future developments within the Swedish power system. To get valid and relevant study cases new data can be used in Quasi-Dynamic simulations and then taken to be used in RMS simulation for observing transients. A recommendation from [32] is to only take data from one source to avoid the problem of errors in the power balance. Some issues with the model are system losses not being correct, the slack generator leading to errors in the active power transfer, simplified modelling of generators not representing the reactive power compensation as well as the dynamic properties properly when compared to reality and reactive power elements only being represented by static elements and SCs.

2.5.2 The 2018 Scenario

The edited Nordic34 model is presented in Figure 2.12. Parts that are marked in black represent the original Nordic32 model apart from the wind turbines which were added for this project. In green are the added parts which together with black constructs the Nordic34 model. Generators are coloured to show if it is hydro based (blue) or thermal based (red) production.

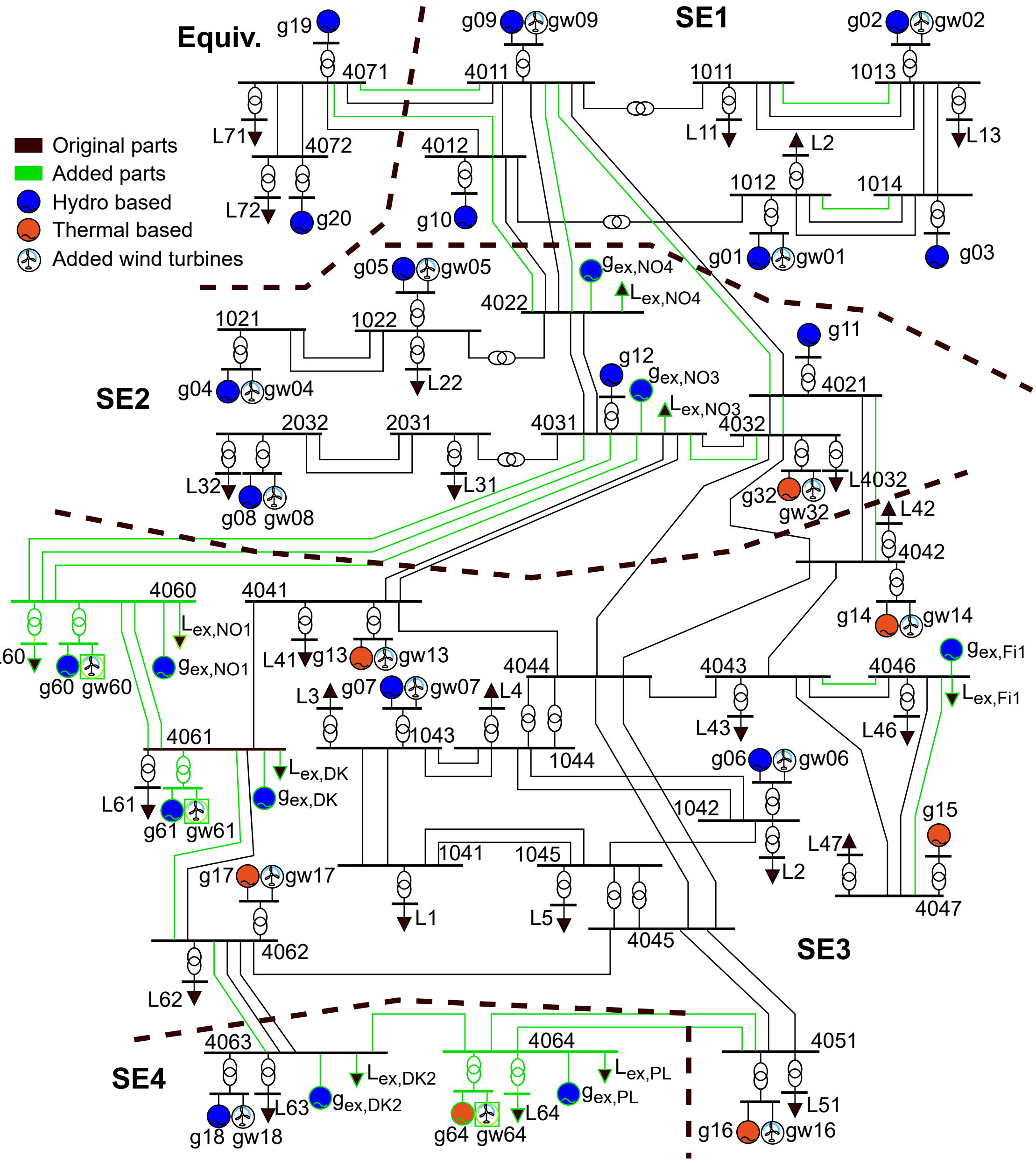

Figure 2.12: Nordic34 model.

Wind turbines were added to split the previously lumped generators to represent the production types individually. The reason behind this was to allow for a future scenario of year 2040 with the nuclear and fossil-fuel-based power plants replaced by wind [34]. The ratings were chosen according to the original calculations from [32] and are shown in

Table 2.2 with both the separated generator values and the split values.

Table 2.2: Apparent power of the generators, both the combined total and the separated values according to [32].

		Combined	Separated	
Generator Type	Generator Name	Total S [MVA]	Generator S [MVA]	Wind S [MVA]
Hydro/ Wind	g01/ gw01	1352	1088	265
Hydro/ Wind	g02/ gw02	1491	1280	212
Hydro	g03	916	916	0
Hydro/ Wind	g04/ gw04	844	424	420
Hydro/ Wind	g05/ gw05	900	424	476
Hydro/ Wind	g06/ gw06	270	109	161
Hydro/ Wind	g07/ gw07	205	136	69
Hydro/ Wind	g08/ gw08	1319	424	895
Hydro/ Wind	g09/ gw09	1590	1517	73
Hydro	g10	1074	1074	0
Hydro	g11	3952	3952	0
Hydro	g12	2799	2799	0
Thermal/ Wind	g13/ gw13	2984	2556	429
Thermal/ Wind	g14/ gw14	1391	1245	146
Thermal	g15	4247	4247	0
Thermal/ Wind	g16/ gw16	1695	1598	97
Thermal/ Wind	g17/ gw17	5188	5135	54
Hydro/ Wind	g18/ gw18	1566	294	1190
Hydro	g19	550	550	0
Hydro	g20	4500	4500	0
Thermal/ Wind	g32/ gw32	1731	1018	714
Hydro/ Wind	g60/ gw60	2123	1140	984
Hydro/ Wind	g61/ gw61	870	498	372
Thermal/ Wind	g64/ gw64	2859	2480	538
Hydro	g_{ex}-type	7x2500	7x2500	0
Total	-	66,628	57,354	7,095

The model was adjusted for the purpose of dynamic analysis by extracting one set of production and load values from a time with high load during a day. The chosen scenario from the yearly data was from 12^{th} of September at 10 a.m. The reason for choosing this date was due to potential maintenance taking place at this time of the year. These values were then distributed according to Table 2.3.

Table 2.3: Data for generators and loads for the chosen scenario of 12^{th} of Sep 2018.

Generator Type	Generator Name	Active power P [MW]	Wind P [MW]	Load Name	Active power P [MW]
Hydro/ Wind	g01/ gw01	693.6	136	L1	263.4
Hydro/ Wind	g02/ gw02	648.5	93	L2	175.6
Hydro	g03	575.5	0	L3	136.6
Hydro/ Wind	g04/ gw04	370.8	185	L4	243.9
Hydro/ Wind	g05/ gw05	391.9	208	L5	585.3
Hydro/ Wind	g06/ gw06	138.5	83	L11	343.7
Hydro/ Wind	g07/ gw07	75.0	26	L12	516.0
Hydro/ Wind	g08/ gw08	550.2	374	L13	171.3
Hydro/ Wind	g09/ gw09	956.0	44	L22	409.1
Hydro	g10	674.4	0	L31	76.4
Hydro	g11	1755.4	0	L32	97.4
Hydro	g12	1402.6	0	L4032	1327.1
Thermal/ Wind	g13/ gw13	575.2	83	L41	493.6
Thermal/ Wind	g14/ gw14	228.3	24	L42	463.4
Thermal	g15	2271.9	0	L43	323.9
Thermal/ Wind	g16/ gw16	922.9	53	L46	864.3
Thermal/ Wind	g17/ gw17	2125.1	23	L47	1543.2
Hydro/ Wind	g18/ gw18	795.8	639	L51	169.7
Hydro	g19	300.0	0	L60	2932.4
Hydro	g20 (slack bus)	624.7	0	L61	771.6
Thermal/ Wind	g32/ gw32	779.1	322	L62	787.2
Hydro/ Wind	g60/ gw60	931.8	432	L63	1878.7
Hydro/ Wind	g61/ gw61	363.7	156	L64	925.3
Thermal/ Wind	g64/ gw64	402.2	72	L71	300.0
-	-	-	-	L72	2000.0
Hydro	$g_{ex,DK}$	0.0	-	$L_{ex,DK}$	0.0
Hydro	$g_{ex,DK2}$	0.0	-	$L_{ex,DK2}$	392.5
Hydro	$g_{ex,FI1}$	0.0	-	$L_{ex,Fi1}$	1200.0
Hydro	$g_{ex,NO1}$	895.0	-	$L_{ex,NO1}$	0.0
Hydro	$g_{ex,NO3}$	391.9	-	$L_{ex,NO3}$	0.0
Hydro	$g_{ex,NO4}$	150.0	-	$L_{ex,NO4}$	0.0
Hydro	$g_{ex,PL}$	0.0	-	$L_{ex,PL}$	600.0
Total	-	19,989	2,953	-	19,992

Additional changes had to be made to correct for imbalances during load flow analysis. Correcting transformer tap-changers, deactivating shunts not needed simplified the system and corrected for the errors. Apart from the generator ratings being changed the correct models and parameters were set to match their production type of hydro turbine or steam turbine. The values are presented in Table 2.4.

Table 2.4: Generator parameters.

	X_d	X_q	X'_d	X'_q	X''_d	X''_q	T'_{d0}	T'_{q0}	T''_{d0}	T''_{q0}	X_l	R_a	H
Hydro	1.1	0.7	0.25	0.3	0.2	0.2	5	0	0.05	0.1	0.15	0	3
Thermal	2.2	2	0.3	0.4	0.2	0.2	7	1.5	0.05	0.05	0.15	0	6

The DSL models for the generators were slightly modified and are described in Appendix B. A model for the new wind turbines was also created with PowerFactory's library models according to the wind turbine type 4A, which has the ability to output reactive power for voltage control. The same model was used for each turbine.

2.5.3 Assumptions of the Fully-Renewable Scenario

Lastly what was of interest for this project was to see how the inter-area frequencies would change in the future with more RES in the grid. The year 2040 was used as comparison mainly because the nuclear power plants have reached their lifespan by then and are to be decommissioned and Sweden is to have fully renewable energy production [34]. Additionally [34] estimated that the hydro and thermal based plants will not have a major change while the installed capacity and generation of the wind turbines will increase by 314 and 400 % respectively. The load is also assumed to be increased between 15-26 % [35].

The changes made were the deactivation of generators g15/g16/g17 being the nuclear power plants. Considering all energy production is to be renewable lead to generators g13/g14/g64 also being deactivated due to them being thermal based. To compensate for the removed power production, wind turbines were increased or added with the removed amount at respective bus. No load or other changes were made in the system. This could simulate a scenario where the existing connecting points in the infrastructure could be used together with the new energy sources. However, the impact on the relocation of the generators will not be analysed here. Neither will be the load increase simulated in this scenario.

3

Implementation of Power Oscillation Damping

This chapter is a thorough workflow of what steps were taken during this thesis. The means of how DMD was used together with PowerFactory for choosing which generators to control is presented. The gain and phase tuning of these generators, both for local and wide-area damping signals are then presented. Figure 3.1 illustrates the overall scheme for how the generator terminal voltage was affected through feeding a constructed control signal to the AVR summation point.

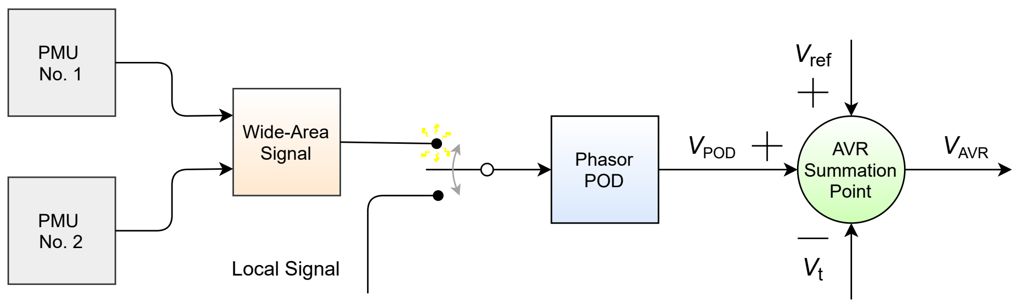

Figure 3.1: Illustration of the overall structure from measured signals to the control signal being fed to the AVR summation point.

3.1 DMD-based Modal Analysis with Phasor Measurements

The DMD algorithm was implemented in Matlab according to the theory in Section 2.3.2 and tested with a test signal. The following signal was constructed to include multiple frequencies of 1, 2 and 5 Hz and damping coefficients 0.13, 0.3 and 0.08.

$$x = \sin(t) \cdot \mathrm{e}^{-0.13t} + \sin(2t) \cdot \mathrm{e}^{-0.03t} + \sin(5t) \cdot \mathrm{e}^{-0.08t}$$

Using 25 s of data with sampling time of 10 ms, with data-stacking of 200 and a truncation rank of 20, DMD gives the same values connected to the above signal and was able to recreate the signal. Figure 3.2 shows the signal together with the recreation.

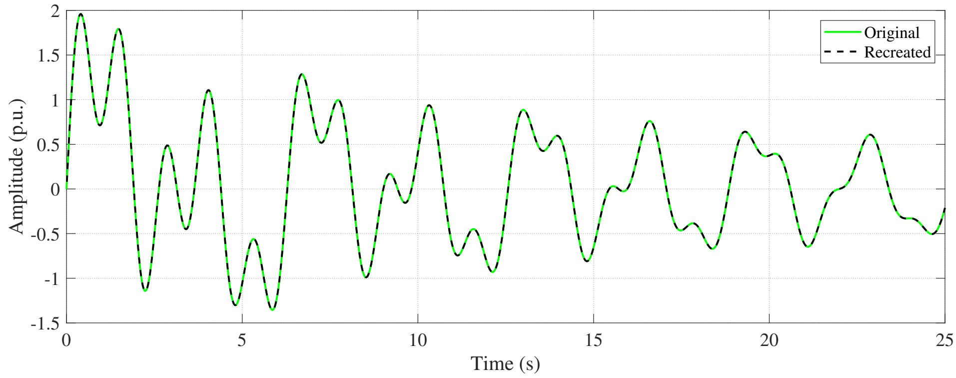

Figure 3.2: Recreation of the test signal with DMD.

The next step was to extract the the oscillation modes from the measured electrical quantities with the help of DMD. This was done by extracting phasor data from each generator bus as if a PMU was there. A 3-phase short-circuit on the line between bus 4032 and 4044 was used to trigger the system dynamics. A time window between 13-18 s was used for the analysis to get a better approximation of the inter-area behaviour as the initial system response from the disturbance was gone.

Figure 3.3 show the right eigenvectors from the electrical or electromechanical quantities of the major participating generators when using the analytical eigenvalue analysis in PowerFactory and the data-based DMD algorithm. The most important observation is that arrows pointing in opposite directions signifying that generators are swinging against each other for this inter-area oscillation. The largest swing being between generators g20 and g17/g64. Arrows pointing in the same direction indicate coherent generators swinging together. The phase shift between the two calculating methods is connected to DMD being affected by the current phase of the signals and the amplitude depends on the calculation method. The orientation also changes with changed truncation for DMD due to this affecting the calculation of the state matrix $\mathbf{A}$ but the relation between the different generators remain the same.

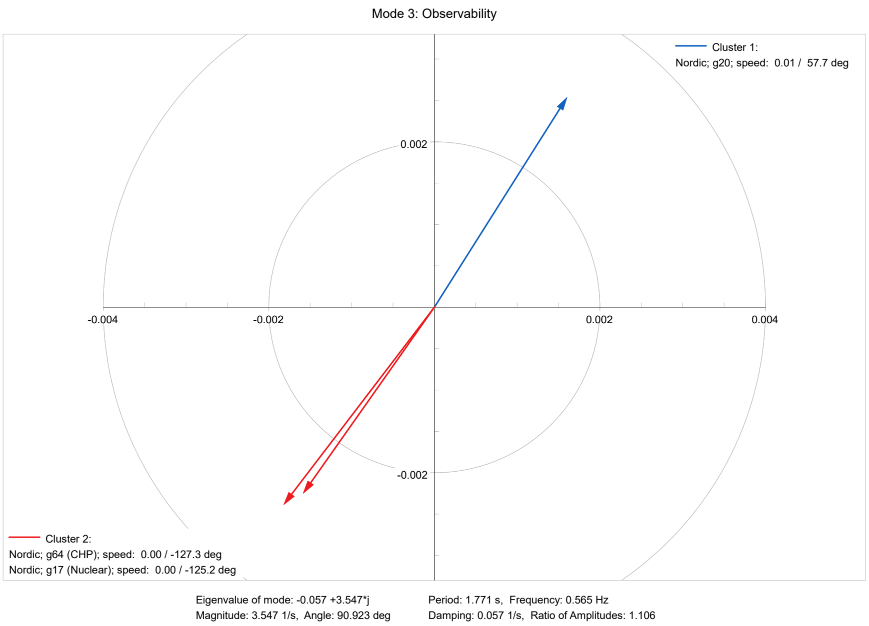

(a) PowerFactory.

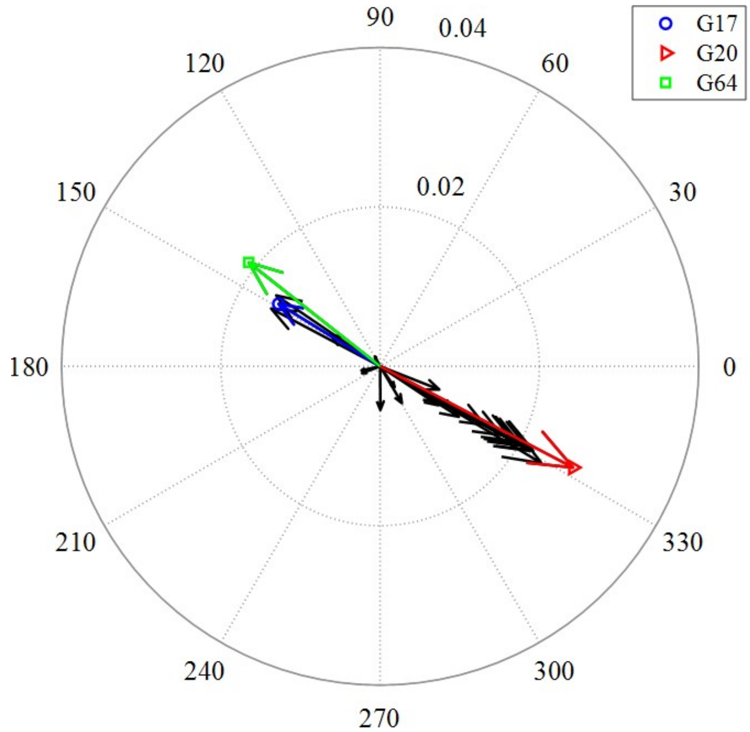

(b) DMD.

Figure 3.3: Right eigenvectors from the two methods for the mode f=0.565 Hz

The participation factor from PowerFactory is shown in Figure 3.4. Generator g20 is the largest contributor in creation of the frequency f=0.565 Hz, with g17 and g64 next. It is unclear how to calculate the participation factor using the DMD algorithm and this will not be investigated further in this work. The modal analysis in PowerFactory was used when deciding which generators to use for the implementation of damping.

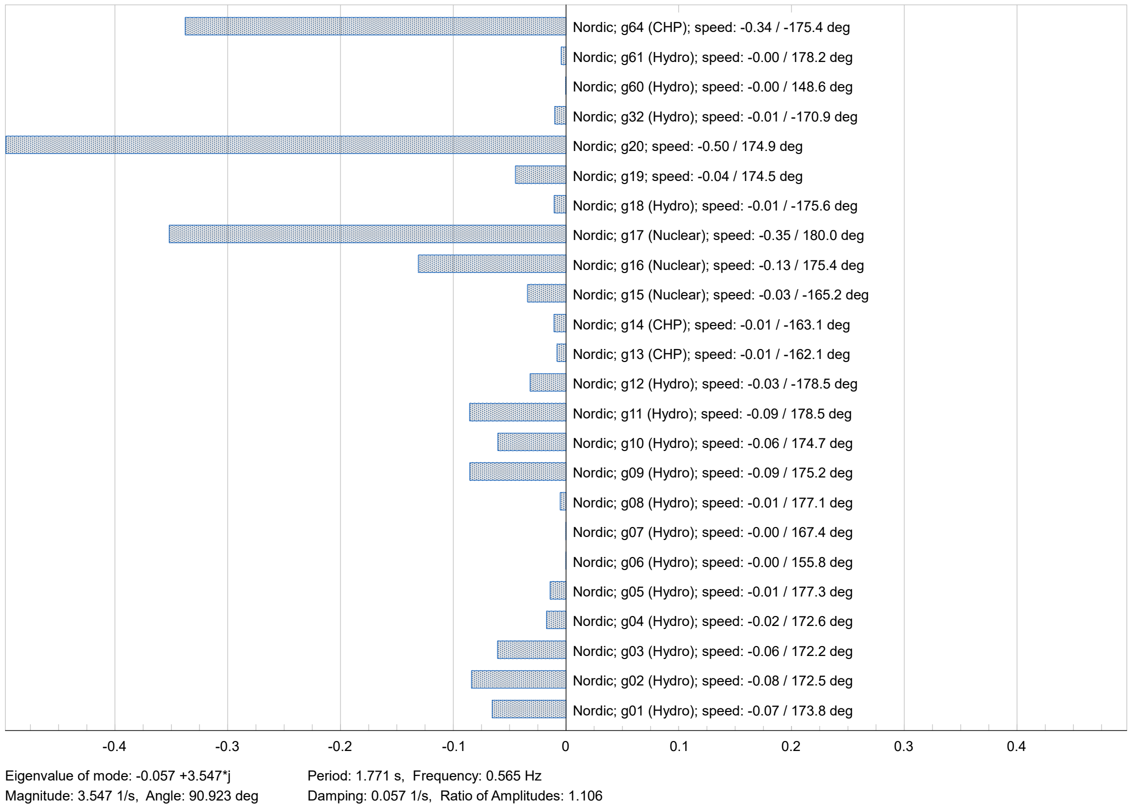

Figure 3.4: Participation factor calculated using PowerFactory.

Two sets of data of P_{sum} over 100 s with a sample time of 10 ms were extracted, where P_{sum} is the power flow between SE2 and SE3. One set with the fault cleared without line tripping and the other with the fault cleared with line tripping. Both were analysed with the DMD algorithm in Matlab. The data window was set to 30-50 s to exclude the transient and data-stacking was used with 200 stacks and a truncation of rank 20. The resulting values of frequency and damping ratio were compared to PowerFactory's own modal analysis and are summarized in Table 3.1. It shows that the resonant frequency in the range between $0.1<f<2$ Hz with a damping ratio of $\zeta<5$ %. As can be seen the values are similar between the methods. P_{sum} was used to extract the oscillation frequency for the tuning of the phasor POD due to it containing the same information as the individual PMU equivalent signals and it was easier to analyse one signal than many as was done before.

Table 3.1: Frequency and damping ratio comparison between the DMD algorithm and PowerFactory's modal analysis.

DMD		PowerFactory	
Fault cleared without line tripping		Fault cleared without line tripping	
Frequency [Hz]	Damping ratio [%]	Frequency [Hz]	Damping ratio [%]
0.564	1.645	0.565	1.610
Fault cleared with line tripping		Fault cleared with line tripping	
Frequency [Hz]	Damping ratio [%]	Frequency [Hz]	Damping ratio [%]
0.550	0.814	0.553	0.772

In the case of the fully-renewable scenario, the same fault was applied and P_{sum} analysed in the same way as previously mentioned. The participation analysis for this scenario resulted in generator g20 being the most dominant contributor followed by generator $g_{\text{ex,PL}}$. Several scenarios were simulated to analyse the behaviour, these were

- Naturally damped, to use as reference
- Reactive and voltage control with wind turbines, due to increased wind production
- Local and PMU control, using g20 being still the dominant contributor to the mode
- Local and PMU control, using g20 with re-tuned POD parameters.

The re-tuning included the same frequency sweep like before. With the new frequency of f=0.692 Hz resulted in a new phase angle of 147°. The phase reference for g20 was changed to the measurement point connected to g64 as tested in Figure 4.11 due to $g_{\text{ex,PL}}$ being the second dominant participant in the inter-area oscillation (see Figure 2.12). Table 3.2 shows the frequencies and damping ratios for the new grid set up when calculated with DMD and PowerFactory.

Table 3.2: Frequency and damping ratio comparison between the DMD algorithm and PowerFactory's modal analysis for fully-renewable scenario.

DMD		PowerFactory	
Fault cleared without line tripping		Fault cleared without line tripping	
Frequency [Hz]	Damping ratio [%]	Frequency [Hz]	Damping ratio [%]
0.691	0.997	0.692	0.741
Fault cleared with line tripping		Fault cleared with line tripping	
Frequency [Hz]	Damping ratio [%]	Frequency [Hz]	Damping ratio [%]
0.671	0.403	0.676	0.175

3.2 Extracting Oscillating Component of a Signal

This section presents methods of extracting oscillatory components from a signal. Both the traditional method of using a washout filter and the method used in this thesis being a phasor extraction algorithm is illustrated.

3.2.1 Washout Filter

Traditionally the classical PSS/POD structure has been used to generate the correct control signal for different applications. The traditional approach has two disadvantages, firstly the washout filter must be well below the oscillation frequency which results in the unwanted average component of the input signal affecting the control signal [36]. Secondly this approach can lead to high output signals for large power swings, it is therefore necessary to limit the signal so the controlled equipment remains within their dynamical range. This has proven to be difficult while at the same time maintaining the correct phase shift [36]. Figure 3.5 shows the bode diagrams of several different washout filters with time constants in the range frequently used.

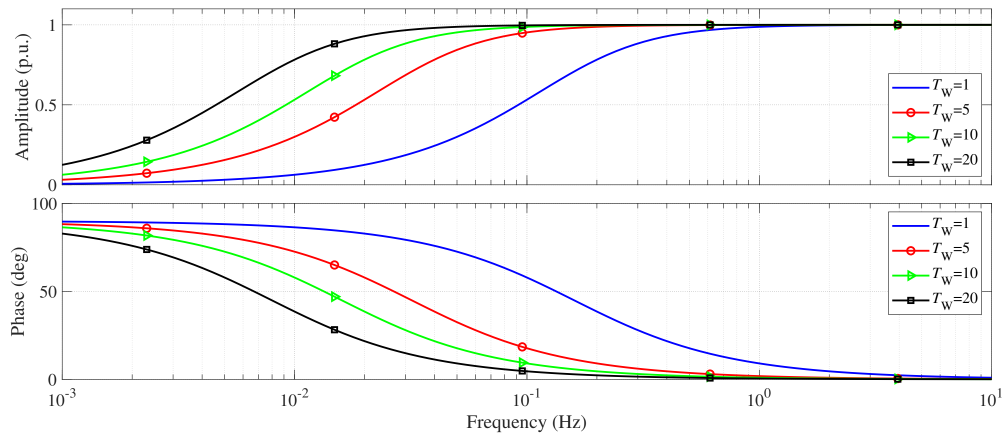

Figure 3.5: Traditional bode plot for washout filter with different time constants.

As can be seen a rather high time constant is necessary to achieve the gain and phase characteristics for the frequencies above 0.1 Hz.

3.2.2 Low-Pass Filter Based Approach

An alternative method for control presented by [36] is a phasor extraction algorithm which uses a specific frequency to extract the oscillatory component with this frequency from a signal. This signal can then be used together with a desired phase shift to control different power system devices.

The phasor extraction algorithm can be described mathematically as follows. The input signal is represented as,

$$p(t) = P_0(t) + P_{\text{osc}}(t) \tag{3.1}$$

with an average component $P_0(t)$ and an oscillatory component $P_{osc}(t)$ which can be written as

$$P_{\text{osc}}(t) = \text{Real}[\underline{P}_{\text{ph}}(t)e^{\text{j}\theta_{\text{osc}}(t)}] = \frac{1}{2}\underline{P}_{\text{ph}}(t)e^{\text{j}\theta_{\text{osc}}(t)} + \frac{1}{2}\underline{P}^*_{\text{ph}}(t)e^{-\text{j}\theta_{\text{osc}}(t)} \tag{3.2}$$

which takes the real part of the complex oscillatory component $e^{\text{j}\theta_{\text{osc}}}$ together with the phasor component $\underline{P}_{\text{ph}} = P_{\text{ph}}e^{\text{j}\varphi}$. The oscillating frequency $\theta_{osc}(t) = \omega_{osc}t$ needs to be known with this approach to get a good estimation. The estimated average component of the signal is lowpass filtered,

$$\tilde{P}_0(t) = H_0\{p(t) - \tilde{P}_{\text{osc}}(t)\} \tag{3.3}$$

with the input being subtracted by the estimated oscillatory component $\tilde{P}_{\text{osc}}(t)$ to further improve the estimation. Rearranging (3.1) gives

$$\underline{P}_{\text{ph}}(t) = H_{\text{ph}}\{[2p(t) - 2P_0(t) - \underline{P}^*_{\text{ph}}(t)e^{-\mathrm{j}\theta_{osc}(t)}]e^{-\mathrm{j}\theta_{osc}(t)}\}. \tag{3.4}$$

Substituting (3.3) into (3.4) provides the estimated value of $\underline{P}_{\text{ph}}(t)$ as

$$\tilde{\underline{P}}_{\text{ph}}(t) = H_{\text{ph}}\{[2p(t) - 2\tilde{P}_0(t) - \tilde{\underline{P}}^*_{\text{ph}}(t)e^{-\mathrm{j}\theta_{osc}(t)}]e^{-\mathrm{j}\theta_{osc}(t)}\}. \tag{3.5}$$

Finally, substitution of (3.1) into (3.5) gives

$$\begin{aligned}\tilde{\underline{P}}_{\text{ph}}(t) = H_{\text{ph}}\{[2P_0(t) - 2\tilde{P}_0(t) + \underline{P}^*_{\text{ph}}(t)e^{-\mathrm{j}\theta_{\text{osc}}(t)} - \tilde{\underline{P}}^*_{\text{ph}}(t)e^{-\mathrm{j}\theta_{\text{osc}}(t)} \\ + \underline{P}_{\text{ph}}(t)e^{\mathrm{j}\theta_{\text{osc}}(t)}]e^{-\mathrm{j}\theta_{\text{osc}}(t)}\}.\end{aligned} \tag{3.6}$$

As can be seen the signal being lowpass filtered is now ideally a constant value leading to the extracted oscillatory component having no phase shift compared to the input. Taking the real part of the output then results in $\tilde{P}_{\text{osc}}(t)$ being estimated as

$$\tilde{P}_{\text{osc}}(t) = \frac{1}{2}\tilde{\underline{P}}_{\text{ph}}(t)e^{\mathrm{j}\theta_{\text{osc}}(t)} + \frac{1}{2}\tilde{\underline{P}}^*_{\text{ph}}(t)e^{-\mathrm{j}\theta_{\text{osc}}(t)}. \tag{3.7}$$

Figure 3.6 illustrates the implementation.

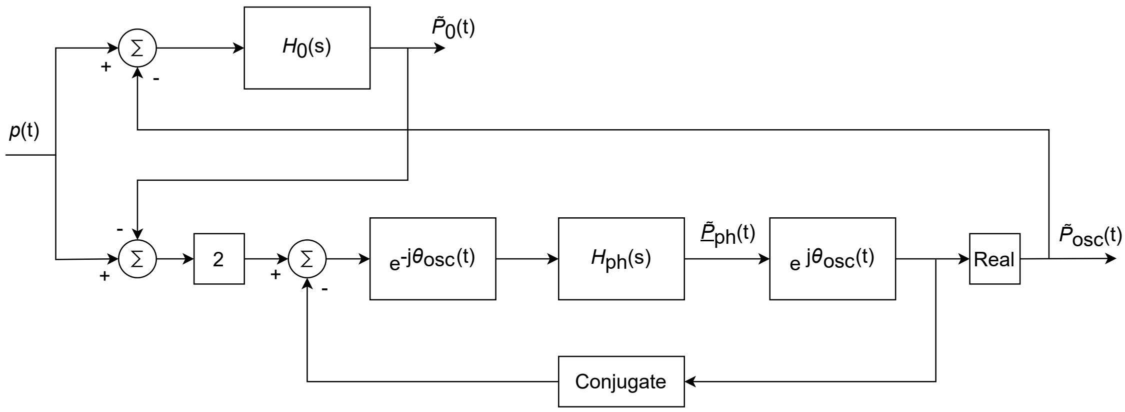

Figure 3.6: Block diagram of the phasor extraction algorithm.

The lowpass filters used can be expressed on the form

$$H_0(s) = H_{\text{ph}}(s) = \frac{\alpha_{\text{LPF}}}{\mathrm{s} + \alpha_{\text{LPF}}}. \tag{3.8}$$

For the extraction to work the cut-off frequency of the filters should be set smaller than the chosen oscillation frequency. A higher value increases the speed but reduces the frequency selectivity. A typical value is between 0.2-0.5 of ω_{osc} [36], but as [37] illustrates, the behaviour of varying the cut-off frequency and a value above 0.4 of ω_{osc} leads to worse performance. Figure 3.7 illustrates the difference between the washout filter and the phasor POD when a time constant T_W=10 s/rad and a cut-off frequency k=0.3 of ω_{osc} is used. The average component resulting from the washout filter is easily observed.

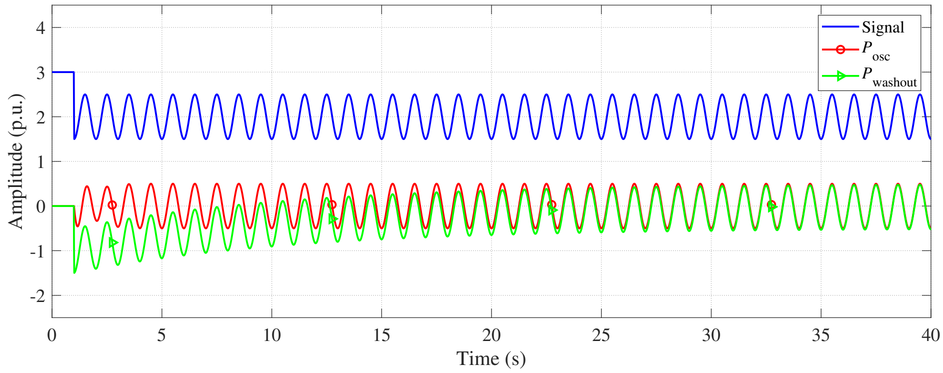

Figure 3.7: Comparison between washout filter and phasor POD for extracting oscillation.

Figure 3.8 shows the bode diagrams for the phasor extraction algorithm with different cut-off frequencies at a selected frequency of 1 Hz. The clear downside of the method is observable in the phase characteristics, i.e. a drastic phase shift occurs if the frequency deviates from the targeted one [38].

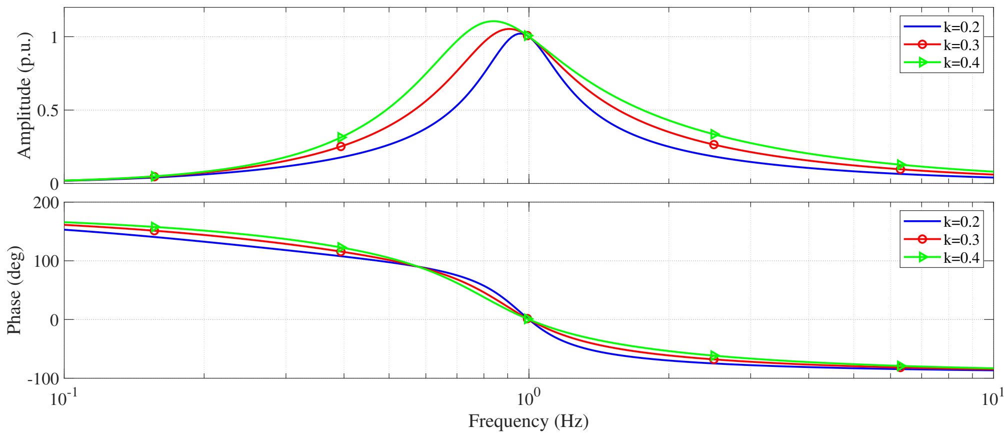

Figure 3.8: Bode plot for the POD transfer function with different cut-off frequencies.

Figure 3.9 shows how the extracted oscillation is affected by wrongly tuned parameters. The signal has a frequency of 0.5 Hz but ω_{osc} is estimated from a frequency f_{osc} that deviates ±0.2 Hz and a k=0.3.

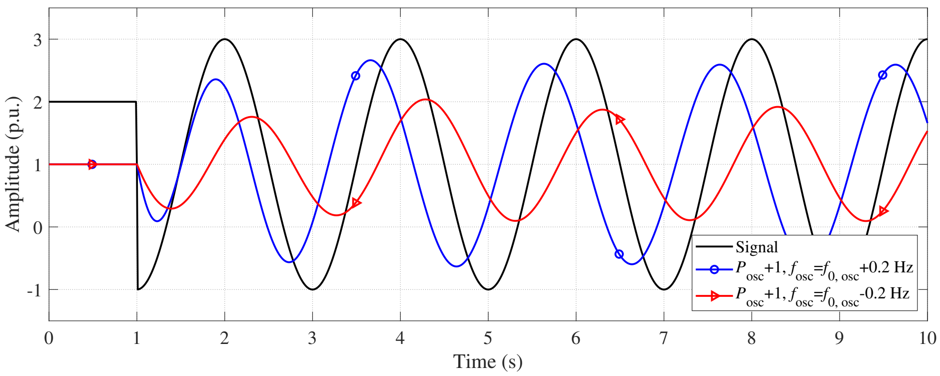

Figure 3.9: Tests of the POD when the signal frequency deviates from the targeted.

Figure 3.10 illustrates how the POD captures the oscillatory component with different cut-off frequencies. A selection has to be done between fast response time and better phase characteristics against worse selectivity of frequencies. To better show the signals matching, an offset was added to the extracted signal.

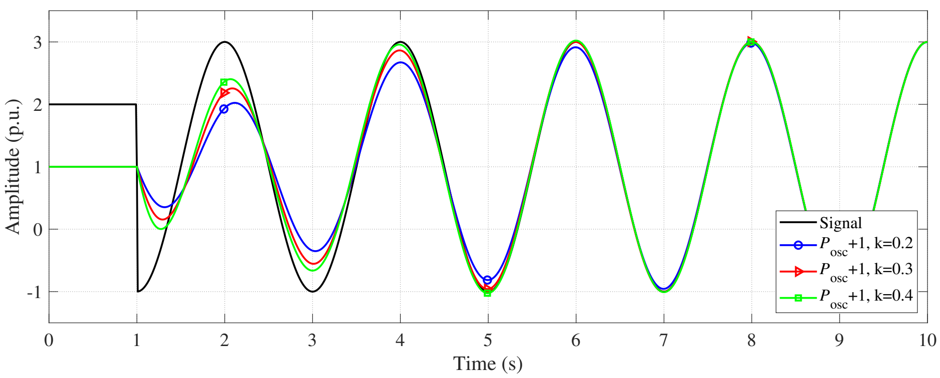

Figure 3.10: Tests of the POD with different cut-off frequencies.

To design a phasor POD, a suitable phase compensation needs to be added to compensate for the delay caused by the exciter and the field winding time constant of the generator. Figure 3.11 shows how the input signal is constructed into a control signal by first adding a phase shift and then also a gain.

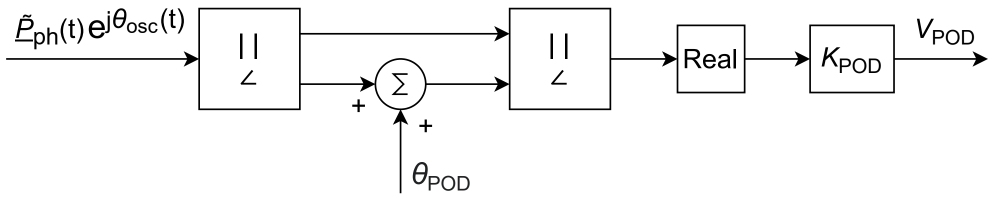

Figure 3.11: Block diagram of phase shift for the phasor POD.

When controlling the terminal voltage of a generator, it is important to limit the output signal to not compromise the secure operation of the generator [39]. A design criteria for traditional PSS is therefore to limit the output to between 5 % and 10 % of the generator terminal voltage.

The POD was firstly constructed and tested in Simulink together with a constructed test signal. The test signal had a frequency of 0.5 Hz and a DC offset of 1 as in Figure 3.10. By starting in steady state and then introducing a transient the behaviour of the POD could be observed. With the method working in Simulink it was then built up in PowerFactory as a DSL model which is shown in Appendix B.3. Figure 3.12 shows the working POD with the cut-off frequency set to k=0.3 and the control signal having a phase shift of 180°. The response was identical in both Simulink and PowerFactory and this value for the cut-off frequency was used for the rest of the project.

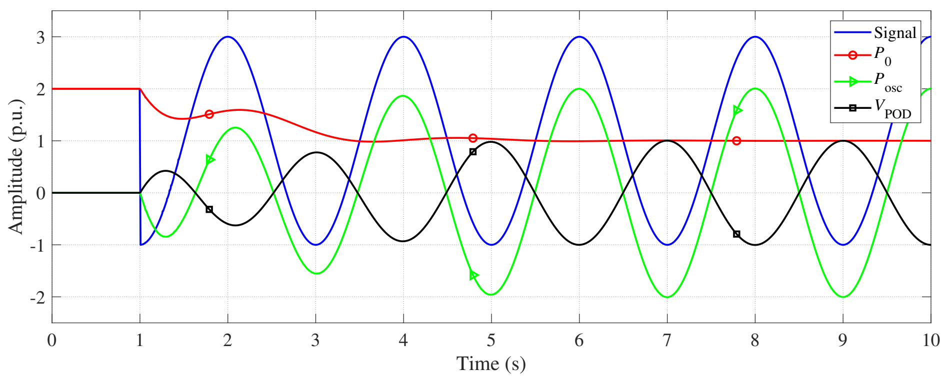

Figure 3.12: Test of the POD in PowerFactory with a test signal.

PowerFactory does not work with complex numbers as Simulink. The real and imaginary parts were therefore separated and processed individually in the DSL model seen in Appendix B.3.

3.3 Evaluation of Phase Angle Compensation

To be able to inject the correct phase to the control signal in the phasor POD the inner dynamics of the synchronous generators had to be modelled. There are multiple parameters affecting the phase delay as explained in Section 2.1.2, the derivation of these are explained here. The different rotor types have different exciter system parameters also contributing to the difference between the categories. These parameters are displayed in Table 2.4.

3.3.1 Analytical Evaluation Based on Linearised System

All the generators in PowerFactory have a specified saturation curve assigned to them. For this thesis an exponential curve was used so an exponential fit was done according to (2.13) with the procedure explained in Section 2.1.3. Figure 3.13 illustrates the chosen points together with the saturation curve.

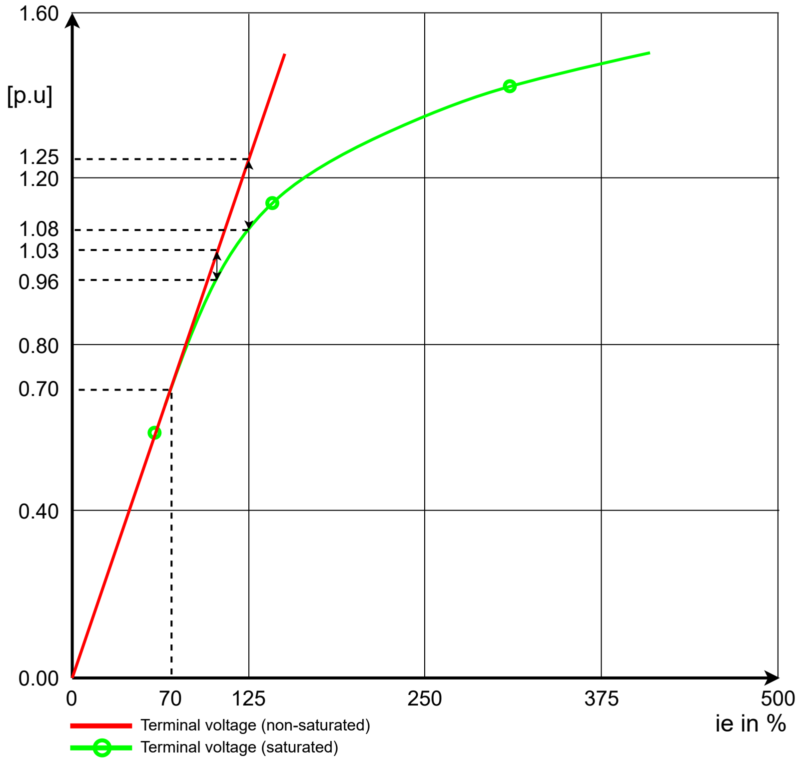

Figure 3.13: PowerFactory saturation curve together with data used for modelling saturation.

The approximated A and B are

$$\Psi_{\mathrm{at1}} = 0.96, \Psi_{\mathrm{I1}} = 1.03 - 0.96 = 0.07$$

$$\Psi_{\mathrm{at2}} = 1.08, \Psi_{\mathrm{I2}} = 1.25 - 1.08 = 0.17$$

$$k = \frac{0.07}{0.17} = \frac{A \cdot e^{0.96-0.7}}{A \cdot e^{1.08-0.7}} = e^{B(0.96-1.08)} = e^{B(-0.12)}$$

$$B = \frac{\ln(k)}{-0.12} = 7.4$$

$$A = 0.07 \cdot e^{-B \cdot 0.26} = 0.01.$$

The steady state excitation currents for the base operation scenario with the current for the different generators varied according to Table 3.3, fitting these in Figure 3.13 and using (A.3) results in the saturation coefficient being close to 0.9. A value of 0.9 p.u. was therefore chosen for the rest of the modelling.

The phase and magnitude characteristics of the generators are dependant on the equivalent grid impedance that the generators see. To get the impedance, short circuit calculations were made at the bus between the generator and the transformers as described in Section 2.1. The Thevenin equivalent impedance was then transformed to p.u. with the generators respective ratings.

The rest of the relevant generator quantities were taken by looking at the steady state load flow of the base scenario. Table 3.3 shows all the resulting values and Figure 3.14 shows the phase characteristics for the three major contributors to the inter-area oscillation.

Table 3.3: Parameters for all the generators.

Generator	V_t	I_t	i_e	$\cos(\phi)$	R_E	X_E	K_{sd}
g17	1	0.41	1.4	1	0.03	0.50	0.9
g20	1	0.26	1.16	1	0.09	1.08	0.9
g64	1	0.13	1.14	1	0.01	0.21	0.9

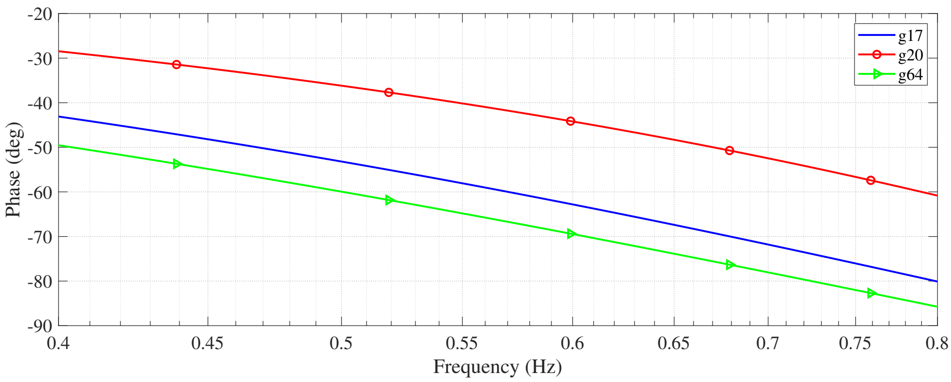

Figure 3.14: Phase characteristics comparison between the different generators from modelling.

3.3.2 Numerical Approach

Compared to the purely theoretical modelling seen in Figure 3.14, a more practical approach was used for comparison. By sending a small reference signal, the open loop response from V_{ref} to ΔV_t seen in Figure 2.10 was obtained. A sinusoidal wave with frequencies varying between 0.4-0.8 Hz and a gain of 0.001 was used as reference input, the phase shift was noted and the result can be seen in Figure 3.15. The results correspond rather well except for the frequencies around 0.565 Hz which happen to be the inter-area frequency in the system. The sharp phase shift is a result of resonance. Even though the resonance introduces a different phase for the compensation, the curves in Figure 3.15 were used for the tuning of the phasor POD as they were directly connected to the system analysed. Connected to the theory in Section 2.1.4 this would result in an undercompensation anyway desirable.

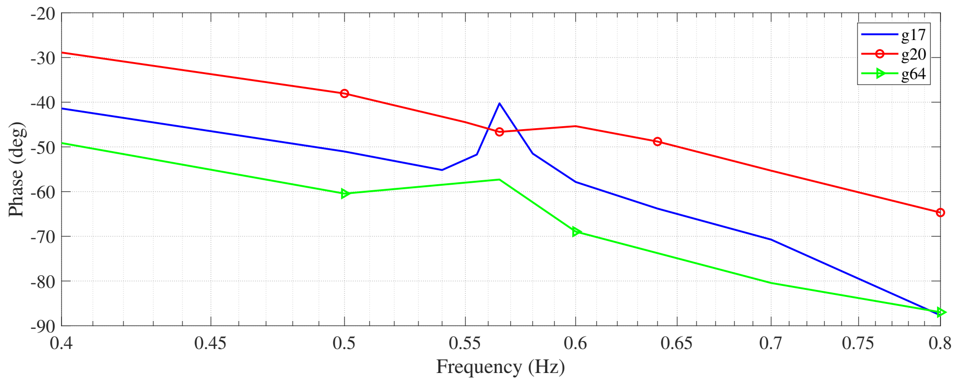

Figure 3.15: Phase characteristics for generators g17, g20 and g64.

The phase characteristics of the participating generators in Figure 3.15 together with the consideration that power is lagging the rotor speed by 90° (according to the swing equation (2.8)) resulted in the phase angles seen in Table 3.4. These angles were used as the inputs illustrated in Figure 3.11 for the first comparisons without tuning.

Table 3.4: Phase lag at frequency f=0.565 Hz for each generator.

Generator	g17	g20	g64
Phase lag from freq. sweep	40	47	57
Phase lag including 90°	130	137	147

3.4 Gain Tuning of Phasor POD

Two methods of damping were compared connected to traditional and Wide-Area Control System (WACS). Method number one was to use the local electric power P_{pgt} from a generator being feed directly into the phasor POD as seen in Figure B.1. The second method being WACS, was to instead use a scaled power signal as input which could be calculated from real PMUs. The signal was calculated according to

$$P = K_{\mathrm{POD}} \cdot \sin(\Phi_1 - \Phi_2) \tag{3.9}$$

where K_{POD} is the scaling factor being the gain and Φ_1 and Φ_2 are bus angles at the PMU locations. Comparing this signal with (2.7) the signal being scaled can be seen in how the first variables in the power transfer equation are set to the gain. A consequence of this relation is that the signal is directly connected to a scaled active power flow between the areas where the measurements are taken from. The equations in the DSL model is shown in Figure B.5.

The participation factor given by PowerFactory's modal analysis seen in Figure 3.4 pointed out generator g20 and g17 as the two largest contributors to the dominant mode of 0.565 Hz. The control signal to these two generators was therefore created by using the measurements of Φ_1 and Φ_2 at these locations. A generator reference was used meaning Φ_1 was taken from the own generator location while Φ_2 was taken from the others location. This was set in the respective generator frame seen in Figure B.1. Generator g64 used its own measurement point as Φ_1 and g20s as Φ_2.

The wind turbine ratings at these three locations are much smaller compared to the size of the synchronous generators. Thus, the wind turbines have little impact on the electromechanical oscillation of the system. No visible change in P_{sum} could be observed and the wind turbine dynamic models were therefore deactivated for the analysis of the base scenario.

The gain K_{POD} had to be tuned for each generator connected to the different cases. A damping ratio of 5 % was used as a reference for setting the gain according to Transmission System Operators (TSOs) having this as a minimum for system operation [40]. The procedure followed was to activate the local power signal for one generator at a time and increase the gain while observing how the damping ratios changed using modal analysis tool in PowerFactory. When the desired damping was reached the corresponding gain was taken. For each generator under evaluation, the gain is increased until the damping ratio of the dominant mode can no longer be increased or that of the other modes is reduced. Table 3.5 shows the corresponding values.

3.4.1 Local Signal Based

The phases used for the gain tuning were the values in Table 3.4. No additional over or undercompensation was used. When doing additional testing with different phases it showed an overcompensation was beneficial. In [41] similar behaviour was observed but overcompensating is not desirable as described in Section 2.1.4.

Table 3.5: Damping ratios ζ [%] during local gain adjustment for each generator.

	Frequency [Hz]	K_{POD}=0	K_{POD}=1	K_{POD}=2	K_{POD}=3
g17	0.565	1.601	2.602	2.910	2.927
	0.648	4.977	5.810	6.139	6.231
	1.087	5.138	5.134	5.131	5.129
	Frequency [Hz]	K_{POD}=0	K_{POD}=1	K_{POD}=2	K_{POD}=2.5
g20	0.565	1.601	3.140	4.696	5.478
	0.648	4.977	5.520	6.086	6.381
	1.087	5.138	5.214	5.479	5.610
	Frequency [Hz]	K_{POD}=0	K_{POD}=2	K_{POD}=4	K_{POD}=5
g64	0.565	1.601	3.098	3.651	3.769
	0.648	4.977	5.069	5.127	5.148
	1.087	5.138	5.138	5.140	5.142

The final gains used were K_{POD}=2 for generator g17 due to the damping ratio having minimal changes with a higher value for the frequency f=0.565 Hz. The value K_{POD}=2.5 was used for generator g20 due to the same frequency reaching the targeted value of 5 %.

The gain for generator g64 was set to K_{POD}=4 because a higher value had low affect on the frequency f=0.565 Hz as well as the control signal being cut by the limit of 10 % seen in Figure 3.16.

3.4.2 Wide-Area Signal Based

The gain adjustment for the WACS measurement damping (PMU damping) was made by comparing the local and PMU amplitudes of the control signals V_{POD} when they were disconnected from the AVR. A ratio of the amplitude difference between the signals at the time 30 s was taken to set the PMU gain to match the local signal. At 30 s the inter-area oscillation was observable in both of the signals without any other disturbing frequency content and the matching was therefore made at this time. The resulting gains for the PMU signals are shown in Table 3.6 together with the damping ratios. After the initial transient both control methods produce the same control signal which is good for comparing the two. The damping ratio decreases for both g17 and g20 while it is increased for g20 for the frequency f=0.565 Hz.

Table 3.6: Damping ratios ζ [%] with PMU gains for each generator.

	g17	g20	g64
Frequency [Hz]	K_{POD}=0.367	K_{POD}=0.438	K_{POD}=1.218
0.565	2.664	6.683	3.268
0.648	5.910	6.073	5.005
1.087	5.135	5.133	5.138

The local and PMU control signal comparison is shown in Figure 3.16 with the local signals as solid lines and the PMU signals as dashed lines. From the top down is generator g17, g20 and g64.

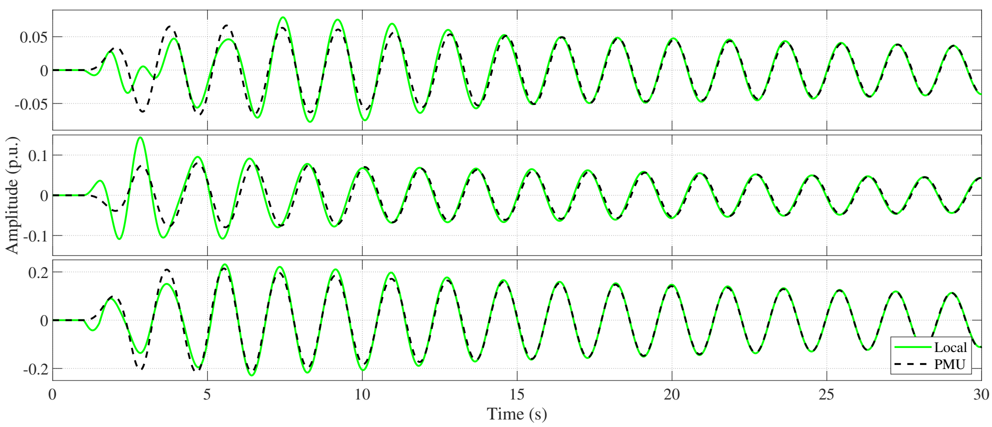

Figure 3.16: PMU gain tuning with unconnected control signals, from the top: g17, g20 and g64.

4

Results

This chapter will present the results achieved throughout this thesis work. A variety of different scenarios will be discussed and conclusions connected to theoretical principles will be laid out.

4.1 Description of Case Studies

The analyses are organised in the following order:

1. The effect on POD when using local signal vs. WACS with PMUs
2. The effect of generator selection for implementing phasor POD
3. The effect of measurement location where PMUs are installed

The main signals and electrical quantities observed include:

- Feedback signals

  These are the signals used together with the phasor POD to construct the control signals. For the local control the feedback signal is the terminal power of the controlled generator. For the WACS the feedback signal is the sinus with the angle difference as shown in (3.9).

- Control signals

  The control signals are the feedback signals after they have been changed by the phasor POD to extract the oscillatory component, added phase compensation as well as amplitude adjustment with a gain. This signal is the one sent into the AVR to control the voltage.

- P_{sum}

  This signal represents the total power flow between all the transmission lines going from price area SE2 to SE3. The dashed line in Figure 2.12 separating these areas are also the cross section for this power flow.

- P_{pgt}

  P_{pgt} is the local power output from the generators, the subscript "pgt" stands for "power generator terminal".

The settings used for the control systems are the values presented throughout Chapter 3. The filter setting for the phasor POD is set to k=0.3 according to Section 3.2.2, the phase according to Section 3.3.2 with the values displayed in Table 3.4 and the gains as presented in Section 3.4 throughout Table 3.5 and Table 3.6.

DMD analysis for frequency and damping ratio extraction was done between 13-18 s, using data stacking of 200 and a truncation rank 20 for the reasons described in Section 3.1. The time window was chosen later in the simulation to exclude the initial behaviour caused by the fault. P_{sum} was used as the analysed signal for frequency and damping while generator speed was used for the modal analysis of the system.

4.2 Use of Local vs. Wide-Area Signal for Damping

Figure 4.1 shows the power from generator g20 together with the feedback signal when WACS is implemented in g20. Due to g20 being the major contributor to the mode the local power changes similarly to how the feedback signal from the WACS changes, as the signal is directly connected to the transfered power described in Section 3.4. This is not necessarily the case as can be observed in Appendix C.1 for g17 and C.6 for g64 and is also discussed in Section 4.2.1. If the controlled generator is the main contributor to the oscillatory mode, the WACS signal representing the inter-area power swing and the local generator terminal power are swing at a similar phase. If the connection is not strong enough the local power will start to deviate from the WACS signal, the wide-area signal will no longer represent how the generator is participating to the oscillation potentially worsening the damping.

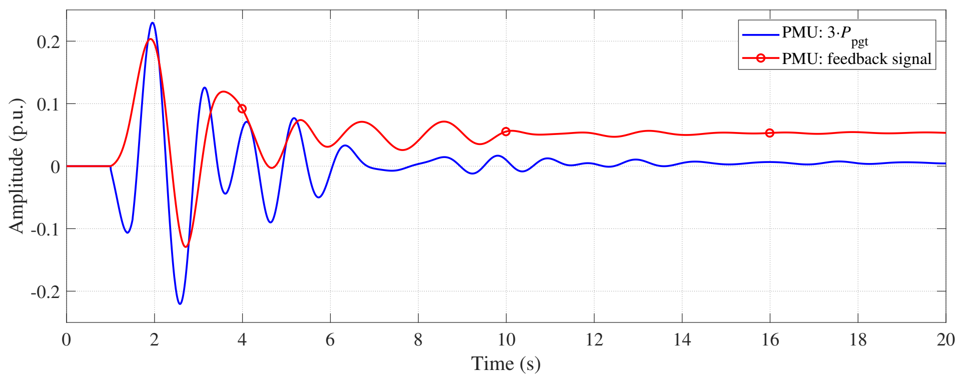

Figure 4.1: Comparison between the generator terminal power from g20 scaled by three and the feedback signal for using WACS method when g20 is used for damping, offset to start at 0.

Figure 4.2 shows the feedback signals for the different methods when g20 is controlled for damping the power oscillation. The local power signal used for the local control contains a higher frequency of 1.12 Hz not observable in the PMU generated signal. The reason for this is the WACS signal is calculated with the phase angles at generator g20 and g17 which are connected to the larger power transfer over the whole system and not local phenomena. The initial decrease in the local power, related to the disturbance is also cut out from the WACS for the same reason. The implications of this is if it is desirable to only focus on the inter-area oscillation the WACS feedback signal could be used with the benefit of including less of local phenomena.

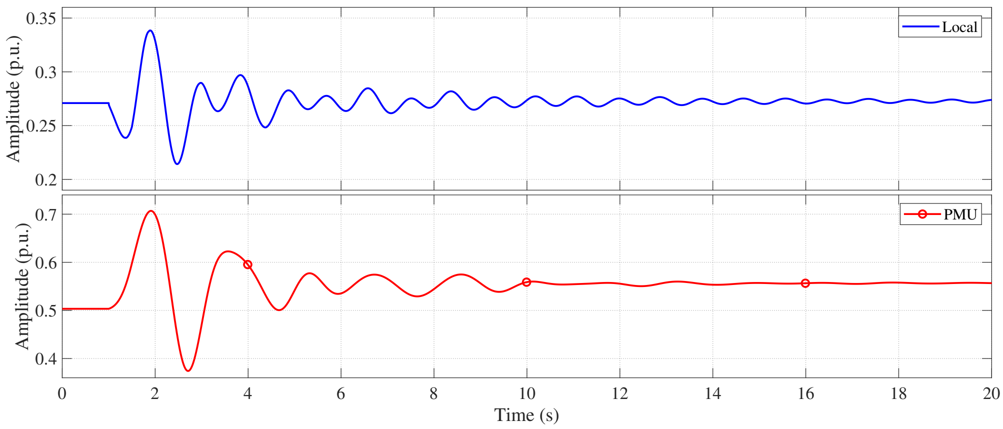

Figure 4.2: Comparison between the feedback signals for the different control methods when g20 is used for damping.

Figure 4.3 shows the control signal output into the AVR for the different simulation cases. With the gains for the different methods the control signal limit of 10 % described in Section 3.2.1 is not reached. The signals differ from each other due to them being based on different measurements as shown in Figure 4.2. The gain scaling also greatly contributes to how the signals compare in the different stages of time. The phase shift between the signals when comparing Figure 4.2 and 4.3 comes from the phase injection to compensate for the phase lag of the generator. With the WACS signal filtering out the local oscillation modes by taking into account the larger dynamics this makes it more fit for usage together with the characteristics of the phasor POD shown in Figure 3.8. With the gain tuning between the methods done in the later stage when the first transient state is over the result is as follows.

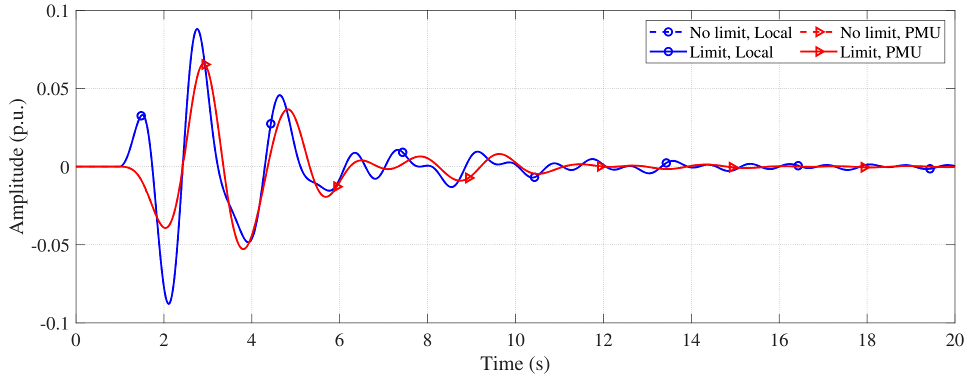

Figure 4.3: Comparison between control signals for the different control methods when g20 is used for damping.

Figure 4.4 shows a comparison between the damping methods on the power transfer P_{sum}. The methods are very similar in there performance with the set settings. Firstly, with the used control of Figure 4.3 it should be noted that WACS uses less control action to produce similar results as the local. Secondly, the non-targeted frequency content included in the control signal for the local method can cause a counter active measure on the larger power transfer. This is not necessarily a fault of the local power signal itself but can be exaggerated by the phasor POD introducing a further phase shift.

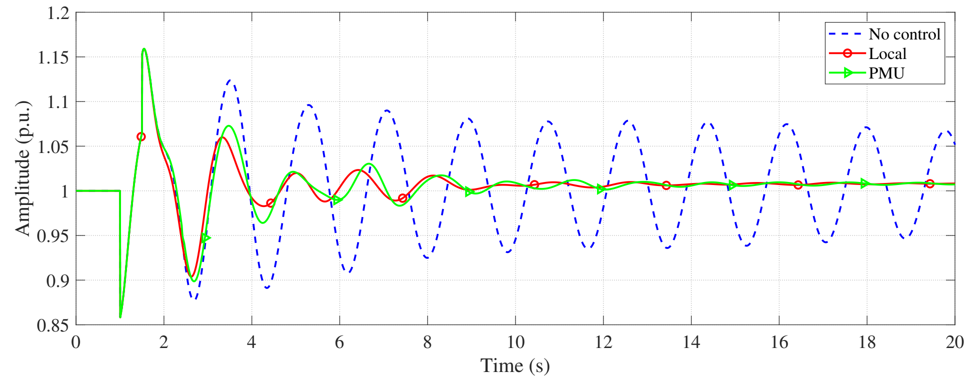

Figure 4.4: Comparison of P_{sum} when g20 is used for damping.

Table 4.1 presents the frequency content and damping ratios for the different P_{sum} signals in Figure 4.4 for the inter-area oscillation. With the theory from Section 2.1.2, the dominant mode frequency changes when the damping is applied. The higher frequency caused by the damping can be seen in the phase shift comparing the signals to the no control reference. This phenomena would worsen the damping due to the gain being reduced when the frequency deviates from the targeted mode.

A feedback process could be set in motion by the initial frequency deviation leading to further deviation. The characteristics of the phasor POD with the initial frequency setting would lead to a negative phase shift being introduced as the frequency increases. The negative phase shift could, depending on the phase added in the phasor POD increase the synchronising torque causing the frequency to increase further and this process would happen until an equilibrium point is reached. The frequency changing is explained by (2.5) and (2.6).

Table 4.1: Frequency and damping ratios from DMD for P_{sum} with g20 used for damping.

No control		Local		PMU	
f [Hz]	ζ [%]	f [Hz]	ζ [%]	f [Hz]	ζ [%]
0.565	1.816	0.650	4.803	0.634	2.960

Figure 4.5 shows the generator g20 power output when the phasor POD uses the local power signal or the wide-area signal from the PMUs. The performance between the two are similar but a higher frequency component is sustained for the local. The phasor POD has good filter characteristics but as can be seen here and in Figure 4.3 it still acts on the non-targeted frequencies. The phase shift added from the frequency being off the targeted mode are probably the reason for the worse damping for this local mode.

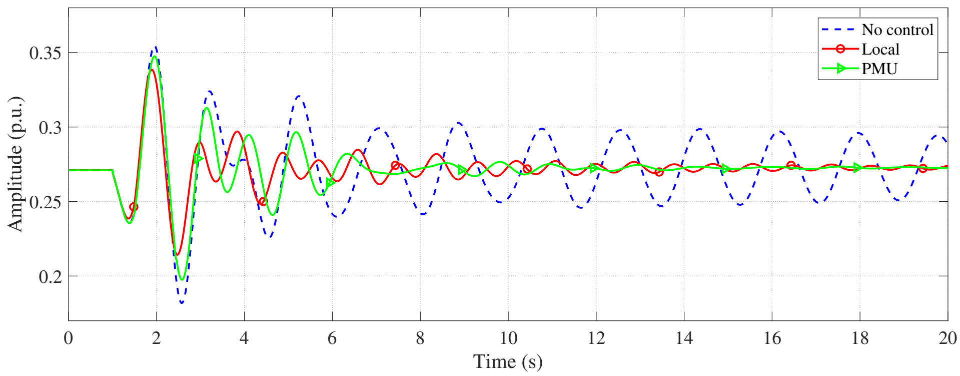

Figure 4.5: Comparison of P_{pgt} when g20 is used for damping.

4.2.1 Impact from Simultaneous Control of Generators

Figure 4.6 shows a comparison between different combinations of generators used for damping with local control. Due to g20 being a large contributor to the inter-area oscillation the additional help from g17 does not contribute noticeably. The same can be said for the combination of g64 and g17 as compared to g64 alone. The similar performance can be linked to the extra damping provided by g17 being counteracted by the change in frequency. Tuning for this deviation is therefore necessary if the extra control is to be useful. This can be explained by the behaviour illustrated in Figure 3.9. The gain is the most obvious factor leading to a worse damping performance while the phase also could contribute negatively. The phase shift does not necessarily lead to worse damping but could lead to instability.

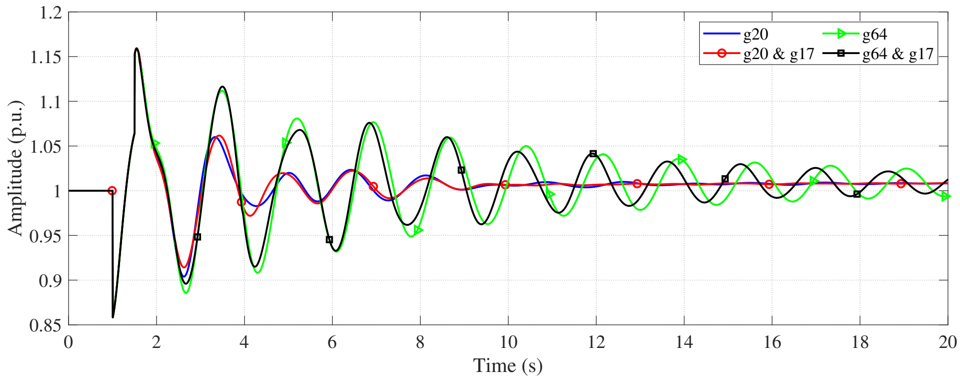

Figure 4.6: P_{sum} when local control is active for multiple generators.

Figure 4.7 shows a comparison between different combinations of generators used for damping with WACS. Similarly to the local control g20 is sufficient for damping. A somewhat worse performance compared to the local can be observed. There could be many reasons for this connected to gain setting, affect on mode frequency but most obvious is the affect from the feedback signal changing phase as shown in Figure 4.8a and Figure 4.9. This is much more observable when comparing the control of g64 and g17 when g20 is not participating in the control. As shown in Appendix C.1 and C.6 these generators change their oscillation pattern therefore coming out of sync with the WACS feedback signal. This leads to a counter active damping effect but not enough to cause instability. Figure 4.8b illustrates how g17 is quick to change oscillation pattern while g64 more slowly wanders away. This most likely depends on where they are situated in relation to the other contributing generators as well as the control action introduced by the disturbance explained in Section 2.4. The consequence of this behaviour is that WACS can be risky due to generators unpredictable behaviour. The local control will always have the direct connection to the controlled generator by using a local signal. The WACS signal is connected to much more complex dynamics with many more generators contributing to the load flow and therefore also the bus angles used for the control signal.

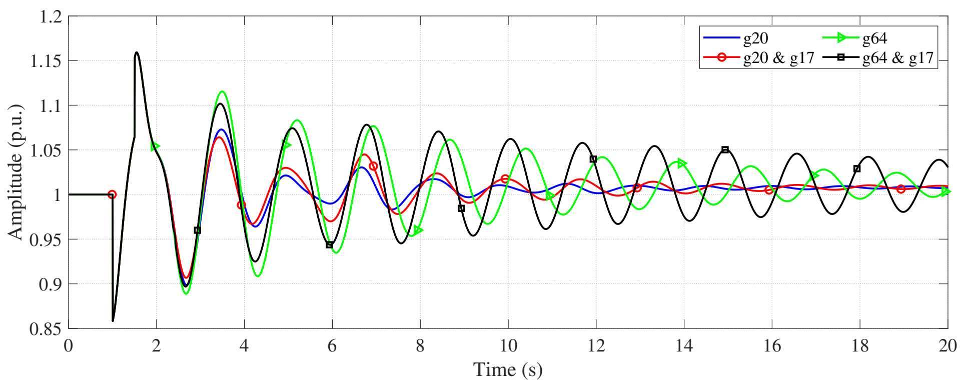

Figure 4.7: P_{sum} when WACS is active for multiple generators.

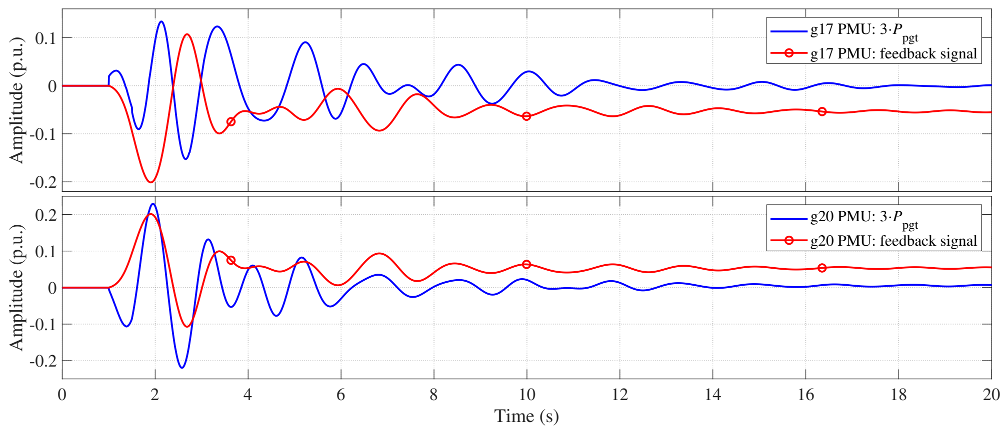

(a) Generators g17 and g20 active for damping.

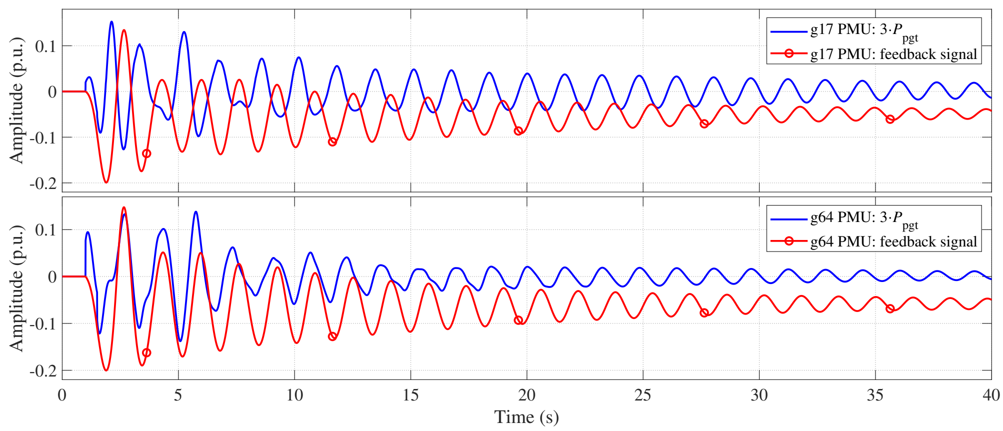

(b) Generators g17 and g64 active for damping.

Figure 4.8: Comparison between the generator terminal power scaled by three and the feedback signal for using WACS with different generators being used for damping, offset to start at 0.

Figure 4.9 shows DMD analysis done at two different time windows for the WACS with g17 and g64. The DMD shows how the generators change oscillation groups over time similar to what the signals in Figure 4.8 indicate, as compared to the no control case shown in Section 3.1. This illustrates an interesting aspect of the DMD algorithm being able to take into account complex changes occurring in the grid due to different control efforts. This seem to be a necessity if WACS where to be implemented to be able to track how the generators behave and adjust the feedback signal to correspond with the current oscillation group.

To summarise, depending on which generators the phasor POD are used together with the results can vary significantly. One factor affecting both the local and the WACS method of damping is the frequency changing with the implemented control, worsening the damping due to the characteristics of the phasor POD. A more severe conclusion is how the WACS feedback signals correlate to generators individual contribution connected to their terminal power. The control action affects how they relate to the other generators contributing to the oscillation. If the generator is not a major contributor it can change its oscillation pattern leading to it no longer corresponding to the WACS feedback signal, being connected to the larger dynamics of the whole system. This partly as the generators damping contribution is not enough to decrease the oscillation quickly enough, but the control effort can also directly change towards which group of generators an individual generator is swinging against. This is not a problem when using local control as it only focuses on the generators own contribution.

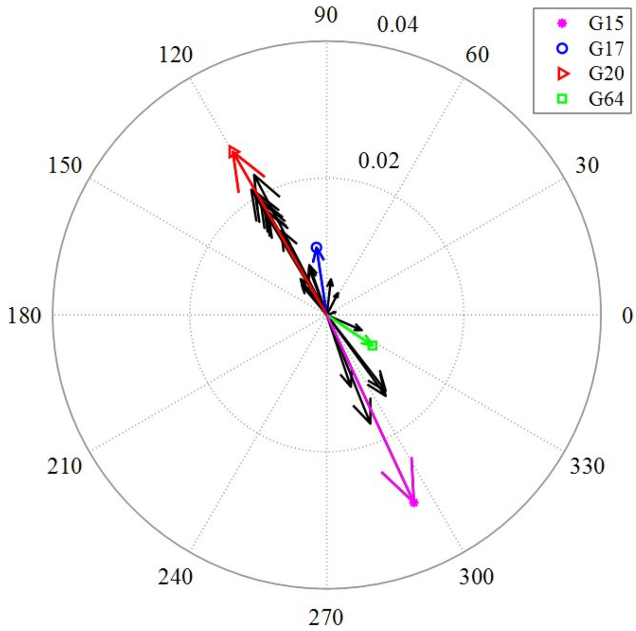

(a) DMD between 5-10 s.

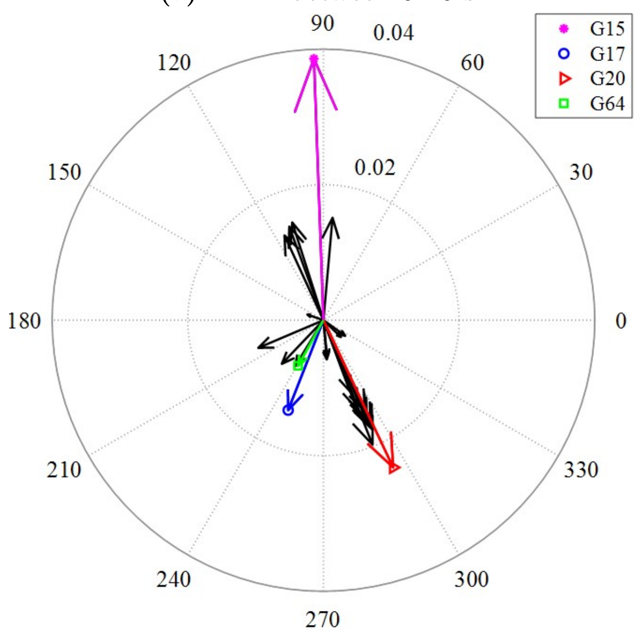

(b) DMD between 30-35 s.

Figure 4.9: Right eigenvectors for multiple generators g64 & g17 at different times with WACS.

4.2.2 Effect of Measurement Location for PMUs

This section presents results connected to the investigation of how measurement points affect the damping. Figure 4.10 shows the feedback signals connected to Figure 4.11. The feedback signal for WACS being directly connected to the power transfer means the initial value represents the initial power flow between the generators. The largest power flow is between areas connected to generators g20 and g17, while the bus feedback signal is connected to the power flow across the bus areas.

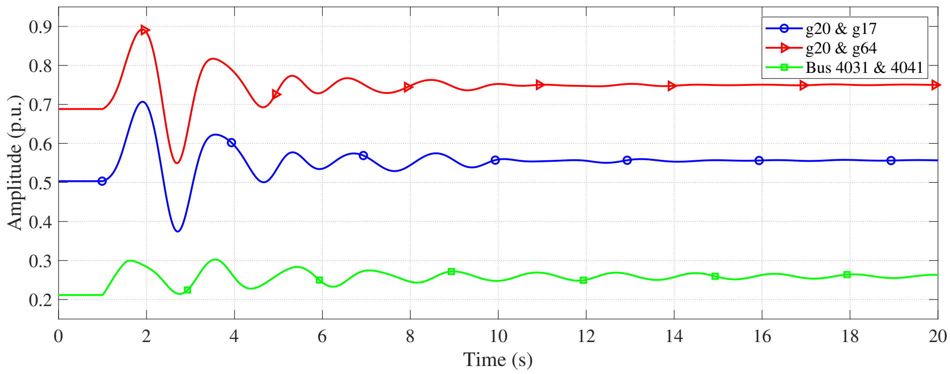

Figure 4.10: Feedback signals when g20 being active for damping with different PMUs used as measurement points.

Figure 4.11 show P_{sum} with only g20 being used for damping but with different phase references for the control. Changing the measurement point between g17 and g64 have minimal significance on the damping. This is due to both generators having similar participation to the mode with similar observability between the references. As for the measurement point being moved to the centre of the grid this decreases the observability with the bus angles deviating less as seen in Figure 4.10. To achieve a similar damping a higher gain is required for this scenario. The option of using distant PMUs for control could be an interesting aspect. The higher gain setting could come with potential problems though connected to instability.

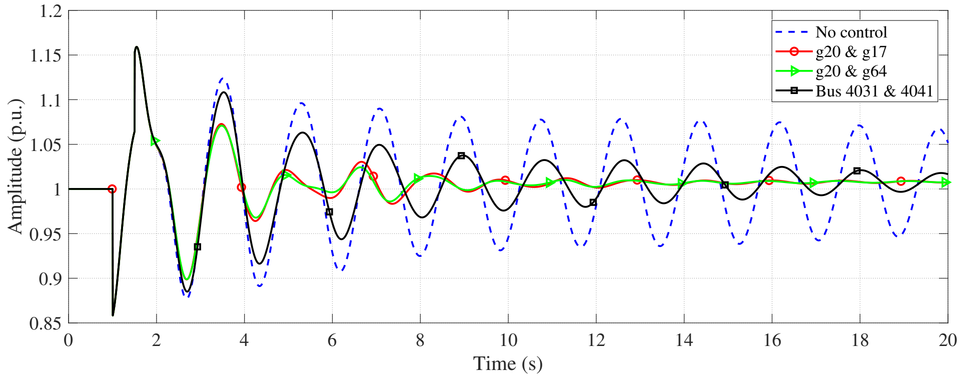

Figure 4.11: P_{sum} when g20 being active for damping with different PMUs used as measurement points.

4.3 Fully-Renewable Scenario

In this section the results and discussions are presented after the future scenario have been implemented. For this case only generator g20 is considered due to the g17 and g64 being replaced by wind turbines. Additionally a figure of results is shown in Appendix C.3 looking at when the wind turbine control system is active for all wind turbines.

Figure 4.12 shows the damping of the inter-area oscillation with the changes described in Section 2.5.3 together with the same fault applied for the fully-renewable scenario. The tuning settings for the 2018 grid configuration provides good damping but re-tuning results in better performance for both methods. The frequency of the oscillation after the disconnection of the faulted line was 0.671 Hz according to the DMD algorithm in Table 3.2. This is a higher frequency than that for the 2018 scenario and is a consequence of the reduced inertia in the system. The phenomena can be traced to (2.6), the reduced system inertia increases the frequency while weaker grid reduces the synchronising torque coefficient according to (2.5). Figure 2.5 illustrates the shift in operating point caused by the line disconnection.

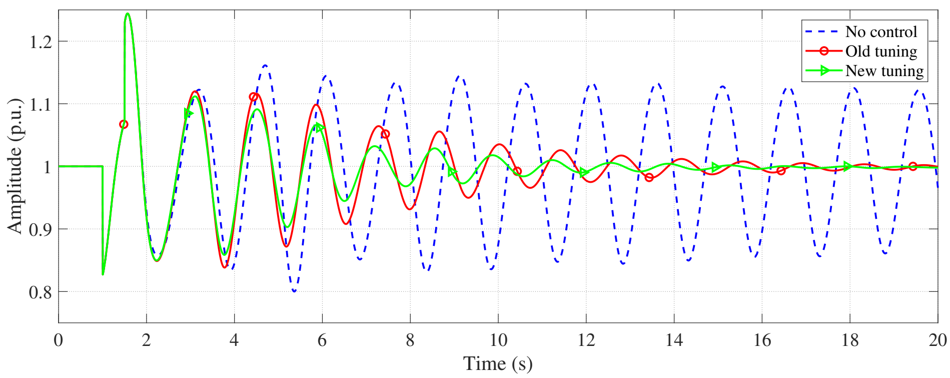

(a) Local control.

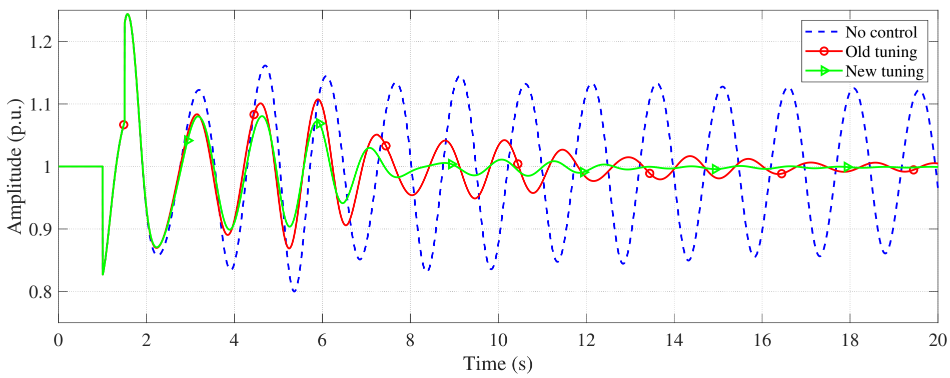

(b) WACS.

Figure 4.12: P_{sum} when g20 is being controlled with the different methods for scenario with increased wind power.

The implications of these results indicate potential problems regarding stability. The existing control systems performance for generators in the power system could deteriorate if the oscillation frequency changes significantly due to the phase compensation needed being affected by frequency. Looking at the phasor PODs characteristics an inter-area frequency closer to a local mode would make it less problematic as the there would be less of an added phase shift from the frequency deviating from the tuning setting. Similar reasoning could be made connected to the traditional PSS structure shown in Figure 2.8 where the phase compensation could be made more preferable for both local and inter-area modes if they are closer to each other.

5

Further Discussions

In this chapter additional discussions are presented regarding the DMD algorithm, with minor problems that occurred and decisions that were made. Additional points regarding the two damping methods are discussed. The fully-renewable scenario is brought up regarding potential future changes in the grid. Sustainable and ethical aspects concerning the project are also discussed. Recommendations of potential future work are presented with thoughts and changes that might have been done differently.

5.1 Participation Factor & Truncation

As was mentioned in Section 3.1 the participation factor did not correlate between the DMD algorithm and PowerFactory. An obvious reason is DMD being a measurement based technique. This would result in the other dynamics such as faults affecting certain generators in the proximity being affected more than a small-signal analysis study would indicate. With the right eigenvectors being similar, a difference emerges from how the left eigenvectors are calculated. The connection of the left eigenvectors projected to the original space in connection to traditional control theory should be investigated further to see the validity of the traditional way of calculating participation factor. Other factors such as size of truncation and time interval of the signal should also be considered.

In Section 2.3.2.1 it was mentioned the right eigenvectors are projected to the original space giving the correct right eigenvectors and then together with the correct left eigenvectors getting the participation factor. The way of calculating the left eigenvectors mentioned in [7] states $\mathbf{\Psi}_i\mathbf{\Phi}_i$=$\mathbf{I}$, meaning the left eigenvectors are the inverse of the right eigenvectors. This is problematic considering this operation only works for square matrices, not being the case for the truncated and projected right eigenvectors. The method used for calculating the left eigenvectors, being mathematically correct, was done according to $\mathbf{\Psi} = \mathbf{RU}^*$.

The size of truncation have most likely affected the results in this thesis. The two methods mentioned in Section 2.3.2.2 varied from each other, with the hard threshold method usually giving a value larger than was needed while the energy method sometimes gave a smaller value. The truncation also changes depending on which time window was chosen and size of data-stacking. The most important aspect of choosing the time window is to not include the first transient. Otherwise the rank increases and no recreation of the signal is possible. From tests with these parameters the final values used which have been mentioned numerous times in this thesis were 200 data stacks and a rank of 20. These parameters, maybe not ideal, gave out similar results to PowerFactory, indicating no important parts of the signals were lost.

5.2 Local Signal vs. Wide-Area Signal

When looking at the comparison between the local and the WACS there are multiple factors which needs to be considered when evaluating if there are any major benefits with the WACS. A discussion of these are done below.

5.2.1 Input Signals

The comparison for the different methods was done connected to feedback signals being related to power. The local power is an easily accessible signal to be used for control. For damping, with the oscillation being well observable in the local power from the participating generators it is well suited to be used for POD. The downside compared to the WACS when only looking at inter-area oscillations are the included local modes. In reality these frequencies should also be damped, so the exclusion could be a down side and a need for a separate control signal might be necessary.

For a more fair comparison between the methods the frequency could be used as an input signal. For the local control the local frequency (equivalent to the generator speed) could be used while for the WACS the frequency difference between the areas. This would result in the gain being more relatable between the methods and as a result the gain settings would not be such a big factor for the comparison.

5.2.2 Gain Setting

The method used for setting the gain was to try to make the different control methods have similar control effort. The behaviour of the feedback signals are inherently different and the results would therefore be different. But, as can be seen from the control signal figures throughout the results they are rather similar when amplitude is of focus. This is a result of the chosen method.

Any different method of tuning the gain would potentially have led to rather different results. However, as long as the actual control effort is being taken into account, the comparison between local and wide-area damping should be valid.

5.2.3 Phasor POD

The chosen method of constructing the control signal also affects the result. The sharp characteristics of both the gain and phase would have given both worse and better results than if the conditions (being phase compensation and targeted frequency) were matching perfectly. The frequency deviation from the filter frequency in the phasor POD would have reduced the amplitude of the control signal leading to worse damping. The same phenomena would also lead to a phase angle deviation changing the damping performance. Depending on how accurate the phase compensation was, together with the knowledge that overcompensation is more efficient for damping torque, the different phenomena would change the performance. An initial undercompensation connected to the phase modelling would worsen the damping. The frequency increasing with the applied damping, leading to a negative phase shift, would worsen the damping performance while increasing the synchronising torque. For stability reasons this is more preferable than the opposite, an increase in phase compensation leading to increased damping while reducing the synchronising torque. Choosing to set the target frequency at a lower frequency than the closed-loop frequency is therefore more secure than the opposite.

5.2.4 Operation Scenario

The operation point of generators affects the phase characteristics and for practical applications the changes would have to be considered. As for this comparison with the underlying conditions being the same it should not make the comparison less valid. A potential factor affecting the performance is how the phase characteristics change with frequency. Depending on how the oscillation frequency change between the methods this could affect the results slightly.

5.2.5 Security

Maybe the most important factor when weighing between the methods are stability and security reasons connected to grid operation. There are multiple factors following the implementation of a WACS not necessary when using local control. Factors as delay connected to the feedback signals, communication error leading to loss of signal as well as having local control as backup in case the WACS fails. The power system is an extremely advanced system. To increase the complexity further without any significant gain would be counterproductive. From the results seen in this study it does not seem like there are sufficient benefits to strive towards implementing these new systems connected to generator control. The phenomena of generators switching toward which generators they are oscillating against would also have to be taken into account when feeding a WACS control signal. To what degree this occures in the real power system as compared to the simulation environment is not certain but would have to be investigated further. Here a potential use of DMD together with PMUs could be used.

5.2.6 Potential Uses

Even though it can be hard to see any clear benefits connected to the WACS in this study there might be certain unique applications worth having in mind for the future. One of the clear benefits of using PMU signals for generating a control signal is the exclusion of frequency content not connected to the inter-area oscillation. This alone also makes the feedback signal more fit for use in combination with the phasor POD with its unique characteristics. A separately fed PMU signal into the AVR as shown in Figure B.2 could potentially be used with the existing control systems for a generator participating to a inter-area oscillation. This would only be an interesting option if the current control system damped the inter-area oscillation poorly, due to its setting for a local mode, while the generator was a major contributor to the inter-area mode. How the two different control signals interacted would then also have to be looked at.

5.3 Grid Reinforcements in the Future

The main reason why other changes were done compared to what is predicted for the future power system, was due to major reinforcements having to be made. With increasing installed capacity for wind turbines the transformers connected to them would need higher ratings. A load flow analysis for the scenario resulted in several voltage drops and thermal transfer limits being reached. Adding extra parallel lines solved the problems but then the system had been changed and would not be valid for comparison any longer. In short, the current Nordic34 model would have to be reinforced to withstand the predicted future scenario. If the thermal generators would instead be replaced with wind turbines as performed for the fully-renewable scenario, this would not be necessary.

5.4 Sustainable and Ethical Aspects

As of late the need for energy in terms of electricity, heat and transport stands for 73.2 % of the world's greenhouse gas emissions [42]. Any work aimed at lowering this percentage can therefore have a large global impact. There is a large shift towards introducing more renewable energy sources into the world's power systems but this is not without concern. This thesis analyses how this generation technology shift affects the small-disturbance stability of the power system and evaluates if the system stability is worsened, and if so, to what extent. In this way, the thesis work contributes with allowing the integration of RES helping with the shift towards a more environmental friendly energy production.

The power system is a complex system which has to be functioning at all times. If not, severe consequences would fall on peoples health, nations economies and on many other areas. This thesis looks into the potential benefits and possibilities of implementing another degree of complexity into the power system. If proceeded, this should be done with great care as the consequences are as severe as they are. Many questions regarding security must be answered connected to how a real implementation would be.

Looking at the IEEE Code of Ethics there are many relevant points to be considered. The most general, not only limited to this thesis, is the "Golden rule". Over the duration of the thesis many people will be involved both directly and indirectly, it is therefore in everyone's best interest to apply the "Golden rule". This together with Code of Ethics number 5, to take criticism, be honest when presenting results and giving credit to the contributors are what will be most relevant during this thesis.

5.5 Future Work

An interesting topic is the choice of control signal for damping. For this thesis a scaled power signal was used which might be problematic with respect to a branched network. Another interesting choice is using frequency as this is a quantity supplied by PMUs. The frequency, being connected to generator speed, is directly connected to power oscillations and could therefore be used both as a local signal but also as a WACS signal taking the difference between frequencies in different areas. A similar option to the signal used in this thesis is using the phase difference directly without the sinus function as done in [11].

One might also look into other means of damping. For this thesis the main focus was damping oscillations using generators with the plan of performing physical tests and only a generator being available. This unfortunately did not happen but it is something that could be investigated further.

A major topic for the future is POD with wind turbines. Included in the simulation environment used is the possibility of activating control for wind turbines as done in Appendix C.11. Unfortunately there was no time to investigate this topic further. Looking into the possibility of having POD functions included in wind turbines for reducing the participation of close by generators to inter-area oscillations is an interesting option as to controlling the generators themselves.

6
Conclusions

This thesis has looked into the possibility of damping inter-area oscillations by controlling generators using data from Phasor Measurement Units (PMUs). A method of damping with a Wide-Area Control System (WACS) was compared to damping with a local power signal. The WACS signals were equivalent to a scaled transfer power by using bus angles in different parts of the system. The control signals were created with the help of a phasor Power Oscillation Damping (POD) algorithm, extracting the oscillatory part of a signal and then manually adding a phase shift. A measurement based analysis algorithm called Dynamic Mode Decomposition (DMD) was used for analysing the system state.

The DMD algorithm was used successfully to analyse the system behaviour connected to frequencies and damping ratios when analysing total power flow P_{sum} as well as mode shape when having speed from all generators simultaneously. However, it is not understood on how to extract the participation factor by using the DMD algorithm if possible.

The local damping with the phasor POD showed good results for damping the inter-area oscillation. The WACS showed similar results with the chosen method for tuning the gain but depending on which generator or generators were used for damping, the results varied. The closed-loop system affects which generator group the generators swing against. Generator g20 being the highest participant is not affected by this because it quickly reduces the power swing. The WACS signal therefore corresponds well with how g20 interacts with the rest of the grid. Generator g17 and g64 are affected in two different ways probably depending on their location. g17 changes oscillation group immediately from the applied control while g64 more slowly moves towards another group of generators. Due to the WACS signals being based on the larger power oscillation between the areas, the connection to the WACS signal is not valid in these cases as it no longer represents the individual generators contribution. The choice of generators for control are therefore crucial regarding whether or not the WACS will have a positive effect. With WACS being much more complicated and local control providing good damping, this study has not found the use of WACS signal to be more advantageous than that of the local signal for POD with generators.

The WACS signals can be seen containing less of local frequencies. A possibility of using these for some control purpose related to inter-area damping could be of interest in the future. Another interesting aspect of WACS is the possibility of using PMUs not located in the vicinity of the equipment being controlled. This study illustrates how remote PMUs can be used as long as the mode is observable. The downside with a worse observability is a higher gain would be necessary to achieve similar damping, potentially creating problems with instability.

With the changes done in the network, disconnecting all thermal production, to represent a fully renewable scenario an increase in the inter-area frequency could be seen. This is a result of the reduced system inertia. This together with structural changes to the grid to allow for increasing loads will affect the synchronising torque coefficient and thus the corresponding resonant frequency of the power oscillation, potentially leading to problems with the current settings for control systems. Re-tuning these would then be necessary to maintain good damping.

References

[1] J. De La Ree, V. Centeno, J. S. Thorp, and A. G. Phadke, "Synchronized Phasor Measurement Applications in Power Systems," *IEEE Transactions on Smart Grid*, vol. 1, no. 1, pp. 20–27, 2010. [Online]. Available: https://doi.org/10.1109/TSG.2010.2044815.

[2] A. Phadke and J. Thorp, *Synchronized Phasor Measurements and Their Applications*. Jan. 2017, ISBN: 978-3-319-50582-4. DOI: 10.1007/978-3-319-50584-8.

[3] European Network of Transmission System Operators for Electricity, *Technical Background and Recommendations for Defence Plans in the Continental Europe Synchronous Area*, ENTSO-E • Boulevard Saint-Michel, 15 • 1040 Brussels • Belgium, 2010. [Online]. Available: https://eepublicdownloads.entsoe.eu/clean-documents/pre2015/publications/entsoe/RG_SOC_CE/RG_CE_ENTSO-E_Defence_Plan_final_2011_public.pdf.

[4] N. R. Chaudhuri, A. Domahidi, R. Majumder, *et al.*, "Wide-area power oscillation damping control in Nordic equivalent system," *Generation, Transmission & Distribution, IET*, vol. 4, pp. 1139–1150, Nov. 2010. DOI: 10.1049/iet-gtd.2009.0478.

[5] E. Grebe, J. Kabouris, S. López Barba, W. Sattinger, and W. Winter, "Low frequency oscillations in the interconnected system of Continental Europe," in *IEEE PES General Meeting*, 2010, pp. 1–7. DOI: 10.1109/PES.2010.5589932.

[6] D. Gautam, V. Vittal, and T. Harbour, "Impact of Increased Penetration of DFIG-Based Wind Turbine Generators on Transient and Small Signal Stability of Power Systems," *IEEE Transactions on Power Systems*, vol. 24, no. 3, pp. 1426–1434, 2009. DOI: 10.1109/TPWRS.2009.2021234.

[7] P. Kundur, N. J. Balu, and M. G. Lauby, *Power system stability and control*, ser. EPRI power system engineering series. McGraw-Hill, 1994, ISBN: 007035958X.

[8] E. Larsen and D. Swann, "Applying Power System Stabilizers Part III: Practical Considerations," *IEEE Transactions on Power Apparatus and Systems*, vol. PAS-100, no. 6, pp. 3034–3046, 1981. DOI: 10.1109/TPAS.1981.316411.

[9] E. Sorrentino and F. León, "Comparison among typical input signals of different types of Power System Stabilizers (PSS)," in *2020 IEEE ANDESCON*, 2020, pp. 1–6. DOI: 10.1109/ANDESCON50619.2020.9272090.

[10] E. V. Larsen and D. A. Swann, "Applying Power System Stabilizers Part I: General Concepts," *IEEE Transactions on Power Apparatus and Systems*, vol. PAS-100, no. 6, pp. 3017–3024, 1981. DOI: 10.1109/TPAS.1981.316355.

[11] K. Uhlen, L. Vanfretti, M. M. de Oliveira, *et al.*, "Wide-Area Power Oscillation Damper implementation and testing in the Norwegian transmission network," in *2012 IEEE Power and Energy Society General Meeting*, 2012, pp. 1–7. DOI: 10.1109/PESGM.2012.6344837.

[12] C. Lu, X. Wu, J. Wu, *et al.*, "Implementations and experiences of wide-area HVDC damping control in China Southern Power Grid," in *2012 IEEE Power and Energy Society General Meeting*, 2012, pp. 1–7. DOI: 10.1109/PESGM.2012.6345363.

[13] P. Schmid and J. Sesterhenn, "Dynamic Mode Decomposition of numerical and experimental data," *Journal of Fluid Mechanics*, vol. 656, Nov. 2008. DOI: 10.1017/S0022112010001217.

[14] P. Schmid, L. Li, M. Juniper, and O. Pust, "Applications of the dynamic mode decomposition," *Theoretical and Computational Fluid Dynamics*, vol. 25, pp. 249–259, Jun. 2010. DOI: 10.1007/s00162-010-0203-9.

[15] A. Alassaf and L. Fan, "Randomized Dynamic Mode Decomposition for Oscillation Modal Analysis," *IEEE Transactions on Power Systems*, vol. 36, no. 2, pp. 1399–1408, 2021. DOI: 10.1109/TPWRS.2020.3012419.

[16] M. Zuhaib and M. Rihan, "Identification of Low-Frequency Oscillation Modes Using PMU Based Data-Driven Dynamic Mode Decomposition Algorithm," *IEEE Access*, vol. 9, pp. 49 434–49 447, 2021. DOI: 10.1109/ACCESS.2021.3068227.

[17] E. Barocio, B. C. Pal, N. F. Thornhill, and A. R. Messina, "A Dynamic Mode Decomposition Framework for Global Power System Oscillation Analysis," *IEEE Transactions on Power Systems*, vol. 30, no. 6, pp. 2902–2912, 2015. DOI: 10.1109/TPWRS.2014.2368078.

[18] C. Zhang, Z. Chen, M. Wang, L. Jia, and P. Zi, "A Novel Identification Method of Power System Oscillation based on Dynamic Mode Decomposition," in *2021 Power System and Green Energy Conference (PSGEC)*, 2021, pp. 713–717. DOI: 10.1109/PSGEC51302.2021.9542185.

[19] A. Alassaf and L. Fan, "Dynamic Mode Decomposition in Various Power System Applications," in *2019 North American Power Symposium (NAPS)*, 2019, pp. 1–6. DOI: 10.1109/NAPS46351.2019.9000261.

[20] S. Mohapatra and T. J. Overbye, "Fast modal identification, monitoring, and visualization for large-scale power systems using Dynamic Mode Decomposition," in *2016 Power Systems Computation Conference (PSCC)*, 2016, pp. 1–7. DOI: 10.1109/PSCC.2016.7540904.

[21] N. Halko, P. G. Martinsson, and J. A. Tropp, "Finding Structure with Randomness: Probabilistic Algorithms for Constructing Approximate Matrix Decompositions," *SIAM Review*, vol. 53, no. 2, pp. 217–288, 2011. DOI: 10.1137/090771806.

[22] S. L. Brunton and J. N. Kutz, *Data Driven Science & Engineering Machine Learning, Dynamical Systems, and Control.* 2017.

[23] J. N. Kutz, S. L. Brunton, B. W. Brunton, and J. L. Proctor, *Dynamic mode decomposition: data-driven modeling of complex systems.* SIAM, 2016.

[24] M. Netto, Y. Susuki, and L. Mili, "Data-Driven Participation Factors for Nonlinear Systems Based on Koopman Mode Decomposition," *IEEE Control Systems Letters*, vol. 3, no. 1, pp. 198–203, 2019. DOI: 10.1109/LCSYS.2018.2871887.

[25] Y. Li, D. Yang, F. Liu, Y. Cao, and C. Rehtanz, *Interconnected Power Systems: Wide-Area Dynamic Monitoring and Control Applications.* Springer Berlin Heidelberg, 2016.

[26] ENTSO-E, *ENTSO-E*, Accessed Mar. 4, 2022. [Online]. Available: https://www.entsoe.eu/.

[27] North American Electric Reliability Corporation, *Interconnection Oscillation Analysis*, Accessed Mar. 16, 2022. [Online]. Available: https://www.nerc.com/comm/PC/SMSResourcesDocuments/Interconnection_Oscillation_Analysis.pdf.

[28] ——, *Detailed Event Analysis*, Accessed Mar. 16, 2022. [Online]. Available: https://www.nerc.com/comm/PC/SMSResourcesDocuments/Detailed_Event_Analysis.pdf.

[29] North American Electric Reliability Council, *Review of Selected 1996 Electric System Disturbances in North America*, Accessed Mar. 16, 2022. [Online]. Available: https://www.nerc.com/pa/rrm/ea/System%20Disturbance%20Reports%20DL/1996SystemDisturbance.pdf.

[30] Dan Trudnowski, Jon Pierre, Matt Donnelly , Mani Venkatasubramanian, Jim Follum, *Bulk Power System Oscillation Terms*, Accessed Mar. 16, 2022. [Online]. Available: https://www.wecc.org/Administrative/Oscillation%20Terms.pdf.

[31] DIgSilent, "PowerFactory," 2022. [Online]. Available: https://www.digsilent.de/en/.

[32] S. Muller, *Development of Nordic 32 System Model and Performance Analysis Based on Real Operational Statistics*, 2019. [Online]. Available: https://www.diva-portal.org/smash/get/diva2:1395253/FULLTEXT01.pdf.

[33] CIGRE Task Force 38-02-08, *Long term dynamics phase ii: Final report*, 1995.

[34] S. W. E. Association, *Roadmap 2040 Wind power: combating climate change and improving competitiveness*, Accessed Apr. 27, 2022. [Online]. Available: https://swedishwindenergy.com/wp-content/uploads/2021/01/Roadmap-2040-ENG-rev-2020.pdf.

[35] Svenska Kraftnät, *Långsiktig Marknadanalys 2018 Långsiktsscenarier för elsystemets utveckling fram till år 2040*, Accessed Apr. 27, 2022. [Online]. Available: https://www.svk.se/siteassets/om-oss/rapporter/2018/langsiktig-marknadsanalys-2018.pdf.

[36] L. Angquist and C. Gama, "Damping algorithm based on phasor estimation," in *2001 IEEE Power Engineering Society Winter Meeting. Conference Proceedings (Cat. No.01CH37194)*, vol. 3, 2001, 1160–1165 vol.3. DOI: 10.1109/PESW.2001.917237.

[37] M. Beza, "Control of Energy Storage Equipped Shunt-connected Converter for Electric Power System Stability Enhancement," Ph.D. dissertation, Jun. 2012. [Online]. Available: https://publications.lib.chalmers.se/records/fulltext/158117.pdf.

[38] M. R. S. Tirtashi and M. Bongiorno, "Phasor-POD based Estimation for the PSS Controller,"

[39] A. Moshref, H. Tagourti, N. Wooster, R. Harrison, and T. Ricioppo, "Power System Stabilizer Tuning with Presence of Torsional Oscillations," *2019 CIGRE Canada Conference*, [Online]. Available: https://cigre.ca/papers/2019/CIGRE-111.pdf.

[40] M. A. Tabrizi, N. Prakash, M. Sahni, *et al.*, "Power system damping analysis on large power system networks: An entergy case study," in *2017 IEEE Power & Energy Society General Meeting*, 2017, pp. 1–5. DOI: 10.1109/PESGM.2017.8274415.

[41] Flexitranstore, "An Integrated Platform for Increased FLEXIbility in smart TRANSmission grids with STORage Entities and large penetration of Renewable Energy Sources," Chalmers, Tech. Rep. [Online]. Available: https://cordis.europa.eu/project/id/774407.

[42] H. Ritchie and M. Roser, "CO2 and Greenhouse Gas Emissions," *Our World in Data*, 2020. [Online]. Available: https://ourworldindata.org/co2-and-other-greenhouse-gas-emissions.

[43] IEEE PES-TR19, *Test systems for voltage stability analysis and security assessment*, 2015.

A

Appendix A. Generator Modelling

The necessary equations that were used during generator modelling in Section 3.3.1 are presented here and are shown in the order they are calculated. The equations are not described in this thesis but in [7]. The parameters needed for the transfer function are K_3, T_3, K_2 and K_6, illustrated in Figure 2.10.

$$\begin{aligned} L_{adu} &= X_d - X_l \\ L_{aqu} &= X_q - X_l \end{aligned} \tag{A.1}$$

$$L_{ads(incr)} = K_{sd(incr)} L_{adu} \tag{A.2}$$

$$K_{sd(incr)} = \frac{1}{1 + B_{sat} A_{sat} e^{B_{sat}(\Psi_{at0} - \Psi_{T1})}} \tag{A.3}$$

$$K_{sq} = \begin{cases} 1, & \text{if salient-pole machine} \\ K_{sd}, & \text{otherwise} \end{cases} \tag{A.4}$$

$$L'_{ads} = \frac{1}{\frac{1}{L_{ads}}} + \frac{1}{\frac{1}{L_{fd}}} \tag{A.5}$$

$$X'_d = X_l + \frac{L_{adu} L_{fd}}{L_{adu} + L_{fd}} \tag{A.6}$$

$$R_T = R_a + R_E \tag{A.7}$$

$$X_{Tq} = X_E + (L_{aqs} + X_l) = X_E + X_{qs} \tag{A.8}$$

$$X_{Td} = X_E + (L'_{ads} + X_l) = X_E + X'_{ds} \tag{A.9}$$

$$D = R_T^2 + X_{Tq} X_{Td} \tag{A.10}$$

$$m_2 = \frac{X_{Tq}}{D} \frac{L_{ads}}{(L_{ads} + L_{fd})} \tag{A.11}$$

$$n_2 = \frac{R_T}{D} \frac{L_{ads}}{(L_{ads} + L_{fd})} \tag{A.12}$$

$$T'_{d0} = \frac{L_{adu} + L_{fd}}{R_{fd} \cdot \omega_0} \tag{A.13}$$

$$a_{33} = -\frac{\omega_0 R_{fd}}{L_{fd}} \left[1 - \frac{L'_{ads}}{L_{fd}} + m_2 L'_{ads} \right] \tag{A.14}$$

$$b_{32} = \frac{\omega_0 R_{fd}}{L_{adu}} \tag{A.15}$$

$$K_3 = -\frac{b_{32}}{a_{33}} = \frac{L_{ads} + L_{fd}}{L_{adu}} \frac{1}{1 + \frac{X_{Tq}}{D}\left(X_d - X'_d\right)} \tag{A.16}$$

$$T_3 = -\frac{1}{a_{33}} \tag{A.17}$$

$$X_{qs} = L_{qs} = K_{sq} L_{aqu} + X_l \tag{A.18}$$

$$\delta_i = \tan^{-1}\left(\frac{I_t X_{qs} \cos\phi - I_t R_a \sin\phi}{E_t + I_t R_a \cos\phi + I_t X_{qs} \sin\phi}\right) \tag{A.19}$$

$$\begin{aligned} e_{d0} &= E_t \sin\delta_i \\ e_{q0} &= E_t \cos\delta_i \end{aligned} \tag{A.20}$$

$$\begin{aligned} i_{d0} &= I_t \sin\left(\delta_i + \phi\right) \\ i_{q0} &= I_t \cos\left(\delta_i + \phi\right) \end{aligned} \tag{A.21}$$

$$\Psi_{aq0} = -L_{aqs} i_{q0} \tag{A.22}$$

$$i_{fd0} = \frac{e_{q0} + R_a i_{q0} + L_{ds} i_{d0}}{L_{ads}} \tag{A.23}$$

$$\Psi_{ad0} = L_{ads}\left(-i_{d0} + i_{fd0}\right) \tag{A.24}$$

$$K_2 = n_2\left(\Psi_{ad0} + L_{aqs} i_{d0}\right) - m_2\left(\Psi_{aq0} + L'_{ads} i_{q0}\right) + \frac{L'_{ads}}{L_{fd}} i_{q0} \tag{A.25}$$

$$\begin{aligned} K_6 = \frac{e_{d0}}{E_{t0}}\left[-R_a m_2 + X_l n_2 + L_{aqs} n_2\right] + \\ + \frac{e_{q0}}{E_{t0}}\left[-R_a n_2 - X_l m_2 + L'_{ads}\left(\frac{1}{L_{fd}} - m_2\right)\right] \end{aligned} \tag{A.26}$$

B

Appendix B. DSL Models

There are two main frames, one for each generator type. Figure B.1 show the frame for the hydro type including the original slots for Generator, AVR, Hydro Turbine and Gov. Each slot has its own DSL model with the same name. The Hydro Turbine and Gov slots are excluded from the thermal based generators. All parameters in the DSL models have not been changed and are set according to [43]. The additions made for this project were the POD slot and the Phasor Signal slot with its inputs of voltage and phase angles.

Frame H PMU:

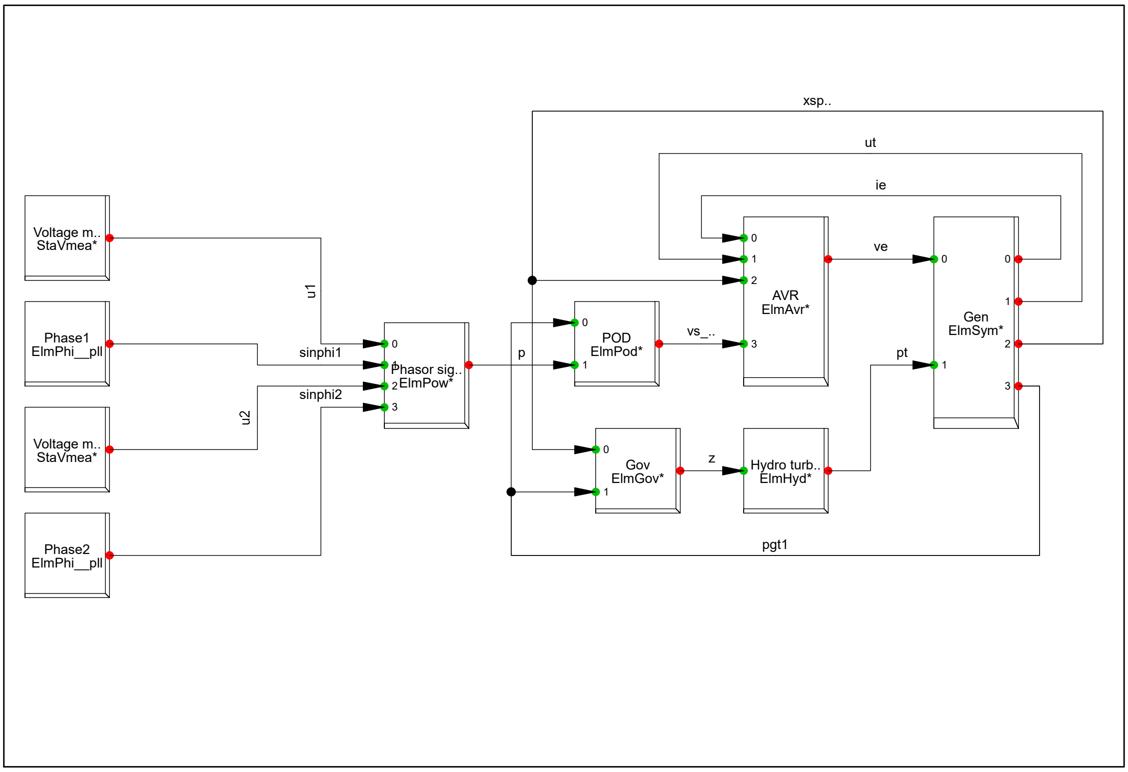

Figure B.1: Diagram of the DSL frame for the hydro based generator.

One small change was done in the AVR model by adding an extra input from the POD slot, with its limit of 10 % and a turn on/off block. Figure B.2 show the AVR DSL model with the new signal at the bottom.

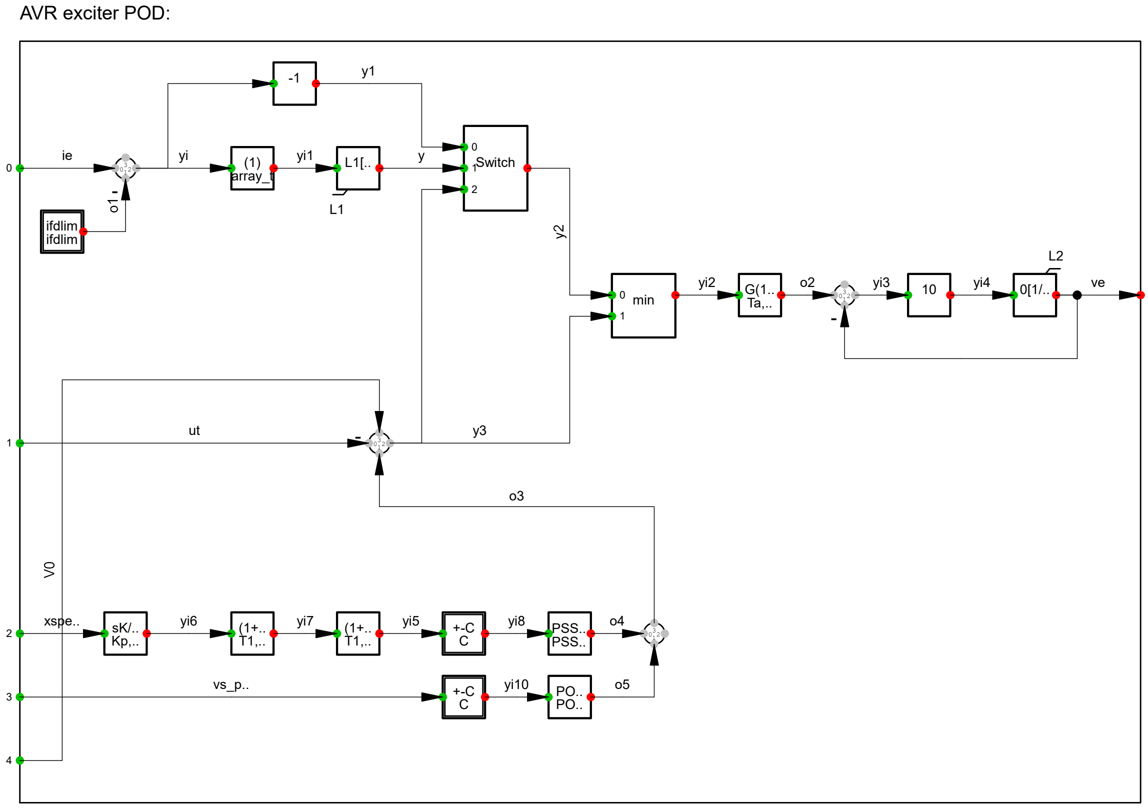

Figure B.2: Diagram of the AVR DSL model.

The next implementation was the phasor POD model which is shown in Figure B.3. The function of this model has been described in Section 3.2.2. The input selector in the top-left allows the user to change which signal is to be used for damping, with the options of local power P_{pgt}, wide-area signal P or a test signal.

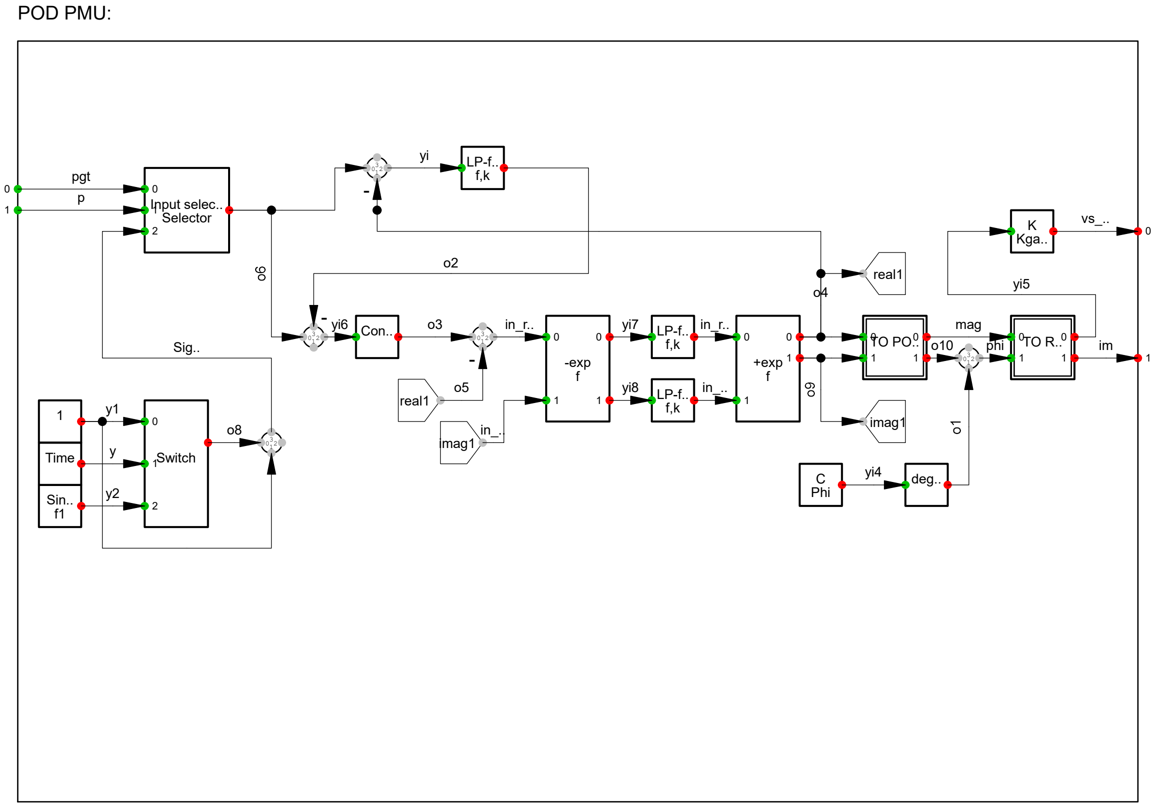

Figure B.3: Diagram of the phasor POD DSL model.

The last added slot was the Phasor Signal slot with its simple DSL model shown in Figure B.4. It consists of a single block where the scaled power transfer is calculated with the input signals. The input signals are voltage and phase angle from desired locations in the system, but only the phase angles are used as is mentioned in Section 3.4. The possibility of choosing to use frequency or angle difference is also included.

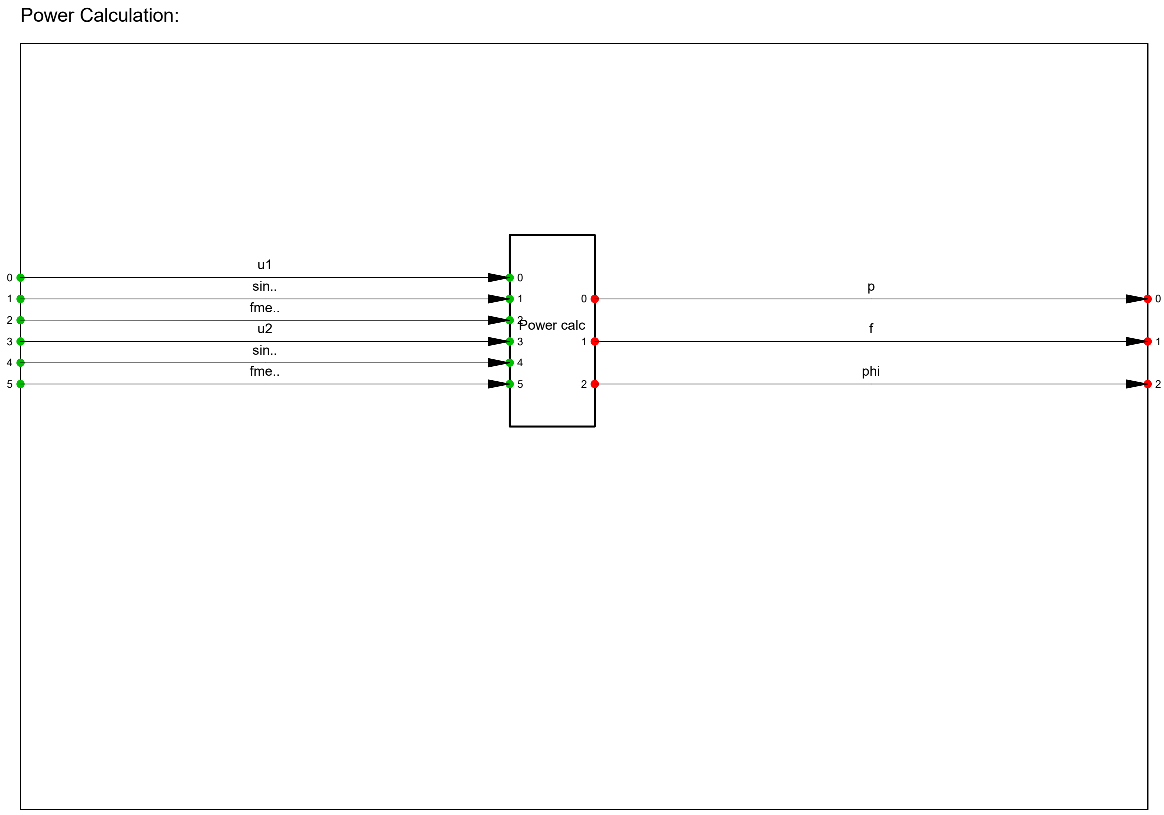

Figure B.4: Diagram of the Power Calculation DSL model.

Figure B.5 shows the equations for the Power Calculation DSL model. Each individual generator frame needs to be connected properly with the measurement points to generate the correct signals. The generator connected to the frame always had its own measurement first (parameters with number one). The scaled power signal was used during this project. The other two signals can also be used by changing the output from the Phasor Signal slot in Figure B.1 to either f or *phi*.

Additional equations

```
Phi1=asin(sinphi1)!*180/pi()
Phi2=asin(sinphi2)!*180/pi()

!Scaled power
inc(p)=sin(Phi1-Phi2) !Generator reference
p=sin(Phi1-Phi2)

!Frequency
inc(f)=fmeas1-fmeas2
f=fmeas1-fmeas2

!Angle
inc(phi)=Phi1-Phi2
phi=Phi1-Phi2
```

Figure B.5: Equations in the Power Calculation DSL model.

The largest frame implemented was that of the wind turbine which is shown in Figure B.6. The DSL models used were from the IEC library connected to the frame.

Frame IEC Type 4A: Frame for wind turbine model of Type 4A acc. to IEC 61400-27-1 Ed.2

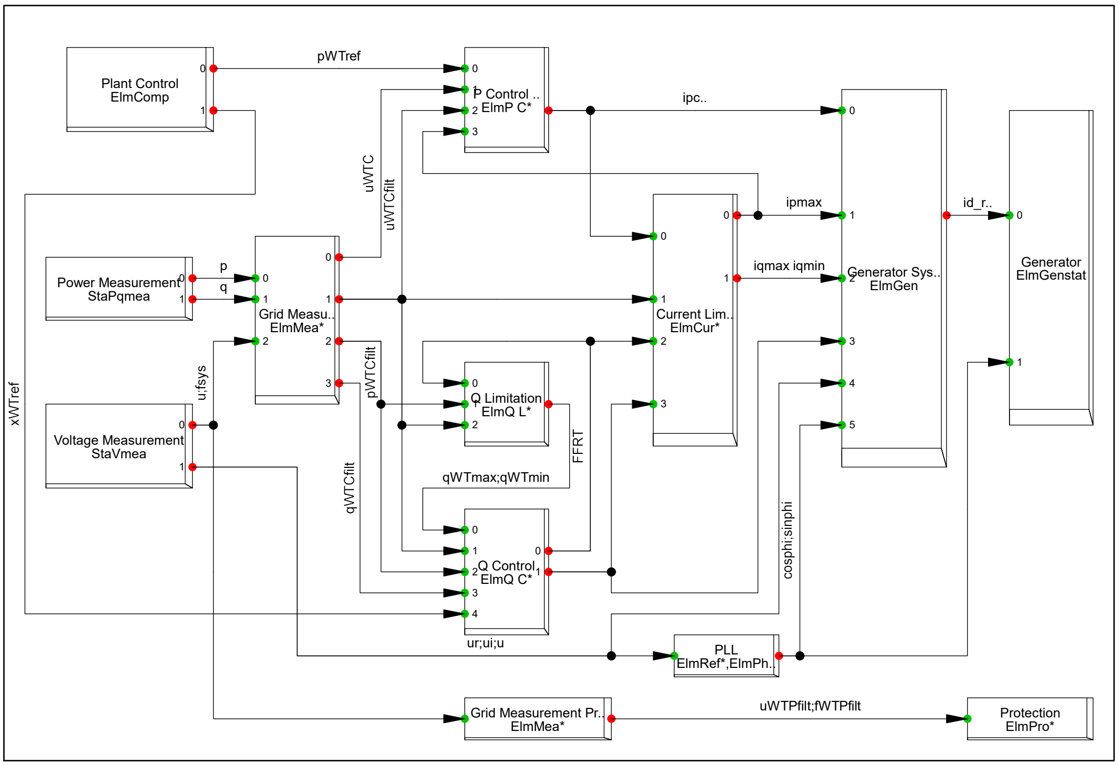

Figure B.6: Diagram of the frame used for the wind turbines.

C

Appendix C. Local vs. Wide-Area Damping

Here additional simulation results are presented following up with what is shown in Section 4.2. The remaining two generators g17 and g64 are shown and discussed here when used separately for damping.

C.1 Generator g17

Figure C.1 illustrates the phenomena of the WACS feedback signal which is connected to the power transfer between g17 and g20, being out of phase with the terminal power. This is a consequence of g17 changing oscillation group as discussed in Section 4.2.1. The feedback signal connected to the power flow between g17 and g20 now no longer represents generator g17s contribution to the power oscillation. It is interesting how this does not lead to instability. A control signal being too much out of phase would lead to a positive electric torque out of phase with the speed deviation, worsening the damping. This is related to the typical closed-loop system directly enhancing the oscillation. The behaviour observed here does not seem to have a link to the traditional theory as the closed-loop is more complex. The effect of the control still contributes with positive damping meaning other phenomena must take place.

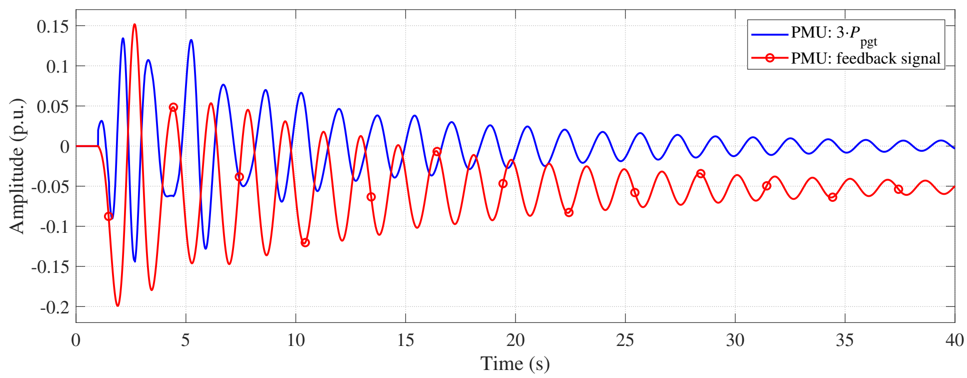

Figure C.1: Comparison between the generator terminal power from g17 scaled by three and the feedback signal for using PMU as control method when g17 is used for damping, offset to start at 0.

Figure C.2 show the feedback signals for each of the methods. The removal of the local frequencies are much more clear here compared to Figure 4.2.

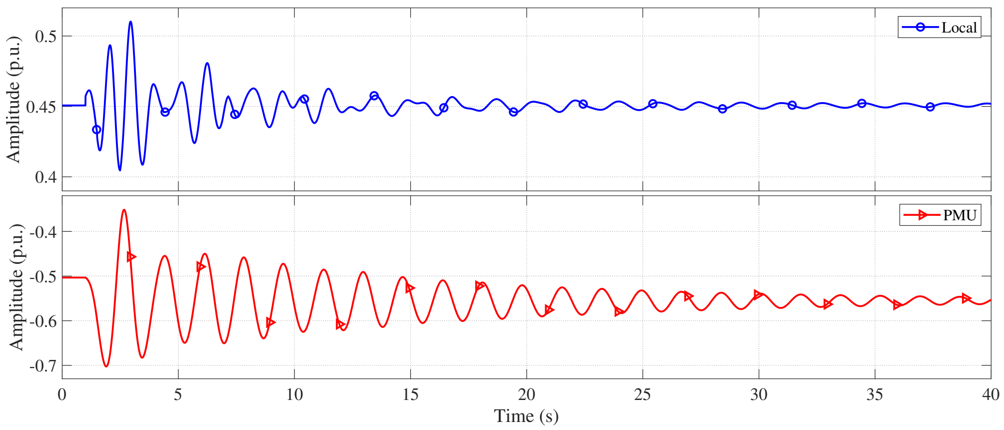

Figure C.2: Comparison between feedback signals for the different control methods when g17 is used for damping.

Figure C.3 show the control signals for each of the methods. The phasor POD removes much of the frequency content seen in Figure C.2 connected to the local feedback. The PMU control signal is mostly changed according to the gain and the phase compensation. Compared to Figure 4.3 the PMU signal has higher amplitude than the local even though the same method was used to set the gain. This is due to a different initial reaction between the generators to the disturbance while the mode observability from the PMUs does not change as much as seen in Figure 4.10.

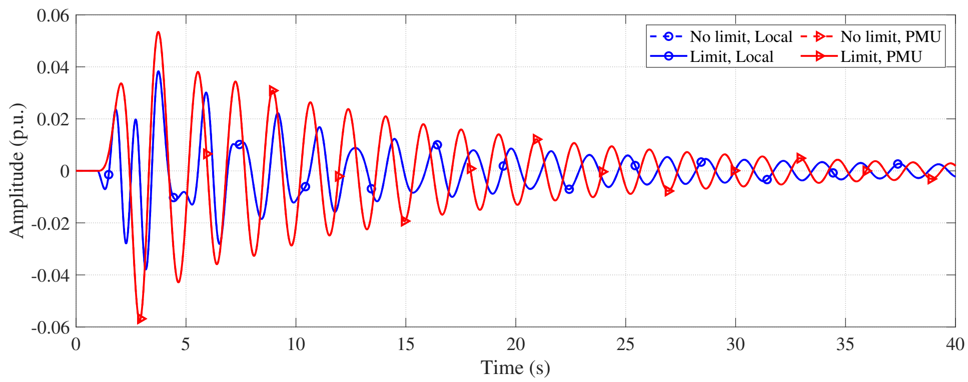

Figure C.3: Comparison between control signals for the different control methods when g17 is used for damping.

Figure C.4 show the P_{sum} signals for each of the methods. The WACS shows better result than the local control but this is with the higher control effort shown in Figure C.3. The higher frequency by the WACS would reduce the control signal amplitude as well as introduce a phase shift, the amplitude is still higher though but the phase shift could have rather detrimental effects. Connected to the phase shift between the WACS signal and the terminal power it is interesting how even though this exists the WACS damps the inter-area oscillation better. The interaction with surrounding generators from the terminal voltage changing must still contribute with a positive effect even though it is unclear how exactly this happens.

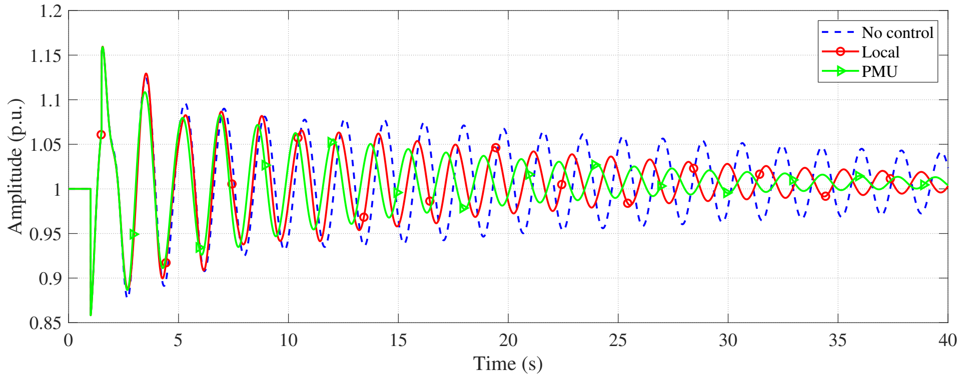

Figure C.4: Comparison of P_{sum} when g17 is used for damping.

Figure C.5 show the P_{pgt} signals for each of the methods. An interesting phenomena can be observed in connection to Figure C.4, the local power is more well damped for the local while the opposite is true for the case of WACS. A possible explanation is the focus of the local, with the feedback signal being the local power, is to reduce its own local oscillation. The effect on other participating generators is therefore not positive in the same manner as for the WACS where it focuses on the inter-area oscillation. Again, it is not clear how this interaction takes place.

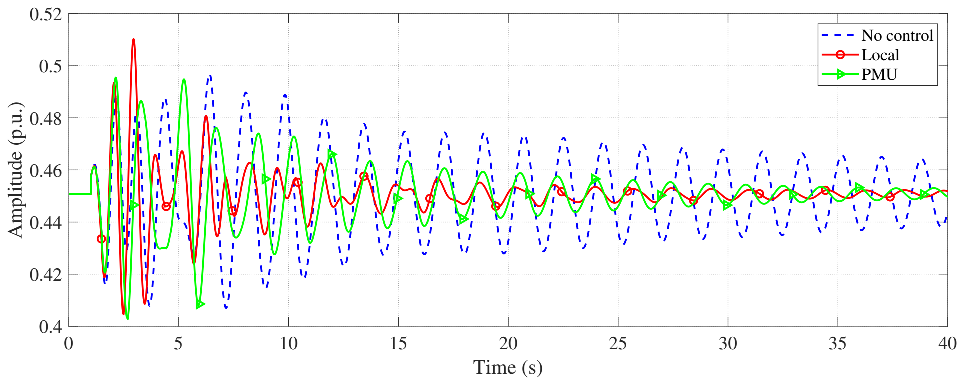

Figure C.5: Comparison of P_{pgt} when g17 is used for damping.

C.2 Generator g64

Figure C.6 shows a comparison between the feedback signal and the terminal power from when g64 was controlled with WACS. Initially the feedback signal is in phase with the terminal power but at around 13 s a shift occures making the signals out of phase. This is the point at which the generator starts swinging against the group of generators it previously belonged to, while the feedback signal still represents the oscillation between g20 and g64.

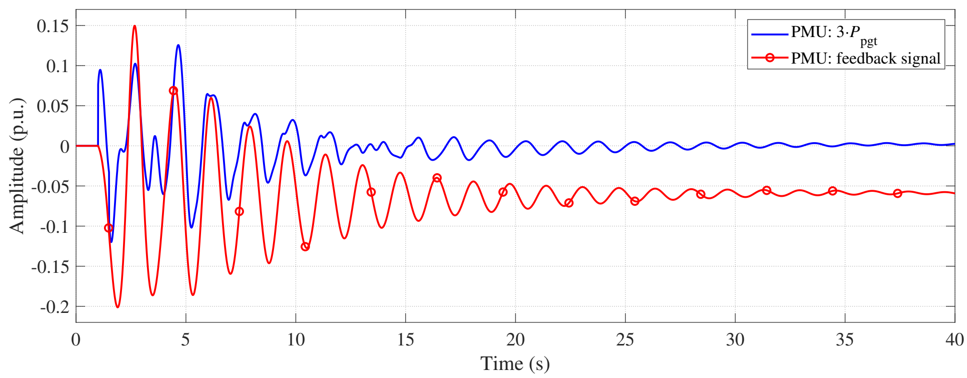

Figure C.6: Comparison between the generator terminal power from g64 scaled by three and the feedback signal for using PMU as control method when g64 is used for damping, offset to start at 0.

Figure C.7 show the feedback signals for each of the methods. Similar conclusions can be made here as for g20 and g17.

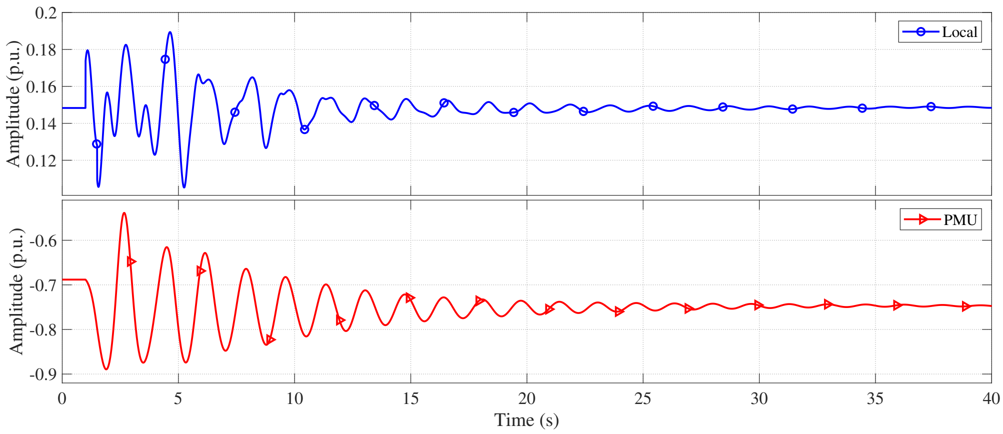

Figure C.7: Comparison between feedback signals for the different control methods when g64 is used for damping.

Figure C.8 show the control signals for each of the methods. The resulting initial control effort due to the AVR limit is similar between the methods as can be seen by the response in power flow. To which degree the phase shift from g64 changing oscillation group affects the damping is unclear. The results indicate it has positive influence on the overall damping which must come from other generators being positively affected.

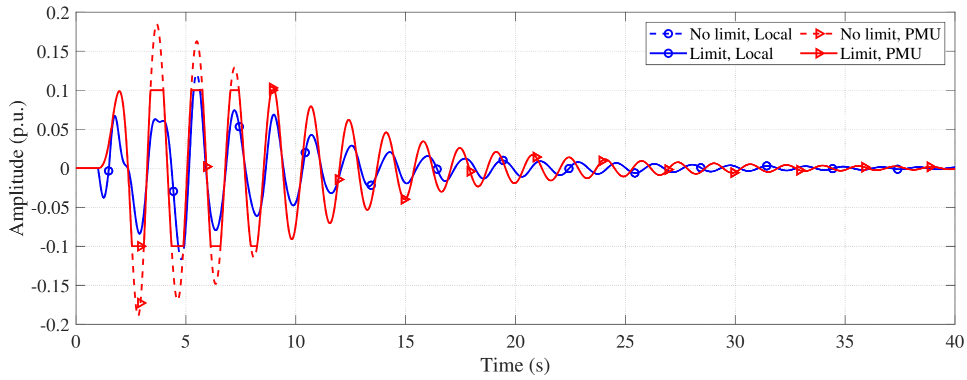

Figure C.8: Comparison between control signals for the different control methods when g64 is used for damping.

Figure C.9 show the P_{sum} signals for each of the methods. The difference is small due to the control effort being similar.

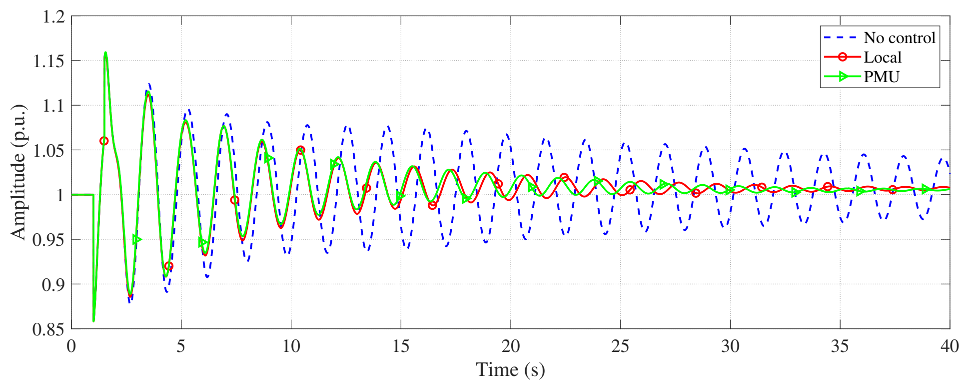

Figure C.9: Comparison of P_{sum} when g64 is used for damping.

Figure C.10 show the P_{pgt} signals for each of the methods. Both the methods lead to some disturbance frequencies in the local power, not seen for the other generators where only the local method produced such behaviour. One reason making this case unique is the control signal reaching the limit which also might be the reason for the new behaviour.

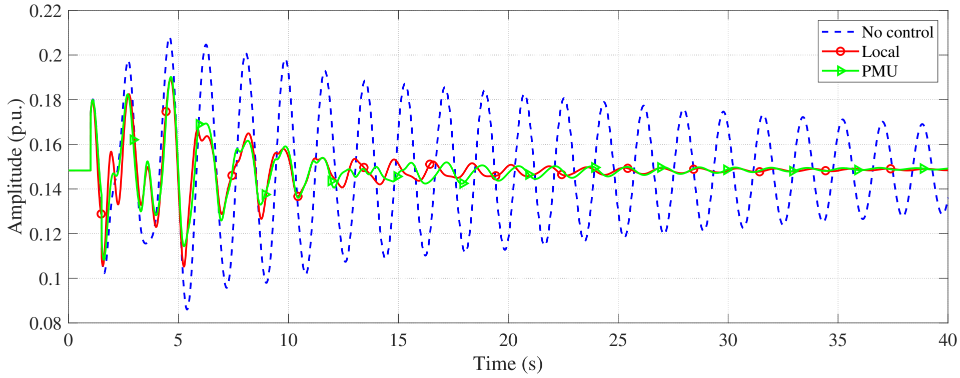

Figure C.10: Comparison of P_{pgt} when g64 is used for damping.

C.3 Wind Turbine Damping for Future Scenario

With an increasing amount of renewable energy the importance of taking into account the effects of these production units become more relevant. Regarding modelling of wind turbines there are a few modern models connected to real life examples. One of these is the IEC Wind turbine Type 4a model which simulates a full-converter connected turbine. It has the possibility of helping with voltage control through reactive power compensation.

Figure C.11 shows a scenario where only wind turbines are used for damping with the fully-renewable scenario. The results indicate efficient damping of the oscillation. The reason for the efficient performance could come from multiple sources. A fast response connected to reactive power output leading to a more stable voltage could be one reason. This could decrease the initial swing of the generators leading to smaller oscillation later on. The topic of power oscillation damping with RES is a large topic which needs to be investigated further. Due to it being out of the scope of this project it is left to future work.

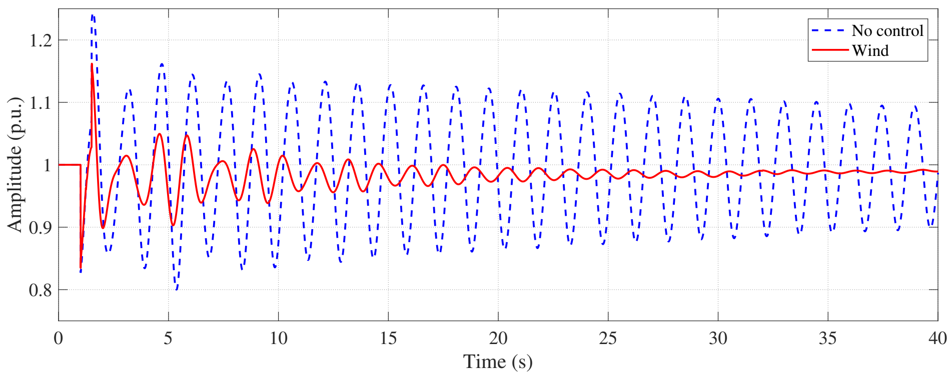

Figure C.11: P_{sum} when wind turbines are controlled with increased wind power.